

DEVELOPMENT OF ALGORITHM FOR EARTHQUAKE EARLY WARNING SYSTEM

Ph.D. THESIS

by

BHANU PRATAP CHAMOLI



**CENTRE OF EXCELLENCE IN DISASTER MITIGATION &
MANAGEMENT**

INDIAN INSTITUTE OF TECHNOLOGY ROORKEE

ROORKEE – 247 667, UTTARAKHAND, INDIA

JULY, 2021



DEVELOPMENT OF ALGORITHM FOR EARTHQUAKE EARLY WARNING SYSTEM

A THESIS

*Submitted in partial fulfilment of the
requirements for the award of the degree*

of

DOCTOR OF PHILOSOPHY

in

DISASTER MITIGATION & MANAGEMENT

by

BHANU PRATAP CHAMOLI



**CENTRE OF EXCELLENCE IN DISASTER MITIGATION &
MANAGEMENT**

**INDIAN INSTITUTE OF TECHNOLOGY ROORKEE
ROORKEE – 247 667, UTTARAKHAND, INDIA**

JULY, 2021



**©INDIAN INSTITUTE OF TECHNOLOGY ROORKEE, ROORKEE-2021
ALL RIGHTS RESERVED**







CERTIFICATE FROM SUPERVISOR

INDIAN INSTITUTE OF TECHNOLOGY ROORKEE

1. Name of the Ph.D. student: Bhanu Pratap Chamoli
2. Name of the Department / Centre: Centre of Excellence in Disaster Mitigation and Management
3. Title of the Thesis: DEVELOPMENT OF ALGORITHM FOR EARTHQUAKE EARLY WARNING SYSTEM
4. Date of Thesis Defense: 12 JULY 2021
5. It is to certify that :

(A) Ms. /Mr. BHANU PRATAP CHAMOLI, Enrollment No. 13929003 has incorporated all the modifications/ corrections pointed out by the examiners, as accepted by her/him, in the final submitted thesis.

(B) The modifications/ corrections suggested during the Presentation and Viva-Voce Examination have been incorporated in the final submitted thesis.

Supervisor(s)

(Prof. Ashok Kumar)

(Prof. Ajay Gairola)

(Prof. Ravi Kumar)

Digitally signed by Ravi Kumar
DN: cn=Ravi Kumar, o=Indian Institute of
Technology Roorkee, ou=Department of
Mechanical and Industrial Engineering,
email=ravi@maie.iitr.ac.in, c=IN
Date: 2021.07.28 15:28:11 +05'30'



ABSTRACT

Part of North-Western Himalaya, Which typically comprised of, Jammu and Kashmir, Laddakh, Himachal Pradesh, and Uttarakhand, particularly Uttarakhand, has been identified by several eminent seismologists as a gap area where large size earthquake(greater than magnitude 7) is expected. The region has witnessed two earthquakes having a magnitude greater than 6 in the last 25 years (28th March 1999 Chamoli earthquake and 20th October 1991 Uttarkashi earthquake), both having an epicenter in the Garhwal region of Uttarakhand. Several studies have shown that a future large earthquake in Central Himalayas can generate severe ground motion in the National capital region of Delhi, which is about 300 km from this expected source. Several densely populated cities and villages having a total population of several million are located between Delhi and Uttarakhand. These towns/cities will be severely affected by a large earthquake having an epicenter in this region. Using advancements in communication technology and real-time seismology, a project to have an earthquake early warning system for Northern India is under progress at the Indian Institute of Technology, Roorkee. In this project, a dense network of 84 accelerometers has been installed, covering an area of about 100 km x 40 km in the Garhwal region. This network has an intermediate station to station distance of less than 10km, and all the sensors are streaming data, which is being processed in real-time at the central server stationed at Roorkee. The cost of the sensor becomes one of the most important parameters on which the viability of an Earthquake Early Warning (EEW) system depends since a dense network of the sensor is required for an effective EEW system. Thus in this study, a detailed analysis is also performed to find out the optimum dynamic range of sensor that is required so that the most relevant information, EEW parameter, and strong motion parameters could be retrieved from the obtained ground motion data. In the study, it is observed that for all relevant EEW parameters, a sensor with ADC with the 16-Bit resolution is quite sufficient, and most of the required information could be retrieved from such data. This thesis describes details of the network, sensors, present status of development, performance of instrumentation during recent events and processing details. The thesis also provides details of the theoretical and numerical analysis done for the ADC dynamic range varying from 24-Bit to 10-Bit and its impact on the most relevant EEW parameter and strong motion parameters.

A new approach for P-phase picking has also been developed in this study. The parameter used is '*Damage Intensity*' which has been widely used in Japan for intensity estimation for UrEDAS. One of the problems faced during the testing of the EEW system was to eliminate far-field earthquakes. By far-field events are those events that have their epicenter at a large distance from the networked region. During testing, one such event from the Hindukush region was picked by the software. Thus it was a concern that such events should not be picked or, if picked, should be ignored by the EEW system. Using this approach, it was found that far-field earthquakes could be eliminated and were not picked if this approach is used.



Acknowledgment

I wish to express my sincere gratitude to my supervisor **Prof. Ashok Kumar**, Professor, Department of Earthquake Engineering, Indian Institute of Technology, Roorkee for their intuitive and meticulous guidance, unwavering support and perpetual inspiration in the completion of this thesis work. I would also like to express my sincere gratitude towards **Prof. Ajay Gairola, Professor**, Department of Civil Engineering, Indian Institute of Technology, Roorkee and **Dr. Ravi S Jakka**, who helped me in all aspects of my research work, starting from identification of the problem to reach a solution, and providing the required facilities to perform the research. Without their painstaking efforts at every stage of the study, this thesis would not have taken this shape. I would also like to express my sincere gratitude towards **Prof. M L Sharma**, Professor, Department of Earthquake Engineering, Indian Institute of Technology, Roorkee, for his guidance and suggestions in various stages of my Ph.D. thesis. I found him always available for discussion, and his suggestions were always helped me in solving several problems. I would also like to thank **Prof. Ravi Kumar**, Department of Mechanical Engineering.

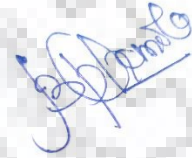
I would like to express my gratitude to **Prof. Mahua Mukharjee**, Centre of Excellence in Disaster Mitigation & Management, members of my student research committee (SRC), **Prof. M L Sharma** (external expert), **Dr. Kamal** (internal expert) for their continuous administrative support, recommendations and useful suggestions in every possible way that helped me to accomplish the thesis work.

I would wish to thank the Ministry of Earth Sciences (MoES), Government of India, for providing funds through Grant No. MoES/P.O.(Seismo)/1(144)/2012, to execute this research. We are thankful to the committee comprising of **Prof. V P Dimri** and **Dr. H N Shrivastav** for helping in the identification of the region to be instrumented. I am thankful to NIC-SWAN, BSNL for providing connectivity and allowing us to use their premises for the installation of the sensor. I am also thankful to **Prof. Yih-Min Wu**, Department of Geosciences, National Taiwan University, for sharing his knowledge and guidance. I am thankful to Mr. Amit Shrivastava and Mr. Ghanshyam Tiwari (Technical staff in the project) for their hard work in the installation of sensors. I am also thankful to the advisory committee, chaired by **Dr. B K Gairola**, for their valuable suggestion and guidance.

I would like to express my sincere gratitude to my friend Mr. Bhavesh Pandey, Assistant Professor, Bipin Tripathi Kumaon Institute of Technology, Dwarahat, Uttarakhand, Uttarakhand, for his support, help, and suggestions all along with my Ph.D. tenure.

I would also like to express special gratitude to Mr. Tahir Husain, who has helped, mentored and resolved all the academic and administrative issues from admission in CoEDMM to the final submission of my Ph.D. thesis.

I am thankful to my friends – Dr. Rituraj Nath., Dr. Pankaj Kumar, Dr. Rajiv Sachdeva, Mr. Amit Goyal, Mr. Govind Rathore, for their valuable help and support at different stages of my Ph.D.



(Bhanu Pratap Chamoli)



Table of Contents

Abstract.....	i
Acknowledgment.....	iii
Table of Contents.....	v
List of Figures.....	viii
List of Tables.....	xiii
List of Abbreviations.....	xiv
List of Notation and Symbols.....	xx
Chapter 1 Introduction	1
1.1 Preamble.....	1
1.2 Motivation.....	4
1.3 Research Objectives.....	5
1.4 Dissertation Outline.....	5
Chapter 2 Literature Review	7
2.1 EEW Parameters.....	7
2.1.1 Predominant Period (τ_p).....	8
2.1.2 Characteristic Period Parameter (τ_c).....	8
2.1.3 Cumulative Absolute Velocity (CAV).....	9
2.1.4 Bracketed Cumulative Absolute Velocity (BCAV).....	9
2.1.5 Windowed Bracketed Cumulative Absolute Velocity (BCAV-W).....	9
2.1.6 Low-Pass Filtered Peak Displacement (Pd).....	10
2.1.7 Squared Velocity Integral (IV2).....	11
2.1.8 The Log-Averaged Period (τ_{log}).....	11
2.1.9 Root Sum Square Cumulative Velocity (RSSCV).....	12
2.2 EEW System Current Status.....	12
2.2.1 UrEDAS.....	13
2.2.2 Compact UrEDAS.....	13
2.2.3 FREQL and AcCo.....	14
2.2.4 EalrmS.....	14
2.2.5 Virtual Seismologist.....	15
2.2.6 EEW system in Taiwan.....	15

2.2.7	PreSEIS.....	16
2.2.8	Early Warning System in Fujian China.....	16
2.2.9	Presto	17
2.3	Suitability of low-cost sensor for EEW and Strong motion studies...	18
2.3.1	OSOP Raspberry Shake 4D.....	18
2.3.2	LIS331DLH (iPhone) Accelerometer.....	19
2.3.3	Quake-Catcher Network.....	19
2.3.4	Urban Seismic Network (USN).....	20
2.3.5	GL-P2B –MEMS for earthquake early warning	20
2.3.6	Palert	21
Chapter 3 EEW System for Northern India		23
3.1.	Region for EEW sensor network.....	23
3.2.	Target location	25
3.2.1.	Plains adjoining Kumaun – Garhwal Himalayas	25
3.2.2.	Western UP and Eastern Haryana	26
3.2.3.	National capital region, Delhi	26
3.3.	Selection of Site for Sensor and Type of Network.....	27
3.4.	Network Time Protocol	36
Chapter 4 Sensor Selection and its Dynamic Range.....		37
4.1	Methodology and Procedure:	37
4.2	Effect on Magnitude using PD or MPD	39
4.3	Effect on magnitude estimation using τ_c	45
4.4	Effect on Spectral Acceleration:.....	49
4.4.1.	Effect on Spectral Acceleration for 5% damping	50
4.4.2.	Effect on Spectral Acceleration for 2% damping	59
4.4.3.	Effect on Spectral Acceleration for 10 % Damping.	66
4.5	Effect on Fourier spectrum or Fourier amplitude.....	75
4.5.4.	Effect on Fourier amplitude	75

Chapter 5 Central Processing unit	87
5.1. Central Processing Unit and Decision Making	88
5.2. Decision Making, Warning dissemination, Simulation and Performance	90
5.2.1.Simulation and Testing	96
5.2.2.Performance of the EEW system during recent earthquakes	99
5.3 New approach for P phase picking using Damage Intensity.	103
5.3.1.Methodology	104
5.3.2.Development of Pick algorithm using recorded data	106
5.3.3.Testing of the algorithm:	108
Chapter 6 Conclusion and Results	113
6.1. EEW System for Northern India	113
6.2. Sensor Selection	114
6.2.1 Effect on Magnitude using PD or MPD	114
6.2.2 Effect on magnitudes using τ_c or $M\tau_c$	115
6.2.3 Effect on Spectral Acceleration	115
6.2.4 Effect on Fourier spectrum or Fourier amplitude.	117
6.3. New Pick Algorithm using DI	118
6.4. Future scope of work	119
List of References	121



List of Figures

Figure Number	Details of Figure	Page No
Figure 3.1	Selected region for instrumentation as well as the most crucial target location for issuing warning, the national capital New Delhi	25
Figure 3.2	The figure shows in the sensor network created for the EEW for Uttarakhand, India.	26
Figure 3.3	THE BASIC CONNECTIVITY DIAGRAM FOR VPNOBB (VIRTUAL PRIVATE NETWORK OVER BROADBAND) CIRCUIT FOR EEW NETWORK. (SOURCE BSNL)	27
Figure 4.2	Number of records vs difference in MPD estimation for 22 Bit converted record	39
Figure 4.3	Number of records vs change difference in MPD estimation for 20 Bit converted record.	39
Figure 4.4	Number of records vs difference in MPD estimation for 18-Bit converted record.	40
Figure 4.5	Number of records vs difference in MPD estimation for 16-Bit converted record.	40
Figure 4.6	Number of records vs change difference in MPD estimation for 14-Bit converted record.	41
Figure 4.7	Number of records vs change difference in MPD estimation for 12 Bit converted record.	41
Figure 4.8	Number of records vs change difference in MPD estimation for 10 Bit converted record.	42
Figure 4.9	The difference in magnitude estimation using T_c is calculated for time histories at different ADC resolutions varying from 22-Bit to 10-Bit with reference to the original 24-Bit data.	43
Figure 4.10	NUMBER of records vs change in MTC estimation for 22-Bit converted record.	43
Figure 4.11	Number of records vs change in MTC estimation for 18-Bit converted record.	44
Figure 4.12	Number of records vs change in MTC estimation for 18-Bit converted record.	44
Figure 4.13	Number of records vs change in MTC estimation for 16-Bit converted record.	45
Figure 4.14	Number of records vs change in MTC estimation for 14-Bit converted record.	45
Figure 4.15	Number of records vs change in MTC estimation for 12-Bit converted record.	46
Figure 4.16	Number of records vs change in MTC estimation for 10-Bit converted record.	46
Figure 4.17	DIFFERENCE in Spectral Acceleration, calculated for time histories at different ADC resolution varying from 22-Bit to 10-Bit with reference to original 24-Bit data and Zero period or PGA.	48
Figure 4.18	Difference in Spectral Acceleration, calculated for time histories at different ADC resolution varying from 22-Bit to 10-Bit with reference to original 24-Bit data and 0.03 second period.	48
Figure 4.19	Difference in Spectral Acceleration, calculated for time histories at different ADC resolution varying from 22-Bit to 10-Bit with reference to original 24-Bit data and 0.05 second period.	49
Figure 4.20	Difference in Spectral Acceleration, calculated for time histories at different ADC resolution varying from 22-Bit to 10-Bit with reference to original 24-Bit data and 0.1 second period.	49

Figure 4.58	Difference in Spectral Acceleration at 10% damping, calculated for time histories at different ADC resolution varying from 22-Bit to 10-Bit with reference to original 24-Bit data and 4 second period	68
Figure 4.59	Difference in Spectral Acceleration at 10% damping, calculated for time histories at different ADC resolution varying from 22-Bit to 10-Bit with reference to original 24-Bit data and 5 second period	69
Figure 4.60	Difference in Spectral Acceleration at 10% damping, calculated for time histories at different ADC resolution varying from 22-Bit to 10-Bit with reference to original 24-Bit data and 7 second period	69
Figure 4.61	Difference in Spectral Acceleration at 10% damping, calculated for time histories at different ADC resolution varying from 22-Bit to 10-Bit with reference to original 24-Bit data and 10 second period	70
Figure 4.62	Difference in Fourier Amplitude, calculated for time histories at different ADC resolution varying from 22-Bit to 10-Bit with reference to original 24-Bit data and 25 Hz frequency.	71
Figure 4.63	Difference in Fourier amplitude, calculated for time histories at different adc resolution varying from 22-bit to 10-bit with reference to original 24-bit data and 20 hz frequency.	71
Figure 4.64	Difference in Fourier Amplitude, calculated for time histories at different ADC resolution varying from 22-Bit to 10-Bit with reference to original 24-Bit data and 10 Hz frequency.	72
Figure 4.65	Difference in Fourier Amplitude, calculated for time histories at different ADC resolution varying from 22-Bit to 10-Bit with reference to original 24-Bit data and 5 Hz frequency.	72
Figure 4.66	Difference in Fourier Amplitude, calculated for time histories at different ADC resolution varying from 22-Bit to 10-Bit with reference to original 24-Bit data and 3.33 Hz frequency.	73
Figure 4.67	Difference in Fourier Amplitude, calculated for time histories at different ADC resolution varying from 22-Bit to 10-Bit with reference to original 24-Bit data and 2 Hz frequency.	73
Figure 4.68	Difference in Fourier Amplitude, calculated for time histories at different ADC resolution varying from 22-Bit to 10-Bit with reference to original 24-Bit data and 1.35 Hz frequency.	74
Figure 4.69	Difference in Fourier Amplitude, calculated for time histories at different ADC resolution varying from 22-Bit to 10-Bit with reference to original 24-Bit data and 1 Hz frequency.	74
Figure 4.70	Difference in Fourier Amplitude, calculated for time histories at different ADC resolution varying from 22-Bit to 10-Bit with reference to original 24-Bit data and 0.5 Hz frequency.	75
Figure 4.71	Difference in Fourier Amplitude, calculated for time histories at different ADC resolution varying from 22-Bit to 10-Bit with reference to original 24-Bit data and 0.33 Hz frequency.	76
Figure 4.72	Difference in Fourier Amplitude, calculated for time histories at different ADC resolution varying from 22-Bit to 10-Bit with reference to original 24-Bit data and 0.25 Hz frequency.	76
Figure 4.73	Difference in Fourier Amplitude, calculated for time histories at different ADC resolution varying from 22-Bit to 10-Bit with reference to original 24-Bit data and 0.2 Hz frequency.	77
Figure 4.74	Difference in Fourier Amplitude, calculated for time histories at different ADC resolution varying from 22-Bit to 10-Bit with reference to original 24-Bit data and 0.14 Hz frequency.	77
Figure 4.75	Difference in Fourier Amplitude, calculated for time histories at different ADC resolution varying from 22-Bit to 10-Bit with reference to original 24-Bit data and 0.75 Hz frequency.	78

Figure 5.1	Figure shows the outcome of the warning display of Early Warning Display Program during simulation of 29th November 2015 Chamoli earthquake of magnitude 4. In the picture, blue dots are the sensors picked, innermost red circle is the estimated epicentre, red circle is S-wave envelop, blue circle is P-wave envelop, the hut in the centre of map is target location, in this case New Delhi. 66.04 is the expected time of S-wave arrival at the target location in seconds.	81
Figure 5.2	P and S wave velocity model derived from Kanaujia et al. (2015)	82
Figure 5.3	The figure showing epicentres of earthquakes that have been used for validation of the regression model for estimation of magnitude of earthquake. Modified after map obtained from http	83
Figure 5.4	Estimated MPD and error in estimation with respect to actual magnitude using Wu et al., 2006.	84
Figure 5.5	Estimated MPD and error in estimation with respect to actual magnitude using Hsiao et al., 2011.	85
Figure 5.6	Estimated MPD and error in estimation with respect to actual magnitude using Kuyuk et al., 2013.	86
Figure 5.7	Average error in estimated Mpd with magnitude using Wu et al., 2006 (Solid line), Hsiao et al., 2011 (Dotted line)	86
Figure 5.8	Acceleration, velocity and displacement time history of 29, November 2015 earthquake having magnitude 4 from station Chinka which was located at 13 km from estimated epicenter. Asterisk denotes the point of P-Onset and diamond shows the maximum displacement of 3 sec window from P-Onset (Pd). Magnitude estimated by EEW system, for Pd equal to 0.0264 cm, calculated at this station was 3.45.	87
Figure 5.9	A schematic diagram to show the EEW process being developed for EEW for Northern India.	90
Figure 5.10	Estimated epicenters and recorded peak ground accelerations (PGA) in gals for 29/11/2015 Chamoli Earthquake of magnitude 4	91
Figure 5.11	Estimated epicentres and recorded peak ground accelerations (PGA) in gals for 25/09/2016 Uttarkashi Earthquake of magnitude 3.5	92
Figure 5.12	6/12/2017 Rudraprayag earthquake of magnitude 5.5	94
Figure 5.13	Plot of DI corresponding to a time history of a seismic event of Magnitude 5.7 recorded at AOMH 05 (Kik-Net) on 15/07/10 at 03	96
Figure 5.14	The figure representing application of DI for picking P phase data	99
Figure 5.15	The figure gives example of candidate record for which event was not picked for far field earthquake.	102
Figure 5.16	Successful pick using DI for near field event	102



List of Tables

Table No	Description of Table	Page No
Table 3.1	EEW stations in Garhwal Region of Uttarakhand installed at SWAN facility	28
Table 3.2	EEW stations in Kumaon Region of Uttarakhand installed at SWAN facility.	28
Table 3.3	EEW stations in Garhwal Region of Uttarakhand installed at BSNL base transceiver station.	30
Table 3.4	EEW stations in Kumaon Region of Uttarakhand installed at BSNL BASE TRANSCEIVER STATION.	31
Table 4.1	Representative periods used for analysis of Spectral Acceleration values	47
Table 4.2	Representative frequencies used for analysis of Fourier Amplitudes. The frequencies are corresponding	70





Abbreviation, Symbols & Notations

General Abbreviation

PGA	Peak Ground Acceleration
PGD	Peak Ground Displacement
PGV	Peak Ground Velocity
BMTPC	Building material Technology Promotion Centre
EEW	Earthquake Early Warning
CAV	Cumulative absolute Velocity
BCAV	Bracketed Cumulative absolute velocity
RSSCV	Root Sum Square cumulative velocity
VS	Virtual Seismologist
CISN	California Integrated Seismic Network
MEMS	Micro-electromechanical system
QCN	Quake catcher network
BOINC	Berkeley Open Infrastructure for Network Computing
USN	Urban Seismic Network
STA	Short Time average
LTA	Long Time Average
CWB	Central Weather Bureau
NTP	Network Time protocol
NTP	Network Time Protocol
TCP	Transmission control protocol
IP	Internet Protocol
DMMC	Disaster Mitigation and Management Centre
MoES	Ministry of Earth Science
NCR	National capital Region
MBT	Main Boundary Thrust
MCT	Main Central Thrust

SWAN	State wide area Network
NIC	National Informatics Centre
BSNL	Bharat Sanchar Nigam Limited
CUG	Close user Group
VPN	Virtual Private Network
SA	Spectral Acceleration
IMD	India Meteorological Department



Abbreviation used for sensor installation location

AGMS	Augustmuni
BHLS	Bhilangana
BKTS	Barkot
CHMS	Chamoli
CLSS	Chinyalisour
CMBS	Chamba
DNDS	Dunda
DVLS	Deval
DVPS	Devprayag
GHTS	Ghat
GOPS	Gopeshwar
HDKS	Hindolakhali
JKLS	Jakholi
JSMS	Joshimath
KOTS	Kot
KRPS	Karanprayag
NGNS	Naugaon
PKRS	Pokhri
PORS	Pauri
PRLS	Purola
PTNS	Pratapnagar
RDPS	Rudraprayag
SRNS	Srinagar
TEHS	Tehri
TRLS	Tharali
UKMS	Ukhimath
UTKS	Uttarkashi
ALMS	Almora (DHQ)
BGSS	Bageshwar (DHQ)
BHKS	Bhikiyasen (BHQ)
BMTS	Bhimtal

BNLS	Bhanoli(THQ)
BRKS	Barakot
BRNS	Berinag (BHQ)
BTLS	Betalghat (THQ)
CHKS	Chaukhutia (BHQ)
CHPS	Champawat (DHQ)
DCLS	Dharchula (THQ)
DHLS	Dhauladevi (BHQ)
DHTS	Dwarahat (BHQ)
DIDS	Didihat (THQ)
DLCS	Dhaulachina (THQ)
DRIS	Dhari (THQ)
GNGS	Gangolihat (BHQ)
GRRS	Garur (BHQ)
HLDS	Haldwani (THQ)
HWBS	Hawal Bagh
JNTS	Jainti(BHQ)
KFLS	Kafligair (THQ)
KKLS	Kosia Katoli (THQ)
KNDS	Kanda (THQ)
KNLS	Kanalichina (BHQ)
KPKS	Kapkot (BHQ)

KTBS	Kotabagh (BHQ)
LGHS	Lohaghat (BHQ)
LMGS	Lamgara
MNKS	Munakot (BHQ)
MNSS	Munsiari
NTLS	Nainital (DHQ)
OKKS	Okhal Kanda (BHQ)
PTIS	Pati
PTRS	Pithoragarh (DEOC)
RMGS	Ramgarh (BHQ)
RNKS	Ranikhet (THQ)
SLTS	Sult (BHQ)
SMSS	Someshwer (THQ)
SYLS	Syaldey (BHQ)
TRKS	Tarikhet (BHQ)
VKBS	Vikas Bhawan (BHQ)
ADIB	Adibadri
AGMB	Augustmuni
AULB	Auli
BHIB	Bhiri
BMKB	Bharamkhal
CDPB	Chandrapuri
CHHB	Chhaam
CMBB	Chamba

CMLB	Chamiyala
CNKB	Chhinka
CYSB	Chinyalisour
DLTB	Dhanaulti
DNTB	Dhauntri
DUNB	Dunda
GAZB	Gaza
GCRB	Gaucher
GDRB	Ghurdauri
GLMB	Gwaldom
GLTB	Gholteer
GNSB	Ghansali
GOPB	Gopeshwar
GRSB	Gairsain
GYNB	Gyanshu
JKDB	Jhaknidhar
JMKB	Jamnikhil
JMTB	Joshimath
KDLB	Kandikhil
KNKB	Khankra
KNPB	Karanprayag
KNTB	Kanatal
KRKB	Kherakhal
KRSB	Khirsu
KSTB	Kanskhet
KTSB	Koteswar
LNGB	Langasu
MDLB	Mandal
MHDB	Mahidanda
MNRB	Maneri
MORB	Mori
MTLB	Matli
NGNB	Naugaon
NNPB	Nandprayag
NRBB	Narainbagar
NTYB	Nauti
PLKB	Pipalkoti

PRLB	Purola
PTHB	Paithani
PTNB	Pratap Nagar
RCRB	Ranichauri
SKTB	Srikot
SMLB	Simli
STKB	Saterakhal
THTB	Thatyur
TLWB	Tilwara
UKMB	Ukhimath
BGSB	Bageshwar
BHWB	Bhawali
BJNB	Baijnath
BKSB	Bhikiasain
BLKB	Baluakot
BRCB	Barecheena
BRNB	Berinag
BSLB	Basoli
BTKB	Bhatrojkhana
BTLB	Betalghat
CBTB	Chaubatia
CHLB	Chillianaula
DGTB	Deghat
DIDB	Didihat
DNYB	Danya
DOLB	Dol
DVDB	Devidhura
DWTB	Dwarahat
GGLB	Ganai Gangoli
GNIB	Ganai
GRMB	Garampani
HWLB	Hawalbagh
JJDB	Jhajjardeval
JRSB	Jaurasi
KFGB	Kafligair
KNLB	Kanalicheena

KPKB	Kapkot
KRBB	Karbala
KSNB	Kausani
LXMB	Laxmeshwar
MCRB	Machor
MKLB	Majkhali
MKTB	Mukteshwar
MNLB	Manila
MNSB	Munsiari
PDGB	Pandey Gaon
RMGB	Ramgarh
SMSB	Someshwar
SYLB	Syaldey
THLB	Thal
TRKB	Tarikhet
WDDB	Wadda

Notation and Symbols

P_D	High Pass Filtered Peak Displacement
M_{PD}	Magnitude estimation using P_D
τ_p	Predominant Period
M_{τ_p}	Magnitude Estimation using τ_p
τ_c	Characteristic Period
M_{τ_c}	Magnitude Estimation using τ_c
τ_{log}	The Log average Period

Chapter 1 Introduction

1.1 Preamble

The Himalaya,; a landmass of approximately 2500 km, was formed due to the collision of Indian and Eurasian plates during the Tertiary period, which is about fifty million years old(Gansser 1964; Molnar and Lyon-Caen 1988; Kayal 2001). The Central Himalaya is situated right in the middle of the Alpine Himalaya zone belt, which is the second most seismically active region in the world. The 800 km stretch of land mass, expanded between river Kali in the west and river Tista in the east in generally referred to as Central Himalayas. The Great Himalaya range attains maximum height in this region of the Himalayas. Few of the world-famous peaks Mt. Everest, Kanchenjunga, Makalu, Annapurna, Gosainthan and Dhaulagiri, are located in the region. The Central Himalayas, within the scope of this thesis, is generally referred to for Uttarakhand and Himachal Pradesh. This landmass had been created; as a result closure of the Tethys Ocean and the process of the collision between the Northward moving African, Arabian, and Indian plates with the Eurasian Plate in general and under-thrusting of the Indian plate under the Eurasian plate in particular (Zhao 1993; Rautela and Sati 1996; Kayal 2008). This under thrusting action results in subsurface internal deformations of rocks, under thrusting along detachment surface. This leads to an accumulation of stresses in the form of strain energy. Researchers have concluded that earthquakes in the Himalayan region are caused due to the release of this accumulated energy (Seeber et al. 1981; Kayal 2001). Continuous observation of Global Positioning System data and average slip deficit studies (Bilham and Ambraseys 2005; Bilham and Wallace 2007), plate convergence rates, and differential shortening rates also points out about continuing seismic activity in the Himalaya(Chen and Kao; Banerjee and Burgmann 2002; Bilham and Ambraseys 2005; Feldl and Bilham 2006; Jade et al. 2007)

The Himalayan belt has been witnessing a large number of earthquakes for a long time. Four most recent earthquakes witnessed in the last century have been reported with magnitude greater than eight viz.; the M 8.7 1897 Shillong(Milne 1911), M 8.5 1950 Assam (Tandon and Srivastava 1954, 1974), M 8.2 1934 Bihar–Nepal(Tandon and Srivastava 1974), and ML 8.0 1905 Kangra (Gutenberg & Richter, 1954) earthquakes. However, no great earthquakes have been observed in the Central Himalayan region in the last few decades (Yeats and Thakur 1998). This non-occurrence of any major seismic activity has resulted in the formation of seismic gaps, which are defined as the region or zones, which have accumulated stresses, but energy has not been released for a long time. The seismic gaps are considered potential zones for future great earthquakes

(Khattri and Tyagi 1983). Seismologists have already forecasted the occurrence of four great earthquakes, having a magnitude greater than 8, in these seismic gaps (Bilham and Ambraseys 2005), which could lead to huge damage to property and life in the region and adjoining regions as well. Gorkha earthquake of 2015 is one such example of a major event in the seismic gaps.

Seismic hazard from the Himalayas and dense population in and around metropolitan cities and industrial hubs in Northern India has made this region vulnerable to large-scale loss of life, and property in case of a large earthquake. To provide housing for all the people, in fast-growing cities, a large number of structures and closely spaced housing complexes have been constructed. Due to a lack of knowledge of local masons or economic considerations, most of these structures are not earthquake resistant which may result in huge damage and loss of life in case of major earthquakes. As per Vulnerability Atlas of India, 2008 (BMTPC, 2008), the region comprising of Uttarakhand, Western Uttar Pradesh, eastern districts of Haryana, and National Capital Region (NCR), has 14,453,897 houses out of which 1,764,619 (12%) are reported under high risk, and 12,088,013 (83.6%) were reported under moderate risk in the event of a major earthquake. Retrofitting such a large number of houses is an economically difficult task to achieve in the near future, and hence a system needs to be developed to mitigate the loss of lives in case of a major earthquake.

In such a scenario, an Earthquake Early Warning (EEW) system could prove to be a boon for short-term earthquake disaster mitigation. An Earthquake Early Warning system is generally defined as a system that can process ground motion in real-time from a remote location and issue a warning before significant ground shaking to industries as well as to the general public. This can be achieved by detecting the ground motion radiating from an earthquake rupture and estimating the resulting ground shaking that will occur later, either at the same location or some remote location.

Early warning can be described as all the actions that can be taken during the lead time of a catastrophic event. The lead time is defined as the time elapsing between the moments when the occurrence of a catastrophic event in a given place is reasonably certain, and the moment it actually occurs. The physical basis behind the earthquake early warning system is that the strong ground shaking is caused by Secondary waves (S-waves) and subsequent surface waves, which travel at a velocity much slower as compared to that of Primary waves (P-waves). Both P and S waves travel much slower than electromagnetic signals transmitted wirelessly or through cables. Thus, depending on the distance from the epicenter of a strong earthquake to the vulnerable urban area, the transmission of information and real-time analysis of the first few seconds of P-wave may provide warnings from a few seconds to a few tens of seconds before the arrival of S-wave and strong ground shaking. An EEW system needs algorithms for estimation of size and location

of the earthquake (maybe relatively inaccurate) from the initial few seconds of ground motion time history to issue the warning. Estimating the size of the earthquake and its location has to be performed in as little time as possible. For this initial few seconds (typically three-second window) of data of record, which means as soon as data is received and picked, for P phase should be analyzed. All the algorithms use recorded data for training the regression models. Thus they may not have an accuracy of one-to-one relation. Still, for all practical purposes of an EEW, the various regression models can be trained to provide near accurate estimation of magnitude and distance.

EEW systems are operational in several countries like Japan (Nakamura 1984, 1988; Odaka et al. 2003; Horiuchi et al. 2005; Nakamura and Saita 2007; Hoshihara et al. 2008; Brown et al. 2009; Kamigaichi et al. 2009), Taiwan (Wu and T.-L. Teng 2002; Wu and Zhao 2006; Hsiao et al. 2009; Chen et al. 2015), Mexico (Espinosa-Aranda et al. 2009; Suárez et al. 2018), Turkey (Erdik et al. 2003; Alçik et al. 2009), Romania (Wenzel et al. 1999; Ionescu et al. 2007), and are under development along the West coast of USA (Allen and Kanamori 2003; Böse et al. 2009), Switzerland (Cua and Heaton 2007; Caprio et al. 2011), China (Peng et al. 2011, 2017, 2019) and Italy (Zollo et al. 2006, 2009).

Several studies (Bhatia et al. 1999; Singh 2002; Parvez et al. 2003; Agrawal and Chawla 2006; P. et al. 2010) suggest that high peak ground acceleration (PGA) of the order of more than 200 gals can be expected in Delhi from a major earthquake in the Central Himalayas. Also, the Indian code of practice for seismic design, IS 1893:2016 (Bureau of Indian Standards, 2002), puts Delhi in seismic zone IV, which suggests PGA of 240 gals for the design of structures. The Possibility and relevance of getting full advantage of the EEW system in India are better in terms of possible lead time in comparison to most of the areas in the world. This is because, for Northern India, a potential source of large earthquakes are located in the Himalayas, whereas the centers of large population and major industrial hubs (including the capital city of Delhi) are in the plains adjoining the Himalayas, which are at least 150 km away from the expected potential source. As mentioned earlier, thick population density and poor adherence to earthquake-resistant practices have substantially increased the seismic vulnerability of this region (BMTPC, 2008). However, in the case of a large earthquake in the Himalayas, most of these places, between the central Himalayas and Delhi, can have a lead time varying from 30 to 70 seconds before the damaging S-waves arrive. If this real-time seismological information is adequately tuned to the operational requirements of technical systems, life and industrial loss could be significantly reduced.

The Indian subcontinent has witnessed earthquakes greater than magnitude 8; this, in turn, has triggered research in the field of seismology and earthquake engineering in India (Dimri and Pandey 2014; Jain 2016).

Northern India is generally defined as the state of the Northern part of India, geographically it includes Indus-Gangatic plains and the Himalayas, which is bounded by Central Asia and Tibetan Plateau. The Ministry of Home Affairs includes the states of Haryana, Himachal Pradesh, Punjab and Rajasthan and Union Territories of Chandigarh, Delhi, Jammu and Kashmir and Ladakh. Ministry of Culture, however, does include Uttarakhand but does not include Delhi as Northern India.

In this study, Northern India generally means Uttarakhand, Himalayas, Haryana, Chandigarh, Western Uttar Pradesh, and the National Capital Region of Delhi.

1.2 Motivation

Rautela (2015) explained how traditional knowledge and practices kept the people and property safe from various natural disasters in general and earthquakes in particular. This knowledge has declined and is lost with rapid industrialization and the migration of population from villages to cities. As a result population of all the adjoining cities in plains has increased many folds. A major (Magnitude 7 or more) or great earthquake (Magnitude 8 or more) will surely cause a large loss of life (H., Singh, and Prasad 2012; Rautela 2015; Rautela and Joshi 2010; R. P. Singh, Aman, and Prasad 1996). The second motivation came through big advancements in communication technology in India. During the last about ten years, almost every city, town, and village of India has got mobile towers and broadband connections. The third motivation came from Bhuj earthquake of 26th January 2001, which caused widespread damage and resulting casualty at Ahmedabad, which was about 300 km from the epicentral region. Other cities of the state of Gujarat, which were more than 100 km, also had several deaths and injuries. An operative EEW system could have saved a large number of lives in Gujarat during the Bhuj earthquake.

Research carried out all over the world on real-time seismology and the success of EEW systems in Japan, Taiwan and Mexico were other motivating factors. But the biggest motivating factor was the internal urge to work for the development of a product that will directly benefit the people of India.

1.3 Research Objectives

The main objective of the study is to develop a prototype of an Earthquake early warning system for Northern India and test its feasibility and potential to mitigate earthquake-related disasters for Indian scenarios. This objective is achieved through the following studies;

- 1) Selection of sensor: Based on connectivity capacity, latency in sending a packet, packet size, and dynamic range.
- 2) Study region and selection of sites for sensor installation for the establishment of EEW network
- 3) Selection of regression algorithm and testing.

1.4 Dissertation Outline

The work performed under this study has been presented in this thesis in seven chapters.

Chapter 2 presents the literature review. The literature review is divided into different sections. The first section describes the EEW theory behind the EEW system and different parameters which have been developed and tested for EEW systems across the world. This section is followed by the current state of the EEW system across the world and a brief description of different EEW systems.

Chapter 3, “EEW system for Northern India”, presents the reasoning behind the necessity and relevance of the EEW system for Northern India. It also discusses the selection of study regions and the selection of sites for the installation of sensors for EEW. Selection of region is broadly done based upon the probability of occurrence of major event and distance of the region from target location which is western UP and Delhi. The site selection for the installation of a sensor is largely a function of logistics, which included network connectivity power supply and ease of maintenance.

Chapter 3, “*Selection of sensor*”, in this section, a detailed analysis of sensor selection is described. A study on the low-cost sensor, with a lower dynamic range, on different EEW parameters and different strong-motion parameters, is done and presented in this section. This chapter concludes that a low-cost sensor with a lower dynamic range can be used successfully for EEW.

Chapter 5, “*The Central Processing Unit*”, Many regression models are available for magnitude estimation and EEW parameter. To select the one which gives the best result for the Indian data set, all available algorithms were tested, and the best one was chosen for implementation. A new regression model is also developed using the Indian data set only. The details of the selection of the regression model and its testing are presented in this chapter.

A new pick algorithm using DI to pick the P phase onset is also evolved during this study; details of this algorithm and its testing are presented in this chapter.

Chapter 6, “*Summary and conclusion*” this chapter summarizes the whole study, our findings and the future scope of the work



Chapter 2 Literature Review

Dr. Cooper first conceptualized earthquake early warning through an article published in the San Francisco Evening Bulletin on the third of November 1868(Nakamura and Saita 2007b). At that time, most of the scientist and seismologist could not comprehend this idea, as it appeared impossible to be achieved. The whole concept was presented as follows:

“A very simple mechanical contrivance can be arranged at various points from 10 to 100 miles from San Francisco, by which a wave of the earth high enough to do damage, will start an electric current over the wires now radiating from this city, and almost instantaneously ring an alarm bell, ... This bell should be very large, of peculiar sound, and known to everybody as the earthquake bell. Of course, nothing but the distant undulation of the surface of the earth should ring it. This machinery would be self-acting and not dependent on the telegraph operators.”

Almost 100 years after this, Japan developed the first P wave earthquake early warning system, and it was named as Urgent Earthquake Detection and Alarm System (UrEDAS).

Since then, a lot of development has happened, and presently most of the seismically vulnerable countries either have a working EEW system or, they are working to develop one for them. In the first section of this chapter, the current stage of various EEW system and different parameters that have been used is discussed.

In the third section of the chapter, the widely used low-cost MEMS-based sensor and network created with a low-cost sensor have been discussed. A few of the most popular low-cost MEMS and their usage in different EEW and strong motion networks have also been discussed.

2.1 EEW Parameters

There are different parameters available in the literature for the early prediction of an earthquake and possible damage at the target locations. Most of these parameters use a few seconds of data from the start of the P-phase. The selection of the right parameter for the system can be based on different aspects such as

- Regional or On-site warning system
- Issuance of warning to society in general or industry
- Kind of industry etc.

The most popular of these parameters are discussed below.

2.1.1 Predominant Period (τ_p)

Small magnitude earthquakes are results of the small patch of rupture over the fault and generate high-frequency energy in comparison to the large rupture (large earthquake) over the fault results in the generation of low-frequency earthquake waves. Therefore the predominant period of the first few seconds of the P phase arrival could be correlated to the magnitude of the earthquake. The predominant period is calculated continuously in real-time, taking into account only the vertical component of the velocity sensor from each station and is defined with the recursive relation. (Allen and Kanamori 2003)

$$\tau_i^p = 2\pi \sqrt{X_i/D_i}$$

Where

$$X_i = \alpha X_{i-1} + x_i^2$$
$$D_i = \alpha D_{i-1} + \left(dx/dt\right)_i^2$$

τ_i^p is the predominant period at the time i , x_i is the recorded ground velocity, X_i is the smoothed ground velocity squared, D_i is the smoothed velocity derivative squared, and α is the smoothing constant. Then the maximum predominant period, τ_p^{max} is used for estimation of the magnitude of an earthquake using linear regression relationship between magnitude and τ_p^{max} . The size of the time window plays a very important role in the accuracy of estimation of magnitude, and it has been studied that a time window of 3 seconds is found to be most economical in terms of magnitude estimation as well as attaining maximum lead time.

2.1.2 Characteristic Period Parameter (τ_c)

The period parameter τ_c is computed by

$$\tau_c = 2\pi / \sqrt{\left[\int_0^{t_0} \dot{u}^2(t) dt \right] / \left[\int_0^{t_0} u^2(t) dt \right]}$$

Where \dot{u} , u is defined as the high pass filtered velocity and displacement of the vertical component of the seismic waveform over a fixed time window t_0 (Wu and Kanamori 2008a).

2.1.3 Cumulative Absolute Velocity (CAV)

Kennedy and Reed (EPRI,1988) proposed a new EEW parameter (cumulative absolute velocity CAV) for the application in nuclear power plant during a study sponsored by Electric Power

Research Institute, Palo Alto, California. It is given as integration of absolute value of ground acceleration over the time history of earthquake record. The velocity content present in the velocity record has a direct relation with the energy associated with the earthquake waves for the corresponding seismic recording station. Therefore, it can be used to estimate the damage potential associated with the impending earthquake. CAV is calculated as follows:

$$CAV = \int_0^{t_{max}} |a(t)| dt$$

Where t_{max} is the total duration of the time-history.

2.1.4 Bracketed Cumulative Absolute Velocity (BCAV)

CAV is not related to the arrival time of different phases of energy, but it is more sensitive to low frequencies (damaging) motions than high frequencies (non-damaging) motion. Therefore EPRI in 1991 modified the CAV calculation by eliminating the non-damaging acceleration's values from the seismic trace. This was achieved by eliminating those earthquake time histories which have maximum acceleration below predefined threshold values, say .025 g within a selected time domain, only earthquake records having acceleration values more than the threshold were considered for calculating modified CAV values and are termed as standardized CAV (Bracketed Cumulative Average Velocity-BCAV). BCAV is computed as:

$$BCAV = \sum \int_{t_i}^{t_i+\Delta t} |a(t)| dt$$

$$\max |a(t)| > 0.025 \text{ g}$$

Where t_i is the time when the value of the seismic waveform is greater than 0.025g, and Δt is 1 second (Alcik et al. 2009)

2.1.5 Windowed Bracketed Cumulative Absolute Velocity (BCAV-W)

BCAV-W is modified from BCAV, where CAV is calculated for all the values of, where acceleration is greater than predefined values. This is performed to remove non-damaging high frequencies from the record. However, the problem still persisted for the sensors which were installed in the industrial facilities and high-rise buildings. To remove the noise from such buildings and also to eliminate data from small and far-field earthquakes, the BCAV is further modified to windowed BCAV,

Onsite earthquake early warning systems employed in the buildings and industrial facilities require some improvements over BCAV due to some reasons. The main reasons are as follows

- To remove the added BCAV values due to reasons like high noise, small earthquakes, and far-field events,
- To take care of the minimum acceleration values which are proposed for the nuclear power plant to consider the lower acceleration level for building type structures to eliminate the very large peak of accelerations for near field impulse from long time earthquake motion with lower acceleration values.
- To identify the short-time earthquake motions with very large peak ground accelerations (near field impulsive) from the long-time earthquake motions with lower acceleration levels (far-field).

BCAV-W is calculated by windowing BCAV calculation on a broader window length (W) basis. Alcik considers window length as 8 sec to perform this algorithm on his dataset. It is calculated as follows (Alcik et al. 2009):

$$BCAV - W = \sum_{W=1}^{\text{win length}} \int_{t_i}^{t_i+\Delta t} |a(t)| dt$$

Where, $\Delta t = 1$ sec and maximum $a(t) >$ minimum acceleration. Level.

2.1.6 Low-Pass Filtered Peak Displacement (P_d)

P_d or low pass filtered peak displacement is defined as the peak displacement amplitude for a time history for the first few seconds after P arrival (Wu and Zhao 2006b).

Wu et al., Using data from Taiwan, concluded that the peak initial displacement amplitude, P_d , correlates well with the peak ground-motion velocity, PGV also when P_d is found greater than 0.5 cm, the event is most likely to be damaging. (Wu and Zhao 2006b; Wu and Kanamori 2008a) It was also concluded that the combination of the τ_c and P_d methods could provide reliable threshold warnings within 10 s after the occurrence of a large earthquake.

(Wu and Zhao 2006b) also arrived at the relationship of P_d with the hypocentral distance R , magnitude M , and obtained the following regression expression:

$$M_{P_d} = A + B \log(P_d) + C \log(R)$$

Wu and Zhao (Wu and Zhao 2006b) also concluded that P_d is a more physically fundamental parameter that is also source-dependent.

Also, it more accurately represents the characteristics of the rupture process, and thus it is more in sync with the study of (Olson and Allen 2005).

Allen and Olson have concluded that the initial characteristics of the initial few seconds of earthquake motion can have a great impact on the actual size of the earthquake.

P_d is also very suitable for the EEW system as it can give very agreeable results by using just the initial 3 seconds after the P-phase arrival.

2.1.7 Squared Velocity Integral (IV2)

A new parameter named squared velocity integral was given and is found to be in good conjunction with the energy associated with the ground motion of the recording site. This new parameter considers the initial portion of P-wave and S-wave and can be formulated as:

$$IV2_c = \int_{t_c}^{t_c + \Delta t_c} v_c^2(t) dt$$

Where the subscript c refers to the P and S phase, t_c is the corresponding first arrival, and v_c is the particle velocity measured on the seismogram. Finally Δt_c is the length of the signal along with analyses is performed (Festa et al. 2008).

2.1.8 The Log-Averaged Period (τ_{log})

This parameter is based on the measurement of the frequency content of the initial portion of P-wave like τ_p and τ_c but has improved over these two commonly used EEW parameters. τ_p and τ_c yield correct solution only in cases where the signal has a very high signal to noise ratio and records are monochromatic while τ_{log} is calculated directly from the actual velocity spectra and therefore corresponds to the actual frequency content of the signal

The log-average period, τ_{log} is calculated from the spectrum of the first few seconds of the velocity seismogram. The calculations are done as follows:

- i. Pre-specified seconds or intervals data is extracted from P phase arrival.
- ii. A Hann window is applied to this extracted data; this helps in reducing sudden end effects.
- iii. The frequency content of this new signal is then calculated by applying Fourier transform, and a set of power spectrum coefficients $P_i(w_i)$ are obtained.
- iv. The set of uniformly spaced P_i is resampled to get a set that is spaced every 0.1 log unit of frequency, between 0.1 and 10 Hz, and finally
- v. The log-average period, τ_{log} is obtained through:

$$\log(\tau_{log}) = \frac{\sum_i (P_i^*(w_i) \log(1/w_i))}{\sum_i (P_i^*(w_i))}$$

Where the asterisk indicates that the power spectrum is resampled according to step IV. It is emphasized that replacing P_i with P_i^* in the above expression, and or multiplying the power spectrum coefficients by L/w_i instead of $\log(1/w_i)$ would result in an average period that is biased

toward the highest frequencies in the spectrum. It was demonstrated that instead of using approximate quantities, such as τ_p^{max} and τ_c to the exact quantity τ_{log} gives better real-time magnitude estimation (Ziv 2014).

2.1.9 Root Sum Square Cumulative Velocity (RSSCV)

The RSSCV is another EEW parameter, which is given by (Bhardwaj 2014; Bhardwaj et al. 2016); this parameter includes the combined effect of both amplitude and time of duration. RSSCV is also an integral EEW parameter similar to CAV and is defined as:

$$RSSCV = \sqrt{\sum_{i=1}^n v_i^2}$$

Where v_i is the velocity vector, which is calculated by performing integration of strong-motion records for n number of samples in the selected window. RSSCV helps in enhancing the SNR and reduces the standard error in earthquake records (Bhardwaj et al. 2016).

2.2 EEW System Current Status

Development in sensor technology acted as the catalyst in the research towards On-site EEW systems. This is because an On-site EEW system issues warning at the location of the sensor's installation. This system was quite efficient to initiate automatic shutdown in the industries, such as nuclear power plants; however, the lead is not enough for the general public to react. In the last couple of decades, the development of communication systems, especially broadband internet, created hope towards the possible development of an effective regional EEW system. Several countries are tirelessly working towards the development of a regional EEW system so that the lead time can be increased. In this section, major EEW systems being developed or functional are discussed. (Santos-Reyes 2019; Allen and Melgar 2019)

2.2.1 UrEDAS

In General, the conventional early warning instruments (seismometers) issue the warning when earthquake motion (seismic acceleration) exceeds a pre-set level. For example, in 1965 in Japan, Alarm seismometers were installed every 20 to 25 km along the Shinkansen railway line to issue an alarm if the acceleration of horizontal ground motion exceeds 40 Gal (= cm/sec²). The first P wave earthquake early warning system UrEDAS, in contrast, first judge the devastating potential of an impending earthquake by observing the initial portion of P-wave in terms of magnitude and location and issue the warning if necessary. The UrEDAS estimates the magnitude and

hypocenter, depth, and epicentral azimuth of the earthquake immediately after the P-wave arrivals at a seismic sensor and, like other seismic observation systems, does not transmit the waveform to remote processing or centralized system. The first pilot test of UrEDAS was initiated in the year 1984, and since the year 1986, UrEDAS has deployed as an early warning system for earthquake-related disasters for Saiken undersea tunnel. (Nakamura 2004; Nakamura and Saita 2007b, c).

2.2.2 Compact UrEDAS

As an aftermath of the Kobe earthquake, a need for a system that could issue warnings even earlier than UrEDAS, which led to the development of a new system. To reduce the time for issuing warning, modifications were done in UrEDAS and the newly developed system was named Compact UrEDAS. Unlike other EEW systems, Compact UrEDAS estimated the damage potential of an earthquake in real-time from the earthquake ground motion; the warning is also issued immediately. To estimate earthquake damage potential, the power of the ground motion is estimated by using the inner product of the acceleration vector and velocity vector. Since this value could be large therefore Destructive Intensity (DI) is defined as the logarithm of the absolute value of this inner product as $DI = \log |AV|$. DI is defined as the maximum value of PI after the arrival of the P-phase. In terms of JMA, the intensity is expressed in terms of real intensity (RI) :(Nakamura and Saita 2007b; Kamigaichi et al. 2009)

$$RI = DI + 2.4$$

And

$$MMI = \frac{11}{7}DI + 4.27 = \frac{11}{7}RI + 0.50$$

The compact UrEDAS has been operational since 1998 for Japan railway network as an on-site P wave detection system.

2.2.3 FREQL and AcCo

It is fast response equipment and integrates the functions of UrEDAS, Compact UrEDAS and AcCO. It estimates earthquake parameters in one second after P-wave detection faster than UrEDAS, judges the dangerousness of the earthquake motion one second after detection of P-wave faster than Compact UrEDAS, and outputs the information and alarm based on both acceleration and RI in real-time in the same way as AcCO does. The FREQL has the functionality to issue earthquake alarms based on both network warnings issued from the regional warning

system as well as take decisions based upon The threshold value of its earthquake parameter based upon data from the local sensor. (Nakamura and Saita 2007c)

AcCO or Accelerator Collector is a small and simple seismometer that is designed to records earthquake time history as well as to issue a warning based upon strong motion data. The advantage of AcCo are as follows:

- It is a very small device, almost the size of a palmtop; thus, it is very easy to install and maintain.
- It is very low in terms of initial cost as well as the cost of maintenance as compared to traditional seismometers or force balance accelerometers.
- In addition to recording strong motion data, it also has the functionality to issue an on-site warning based upon local intensity.
- It calculated 5 HZ PGA and issues warning if this value is found to be more than 5 gals
- Intensity scale can be chosen based upon RI MMI or PEIS.

2.2.4 EalrmS

California Integrated Seismic Network acronym as CISN integrated three different algorithms for the development of EEW, these algorithms are P phase detection, subsequent parameter calculation and SHAKEALERT project, and all these are collectively called EalrmS. EalrmS uses two basic modules waveform processing module and an event detection module. The waveform processing module (WP) runs simultaneously at three locations which are CALTECH USGS, USGS Menlo Park, and UC Berkeley. The main objective of this module is to scan for P phase arrival; Allen's (Allen 1978) short time average divided by long time average is implemented for detection of P phase arrival. The WP module estimates peak displacement, velocity and acceleration, predominant period and signal to noise ratio for a 4-second window. All these parameters and P phase arrival time is sent to the event detection module every second. The event detection module runs only at UC Berkeley. This module, in turn, estimates event location, estimates event magnitude and earthquake warning alert to SHAKE ALERT, where the decision to disseminate warning is taken. (Allen and Kanamori 2003; Allen et al. 2009)

The most advanced version with improved modules for estimating and predicting parameters is called EalarmS-3 or E3 and will be used in the future for ShakeAlert (Chung et al. 2019)

Elarms has also been tested for the region outside California, for which it has been optimized. With the help of simulation and recorded data, the Elarms was tested for Israel, and it was found that it worked fine for a sensor network in Israel. (Nof and Allen 2016)

2.2.5 Virtual Seismologist

The Virtual Seismologist (VS) method is based on the Bayesian theorem in Earthquake Early Warning (EEW) that estimates earthquake magnitude and location using observed ground motion amplitudes, predefined prior information, and envelope attenuation relationships (Böse et al. 2009; Caprio et al. 2011). The application of Bayes theorem in EEW states that the most probable source estimate at any given time is a combination of contributions from prior information (i.e., network topology or station health status, regional hazard maps, earthquake forecasts, the Gutenberg-Richter magnitude-frequency relationship) and the real-time streamed ground motion observations. VS is considered an intelligent and smart automatic system capable enough to imitate the work of human seismologists. Because VS is based on the prior information as well as the currently available real-time waveforms makes it unique, when compared with the other available EEW algorithms. This method can make quick, relatively accurate interpretation from real-time earthquake waveform using the experience and the available streamed ground motion data. This method continuously updates the source estimates and predicts ground motion at each second due to a change in the likelihood function as the arrival of additional data.

2.2.6 EEW system in Taiwan

Taiwan, due to its proximity to the Circum-pacific seismic belt, is highly vulnerable to earthquakes and has seen massive damage due to earthquakes in the past. Central Weather bureau has established a real-time strong motion instrument network and has a functional earthquake early warning system in place. The system has the capacity to issuing a warning within 20 seconds of the occurrence of an event of magnitude greater than 6.5. Taiwan's EEW system works on the P-wave method.

(Wu and Zhao 2006b; Wu and Kanamori 2008b; Hsiao et al. 2009b, a).

Along with the conventional strong motion instrumentation of the Central weather bureau, Taiwan has also installed a very dense network of low-cost MEMS-based sensors. These sensors are capable of sending three-axis acceleration to the remote server using TCP/IP and simultaneously can act as a standalone on-site earthquake early warning system. For onsite warnings, the system uses P_a approach for issuing earthquake warnings. (Rydelek et al. 2007)(Wu et al. 2013; Chen et al. 2015b)

2.2.7 PreSEIS

PreSEIS uses three two-layer feed-forward (TLFF) Artificial Neural Network (ANN) and each network is used for a specific purpose. First TLFF uses the time differences (time difference in P-onset at the first station to the P-onset on the remaining stations in the seismic instruments network) to estimate the hypocentre location, second TLFF uses the hypocentre location and CAV of each sensor to estimate the Magnitude of an impending earthquake and, third TLFF uses the hypocentre location, CAV and Magnitude to estimate the rupture starting and ending location to know the about the rupture.

Training of TLFF is done using some earthquake time histories whose hypocentre location, magnitude and rupture information is known to us. The main purpose of training this network is to set the weight parameters, and this is done by the backpropagation approach. (Böse et al. 2009, 2012).

For warning purposes, the new parameter (ground motion parameter IM) is calculated at each timestamp using the source parameters and site conditions and can be expressed as:

$$\widehat{IM}(\lambda, \theta) = f(\widehat{M}^n, \hat{d}_{rup}^n, site)$$

Where (λ, θ) is the location of the site of interest for which warning needs to be issued, \widehat{M}^n is the estimated magnitude obtained from TLFF, \hat{d}_{rup}^n is the distance between rupture and site of interest at each timestamp and, *site* represents site characteristic of area of interest.

Warning of an impending earthquake will be issued if $\widehat{IM}(\lambda, \theta) \geq IM_{thres}$

2.2.8 Early Warning System in Fujian China

China started the development of the EEW system for the Fujian district in 2009, Fujian which is one of the most important districts in China, is highly vulnerable to earthquakes originating from Taiwan and from the Fujian region itself. Testing has shown that for inland events, almost 6.4 ± 0.97 seconds from the triggering of the first station, whereas for offshore earthquakes, the first alarms were generated almost 13.7 ± 2.9 seconds after the first trigger.

The epicenter is estimated by solving the travel time equation once three of four stations are triggered, and magnitude is estimated by using P_d method. (Zhang et al. 2016)

2.2.9 Presto

PRESTo or PRobabilistic and Evolutionary early warning system is a software system under development and testing in southern Italy. As the name, “Evolutionary” suggest PRESTo uses the most modern algorithm for the development of EEW system, apart from estimating EEW parameter it also keeps on updating them as and when more records are available. Also,

“Probabilistic” suggests that calculations are based on probabilistic earthquake detection and the Bayesian approach. (Satriano et al. 2011; Cauzzi et al. 2016)

The main functionality of PRESTo is dependent upon the following main modules:

- Strong motion data processing and acquisition.
- Detection of event or P phase arrival.
- Determination of Location of the earthquake.
- Estimation of magnitude.
- Prediction of peak ground motion at the target location.

The software is mostly written using C++ language and can be installed on various operating systems from Windows to Linux as well as mac. For the acquisition of data, the seed link format is used.

For estimation of magnitude RTMag technique by Lancieri and Zollo has been implemented. It makes a correlation between P and S phase peak displacements, measured for the first few seconds of the low passed filtered signal. The relationship used is as follows:

$$\log Pd = A + BM + C \log\left(\frac{R}{10}\right)$$

Where,

P_d is peak ground displacement for predefined window length after P phase arrival, two to four seconds window length is generally adopted.

R is hypocentre distance, A, B, and C are regression coefficients

2.3 Suitability of low-cost sensor for EEW and Strong motion studies

Since last decade seismologist has started using low-cost MEMS sensor as an add-on the existing traditional force balance accelerometers, especially in case of creation of a dense network for EEW. (Tu et al. 2013; Alessandro et al. 2014; Chen et al. 2015b; Peng et al. 2019). These low-cost sensors do come at the cost of performance in terms of dynamic range and signal to noise ratio, recording correct ground motion or large frequency range, and choice of such sensors is largely a function of research/technical requirement and availability of funds. However, for a large number of applications that vary from recording maximum amplitudes to strong motion studies, such cost-effective MEMS are quite suitable as most of these applications do not need very high-performing sensors(Anthony et al. 2019), which means that for most of the daily life engineering applications, low-cost sensors can be deployed without much hampering the quality of expected engineering outcome.

In their study (Tu et al. 2013) have categorically found that for strong motion data having frequency more than 0.5 Hz, the velocity-time history, as well as displacement time history, could be extracted from low-cost MEMS without any error.

(Picozzi et al. 2011) have also found in their study that there is no difference in response spectra calculated from data recorded between Guralp sensor and low-cost MEMS as long as the frequency is greater than .5 Hz.

The C class sensor does have suitability and could help in creating SHAKEMAP moreover, few of the sensors do have the potential to be deployed into ANSS network of A and B class sensors for densifying the network (Evans et al. 2014).

2.3.1 OSOP Raspberry Shake 4D

OSOP Raspberry Shake 4D consists of a three-component accelerometer, one channel 4.5 Hz geophone having a vertical component, 24-bit digitizer and real-time data transmission in mini-seed format. It also incorporates a network timing protocol for accurate timing as well as support external GPS, which need to be installed separately.

(Anthony et al. 2019) in their study found that for an earthquake having a magnitude in the range of M_L between 2 - 4 and epicentral distance varying from 20 to 100 Kilometres, Raspberry shake will require events magnitude or order .3 higher than as compared to the broadband sensor for reliable calculation of event magnitude.

One of the most important drawbacks of MEMS-based low-cost sensors is the low signal-to-noise ratio (SNR). However, the study has suggested that for small events, there is overestimating of the magnitude; however, for large events having magnitude M_L greater than 3 and epicentral distance less than 100 Kilometres, the records were extracted with high precision. It was also concluded that the accuracy provided by Raspberry is well with the requirement of EEW purpose, and this sensor is quite suitable for densifying the EEW strong motion sensor network.

2.3.2 LIS331DLH (iPhone) Accelerometer

LIS331DLH is a low-cost three-axis MEMS-based accelerometer that can output data with 16-bit accuracy. It has a user-selectable range varying from $\pm 2g$ to $\pm 8g$ with a frequency range of .1 Hz to 1 kHz. (D'Alessandro and D'Anna 2013) Performed test for LIS331DLH by comparing it with the EpiSensor FBA ES-T sensor using a vibration table arrangement. A constant and damped sign wave with a frequency from 0.2-20 Hz was created to perform the test. The amplitude between 10 to 2000 mg was analyzed for all frequencies in the range.

In the study, it was concluded that for the frequency range which is of most importance for earthquake engineering LIS331DLH has shown accurate and excellent phase and frequency response. It was also found that LIS331DLH records slightly less amplitude of acceleration. It was also found that because of low SNR these sensors are most suitable to be used for strong motion studies for large magnitude events as compared to microseismic events. However, a greater advantage of this sensor is its relatively smaller size, minimal power requirement, and no maintenance once installed. All these make the most suitable to be used in smartphones and smart devices. They can also be used for densifying EEW networks.

2.3.3 Quake-Catcher Network

Quake-Catcher is one of its kind sensor network, in which detection and recording seismic event is performed by involving the general public. It used various sensors installed in smartphones, laptops, and other connected devices of the normal public to record and collect earthquake data. QCN has more than 1400 volunteers who share data from their phones, laptops, and computers. The whole system is developed using the Berkeley Open Infrastructure for Network Computing (BOINC) software for volunteer computing. Most of these sensors can have linear amplitude and phase response for a wide range of frequencies varying from flat to 250 Hz. (Benson et al. 2013; Portnoi et al. 2014; Evans et al. 2014)

(Lawrence et al. 2014) Performed feasibility of using community-based sensor network and tested QCN for recording earthquakes. The study observed that QCN can determine magnitude with error in the range of 1 magnitude and can report an earthquake as early as 9.1 seconds from the start of rupture. These sensors are monitored continuously in the remote private mobiles or laptops and sent the triggered event to the remote central server. The MEMS sensors that have been used by the QCN network have improved greatly with time since the network became operational in 2007. The noise level of the MEMS sensor has decreased from $4 \times 10^{-2} \text{ m/s}^2$ in 2008 to $2 \times 10^{-3} \text{ m/s}^2$ in 2010, and less than $6 \times 10^{-4} \text{ m/s}^2$ for the sensors.

The ease with which these sensors can be installed makes it ideal for recording aftershocks after a great event as a large number of sensors can be deployed within few days to cover a large area and record a large amount of strong-motion data. Like for an M 7.2 earthquake that occurred in Darfield, New Zealand, located just northwest of the urban centre of Christchurch, it was decided to densify the network to record as much as data from the future aftershocks. After 11 days of the main event, 180 QCN sensors were installed in homes and offices in and around Christchurch city. The success of such type of network and the deployment of low-cost sensors will have a

huge impact in the future of the real-time seismic network, especially strong-motion seismology (Cochran et al. 2009; Lawrence et al. 2014; D'Alessandro et al. 2019).

2.3.4 Urban Seismic Network (USN)

USN or Urban Seismic Network has been installed as a community-based network for seismic monitoring as a pilot study in the Acireale municipality area, Sicily, Italy. This region falls under one of the most seismically active regions in the world (Azzaro et al. 2013). MEMS selected for this study is 1044_0 (3/3/3 Phidget Spatial Precision High Resolution) produced by the Canadian company Phidget Inc. This device has a three-axis accelerometer along with a gyroscope and a magnetometer. The MEMS has a resolution in the range of $\pm 2g$ and a dynamic range in the order of 44dB. The system has a linear response from 0 to 497 Hz. There are roughly 200 plus devices connected to the central server and transmitted data through TCP/IP protocol.

The PSD curve was drawn for the self-noise of the sensor obtained for the sensor by acquiring a 72 hour of the signal at a site having low seismic noise. The PSD curve shows that the noise level of the sensor is a bit higher than the desired values as suggested by Peterson (Jon 1993); however, it is well within the limits required for the pilot project (Alessandro et al. 2014).

2.3.5 GL-P2B –MEMS for earthquake early warning

GL-P2B is a three-axis accelerometer that has an inbuilt seismic processing module; it can calculate EEW parameters and can transmit the information to a remote server with little latency. For the automatic pick of P phase, STA/LTA algorithm for Allen (Allen 1978) has been implemented. The whole package consists of three uniaxial MEMS, three digitizers and microcontrollers and other peripheral devices required for data processing and storage.

The amplitude-frequency response of the sensor shows that it has a flat response from 0 to 80 Hz, which is quite in agreement with A-class sensors. The laboratory test has shown that these sensors have a dynamic range of the order 97-99 dB. The performance of this sensor has been found better than sensors traditional strong-motion accelerometers like Namometrics Titan, RefTek RT- 147-01/3, Guralp CMG-5TC, and can be compared with EpiSensor 2. The test results claim that it would be suitable to call it a B class sensor and not a C class sensor. As of 2016, ten numbers of these sensors have been installed in Liangshan Yi Autonomous Prefecture, Sichuan, China. The data is transmitted using mobile internet with 4g connectivity. (Peng et al. 2017, 2019)

2.3.6 Palert

Palert sensor, which is developed by San Lien Corporation Taiwan, has been used to create a high-density sensor network EEW in Taiwan. Palert seismic network, also known as PSN is being tested in Taiwan since 2010 and has more than 700 sensors. The PSN is integrated with Taiwan's Central Weather Bureau seismic network (CWB-SN), which is used both for monitoring earthquakes and EEW in Taiwan. This integration of the traditional seismic network with low-cost MEMS sensors is the first of its kind in the world, and it has demonstrated the suitability of low-cost sensors for EEW systems. The studies suggested that Palert is capable of providing good quality data for EEW purposes, earthquake engineering, structure health monitoring as well as performing an on-site EEW warning system (Wu et al. 2013; Hsieh et al. 2014; Chen et al. 2015b; Wu 2015).

Palert can record ground motion data with a sampling frequency of 100Hz; this data is digitized with the 16-bit digitizer, with a resolution of $\pm 2g$. For accuracy and time stamping of data, a network timing protocol (NTP) is available, which can update time from any self-configured server or internet. Palert can send data to 2 servers (3 in case of the latest Palert plus) simultaneously, data in the form of TCP/IP packet of one-second duration. Each packet is comprised of 100 samples of three-axis acceleration time data as well as parameters computed locally by Palert. Palert can also act as an on-site warning system once it is connected with a siren or warning assembly. The warning threshold for PGA, P_d and/or intensity can be selected using the software.

Despite having a relatively low signal-to-noise ratio it has been found that data from Palert is suitable for P phase picking, location of the earthquake, and estimating the subsequent magnitude of the earthquake. Integrating PSN network with CBW-SN has not only densified the existing CWB network it has also helped in the generation of PGA map with greater and more accurate details. (Wu et al. 2013, 2019).



Chapter 3 EEW System for Northern India

As a first step towards establishing EEW System for Northern India, a network comprising of 84 accelerometers has been installed in Central Himalayas (Uttarakhand) to provide earthquake early warning (Chamoli et al. 2019). This system was installed by the funding provided by the Ministry of Earth Sciences (MoES), Government of India, and is currently being operated by funds provided by the Disaster Mitigation and Management Center (DMMC), Government of Uttarakhand, India. The objective of the project granted by MoES was to test the feasibility and establish a prototype EEW system for Northern India, which was successfully concluded in March 2017. With the successful completion of the first phase of installation, another 85 accelerographs were installed in the Kumaon region of Uttarakhand. This extended network was funded by the Government of Uttarakhand. This system, which is the first EEW system in India, is capable of giving warning of about 76 seconds (Bhardwaj, 2014) to Delhi in the event of an earthquake having a magnitude greater than six and having an epicenter in the instrumented region. Similarly, other important cities such as Dehradun, Haridwar, Roorkee, Muzaffarnagar, and Meerut lead time estimated by Bhardwaj, 2014 were 20, 22, 31, 44, 57 seconds, respectively.

3.1. Region for EEW sensor network

For the initial phase of installation, a region in the central Himalayas which lies between Yamunotri in East (31.0140° N, 78.4600° E.) and Badrinath in the west (30.7433° N, 79.4938° E) was selected. This region was selected because of the following two main reasons:

- Primarily this region has been identified as one of the seismically most active regions in the central Himalayas.
- Secondly, the scope of the project was to establish feasibility to issue warnings to cities falling in western Uttar Pradesh and NCR, which would be most affected by an earthquake having epicentre in the selected region.

During the last 25 years, this region has seen two strong earthquakes, viz—Uttarkashi earthquake of 1991 (Magnitude 6.8) and Chamoli earthquake of 1999 (Magnitude 6.5). The selection of a region for the installation of sensors for the EEW network was done after considering the suggestions of many eminent scientists. Most of them have identified this region as a seismic gap where a large magnitude earthquake (Magnitude greater than 7) can occur. The studies have shown that a large earthquake with a magnitude greater than 7 in Central Himalayas could generate significant ground shaking up to the National capital region Delhi (Singh 2002; Iyengar and Ghosh 2004; Mittal et al. 2012, 2013c, b), which is situated at a distance of nearly 200 km

from Main Boundary Thrust (MBT) and 300 km from Main Central Thrust (MCT). The MCT and MBT are the two most active thrust planes of the Himalayas. The study conducted by (Mittal et al. 2013a) has also estimated that for Magnitude 8.0 and 8.5 earthquakes from the Himalayas, the response spectrum of the postulated time history will exceed the design response spectrum for the zone IV at several frequencies on all soft soil sites for Delhi. Most of the thickly populated cities and industrial hubs in and around NCR have been mapped in zone IV as per seismic zoning map of India provided in IS 1893:2002. Thus a major earthquake in the central Himalayas could prove to be disastrous for NCR and adjoining cities. In the later stages of the research, the region was further extended up to Dharchula so that the Uttarakhand-Dharchula seismic gap (Srivastava et al.; Tandon and Srivastava 1954, 1974) can be exhaustively covered.

Characterized by its thickly populated cities, large population, and by virtue of its proximity with the Himalayas, western UP and Delhi are some of the most vulnerable regions in India for disasters related to earthquakes originating in the Himalayas. It is because of this reason, it was decided that the first-ever EEW network in India must be installed in Kumaun-Garhwal Himalayas so that warning could be given to the whole of Western UP and the national capital region (NCR). Kumaun and Garhwal Himalayas are part of the central Himalayas and lie in the state of Uttarakhand. This region is surrounded by the international boundaries of Tibet (China) in the northeast and Nepal in the east. This region consists of all four Litho-tectonic subdivisions of the Himalayas (Valdiya 1980), viz. Tethys Himalayas, Higher Himalaya, Lesser Himalayas and sub-Himalayas (Shivalik). These subdivisions are further separated from each other by North dipping intra crustal boundary thrust. Shivalik which is comprised of Cenozoic sediments is youngest of all and lie at the southern end, and it reached a maximum height of 1200 meter. South of Shivalik is marked by Himalayan Frontal Thrust and north boundary is delimited by Main Boundary thrust (MBT). The region between South of Greater Himalayas and north of Shivalik is known as the Lesser Himalayas. This region has its boundaries marked by MBT in south and Main Central Thrust in north, and is comprised of mostly Meso and Neo-proterozoic period rocks. The region between MCT and south of the Tethys Himalayas is called Greater Himalayas or Himadri.

3.2. Target location

The target cities in which warning is planned to be issued lie in Western Uttar Pradesh and the national capital region of Delhi, which are approximately at a distance of 100 to 300 km from the instrumented region. Geologically this region mostly comprises of Indo-Gangetic plains. The Possibility and relevance of getting full advantage of the EEW system in India are better in terms of possible lead time, in comparison to most of the areas in the world. This is due to the fact that,

for Northern India, potential sources of large earthquakes are located in the Himalayas, whereas the centers of large population and major industrial hubs (including the capital city of Delhi) are in the plains adjoining the Himalayas, which are at least 150 km away from the expected potential source. As mentioned earlier, thick population density and poor adherence to earthquake-resistant practices have substantially increased the seismic vulnerability of this region (BMTPC, 2008). However, in the case of a large earthquake in the Himalayas, most of these places, between the central Himalayas and Delhi, can have a lead time varying from 30 to 70 seconds before the damaging S-waves arrive. If this real-time seismological information is adequately tuned to the operational requirements of technical systems, life and industrial loss could be significantly reduced.

3.2.1. Plains adjoining Kumaun – Garhwal Himalayas

Morpho-stratigraphically speaking, the Indo-Gangetic plains are comprised of two units which are Bangar, an older upland, which is mostly free from floods, and Khadar, a comparatively younger lowland, which has a high vulnerability for floods. Based upon sediment characteristics and gradient Bangar is further divided into two divisions which are the Piedmont zone or bhabhar and the Varanasi plain. Bhabhar is upland adjoining shivalik and is mostly consisting of coarse clastic sediments of upper Pleistocene age to middle age and also consist of alluvial and colluvial. Most of the seasonal rivers from shivalik moves under the bhabhar and disappear, however, they again emerge at the end of bhabhar zone, in Varanasi plains, and result into formation of swampy region, which is known as tarai region. As compared to Varanasi plain bhabhar zone has a greater gradient and varies from 10m/km to .4m/km from North to south and its boundary is demarked by HFT. Important cities in which warning is to be issued in this zone are: Vikasnagar, Dehradun, Haridwar, Rishikesh, Kotdwar, Haldwani, Khatima, Tanakpur, Roorkee, Laksar, Kashipur, and Udham Singh Nagar.

3.2.2. Western UP and Eastern Haryana

This region is thickly populated and is bounded mostly by Yamuna and Ganga rivers, and sometimes it is also referred as Doab region. Most of this region is characterized by deep alluvial deposits, thus making it highly vulnerable to seismic hazards. The Varanasi plains have a mostly negligible gradient. This region is demarked by a great boundary fault in the southeast and Mahendragarh-Dehradun fault in the northwest. Several other small faults like the great boundary fault, Moradabad fault several other smaller faults and lineaments also characterize this region.

The Ganga basin is one of the most prominent sedimentary basins of India, which forms the northern province of India, and is mostly covered with quaternary alluvial deposits.

3.2.3. National capital region, Delhi

Delhi, the national capital of India, is highly vulnerable to seismic-induced hazards not only because of its proximity to highly active Himalayas but also due to complex nearby tectonics and local site effects. This highly and thickly populated capital territory of India lies in zone IV as per Bureau of Indian standard, 2002, and thus is most crucial in terms of the target location for issuing earthquake warnings.

Many studies have concluded that a major or great earthquake in the Himalayas could have a huge impact on Delhi and surrounding regions. In a study performed by Singh *et al.* (Singh 2002), a scenario for two earthquakes with magnitude 8 and 8.5 in the Himalayas was created; it was concluded that for such events in the Himalayas with distance more than 300 km, Delhi could experience peak ground acceleration of order 96 to 140 gals for rocks sites and 174 to 218 gals for soft soils sites (Bansal *et al.* 2009; Mittal *et al.* 2013a).

Several studies (Agrawal & Chawla, 2006; Bhatia *et al.*, 1999 under the GSHAP program and Parvez *et al.*, 2003; Joshi & Sharma, 2011) suggest that high peak ground acceleration (PGA) of the order of more than 200 gals can be expected in Delhi from a major earthquake in the Central Himalayas. Also, the Indian code of practice for seismic design, IS 1893:2002 (Bureau of Indian Standards, 2002), puts Delhi in seismic zone IV, which suggests a PGA of 240 gals for a maximum credible earthquake.

(Ghosh and Pal 2017) have also discussed the liquefaction hazard in NCR in case of an event.

3.3. Selection of Site for Sensor and Type of Network

The region selected for instrumentation, shown in Figure 3.1, is sparsely populated, and a large part of the area is difficult to be accessed, due to dense forests and extreme weather conditions; hence different kinds of connectivity options were explored.

The most promising option explored was the use of VSAT for connectivity. The advantage of VSAT is that it can be installed at any location of choice and thus enabling to create a network of desired grid size. However latter this option was rejected because it was found that even for a small displacement of few millimeters VSAT could lose its connectivity with satellite and thus making it work all the time perfectly but not when needed, that is right during a seismic event. Thus, VSAT was rejected. Depending upon the availability of connectivity at different sites, it was decided to use two different types of network circuits.

The alternative was to make use of very good mobile connectivity and 4G networks. The region has suitable connectivity with both 3G and 4G enabled mobile networks. This type of network is the most economical and should suit the purpose of the EEW system. However, the kind of algorithm decided for EEW development, a seamless network that can provide a continuous data stream without delay or missing data, is required. In the initial phase of testing, it was found that though the connectivity was good in terms of online streaming of video and all, but there were huge data drops in real-time in terms of seamless, strong motion data streams. This implies that there would be chunks of data, either missing altogether or arriving with network-generated latency, which is not in sync with other sensors. This could break the continuity in data, which in turn will lead to errors in pick and other calculations, as the determining location of earthquake largely depends upon the time stamp of the real-time strong-motion time history. So, the use of mobile connectivity was also rejected.



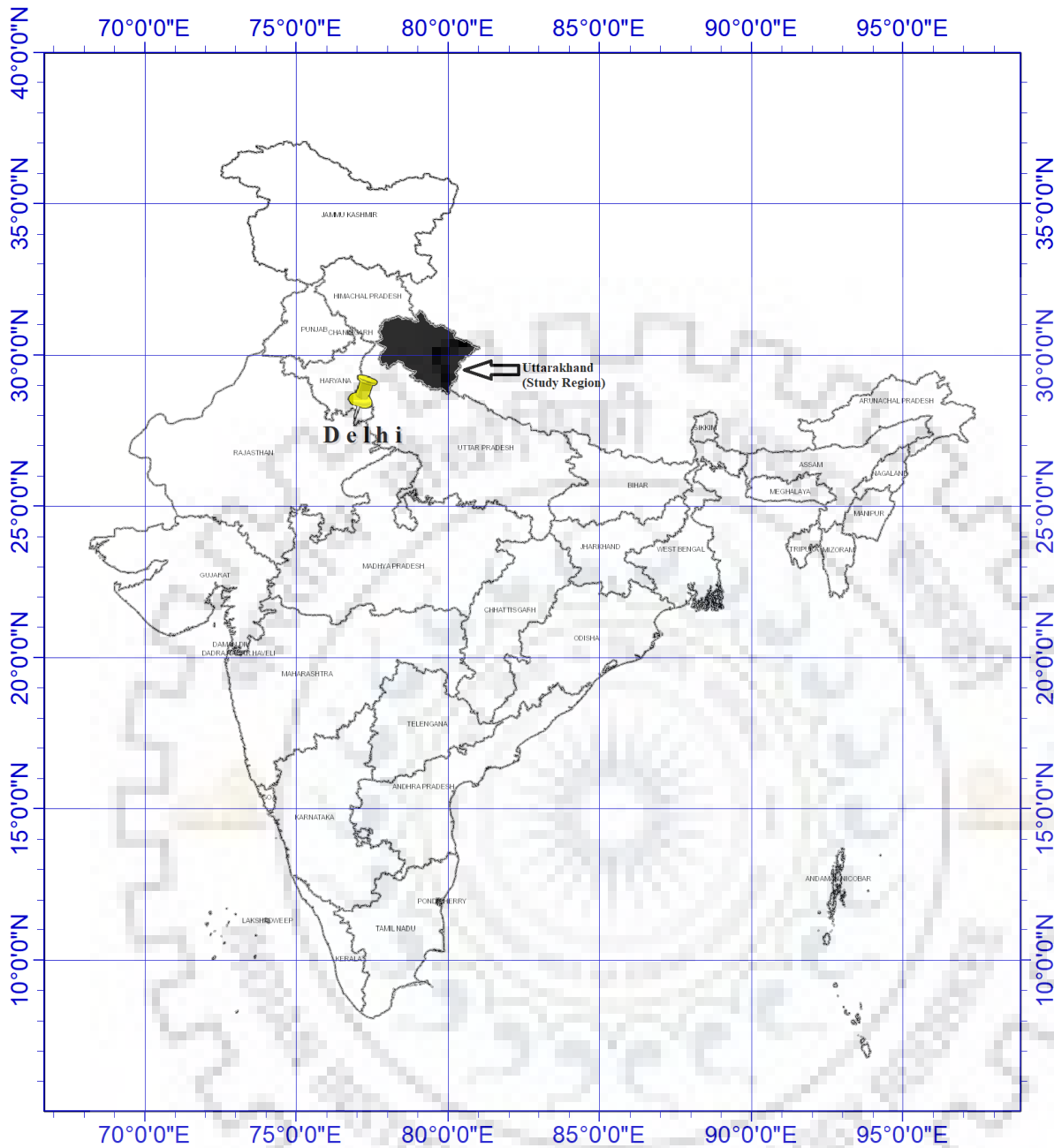


Figure 3.1: Selected region for instrumentation as well as the most crucial target location for issuing warning, the national capital New Delhi
 Thus, finally, a decision was taken to stick to the most traditional copper and optical fiber network. Depending upon the availability of connectivity at different sites, it was decided to use two different types of network circuits.

As discussed, two modes of connectivity had been used for the development of the network of accelerographs in Uttarakhand. These two modes are State Wide Area Network (SWAN) and Virtual Private Network over Broadband (VPN_oBB) through the network of Bharat Sanchar Nigam Limited (BSNL). SWAN is developed under the National e-governance plan of the Government of India. It is one of the core infrastructure components whose purpose is to create a dedicated Closed User Group (CUG) network in order to provide secured high-speed

connectivity for government functioning and provide interconnectivity to State Headquarters, District Headquarters, Block Headquarters. Bharat Sanchar Nigam Limited (BSNL) is an Indian state-owned telecommunications company headquartered in New Delhi, Delhi, India. It provides mobile voice and internet services through its nationwide telecommunications network across India. For the installation of sensors, Base Transceiver Station (BTS) of BSNL were used, and they have been connected to the central server using the VPNoBB circuit.

In the first phase, overall, 84 sensors were installed in the Garhwal region of Uttarakhand. While in the second phase, 85 sensors were installed in the Kumaon region of Uttarakhand (Figure 3.2). Twenty-seven sensors from the Garhwal region and forty-two sensors from the Kumaon region are installed in the SWAN facility (Table 3.1 and 3.2) available in different district administrative offices across the state.

Similarly, 58 sensors in the Garhwal region and 43 sensors in the Kumaon region of Uttarakhand are installed at the BTS of BSNL and connected through Virtual Private Network over Broadband (VPNoBB) with the central server (Table 3.3 and 3.4).

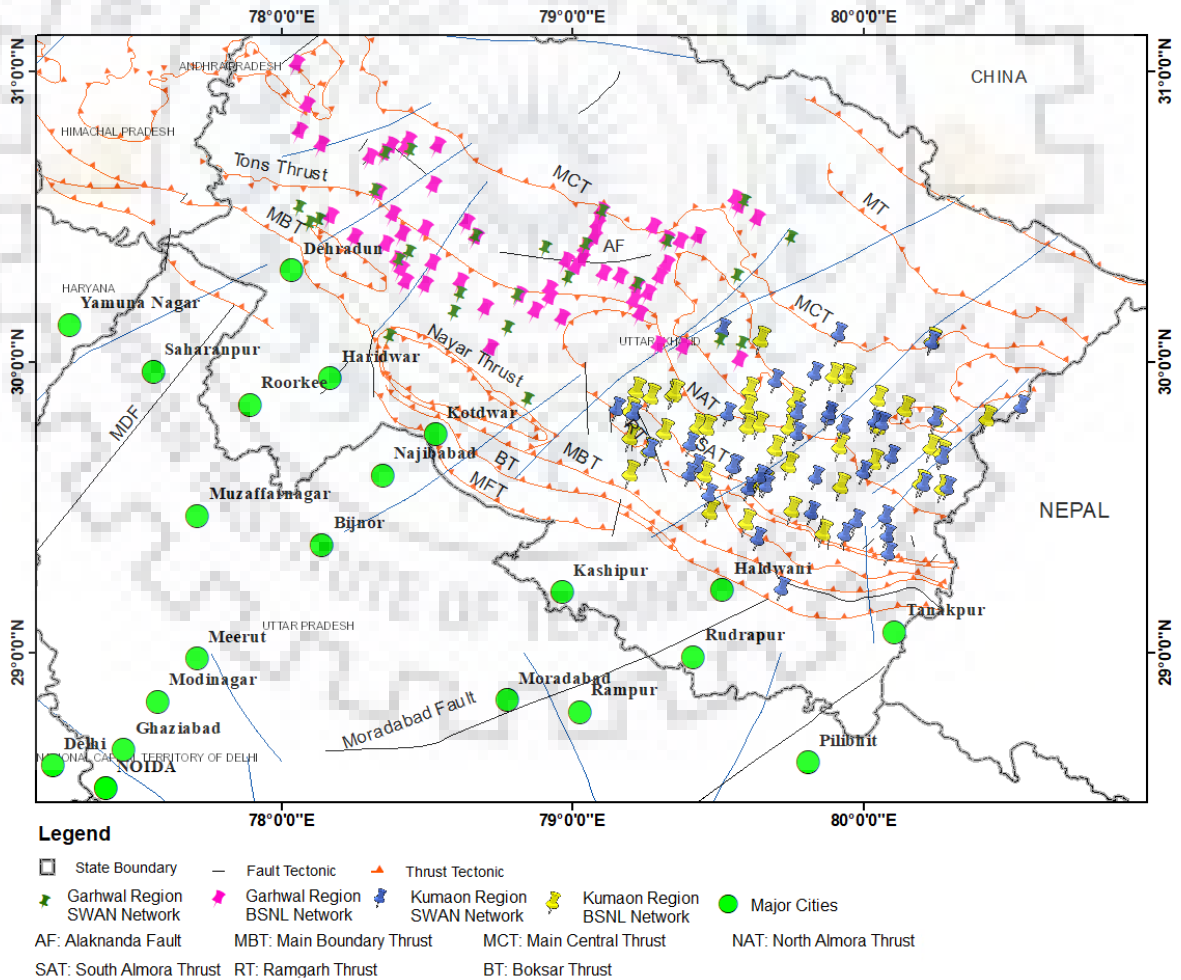
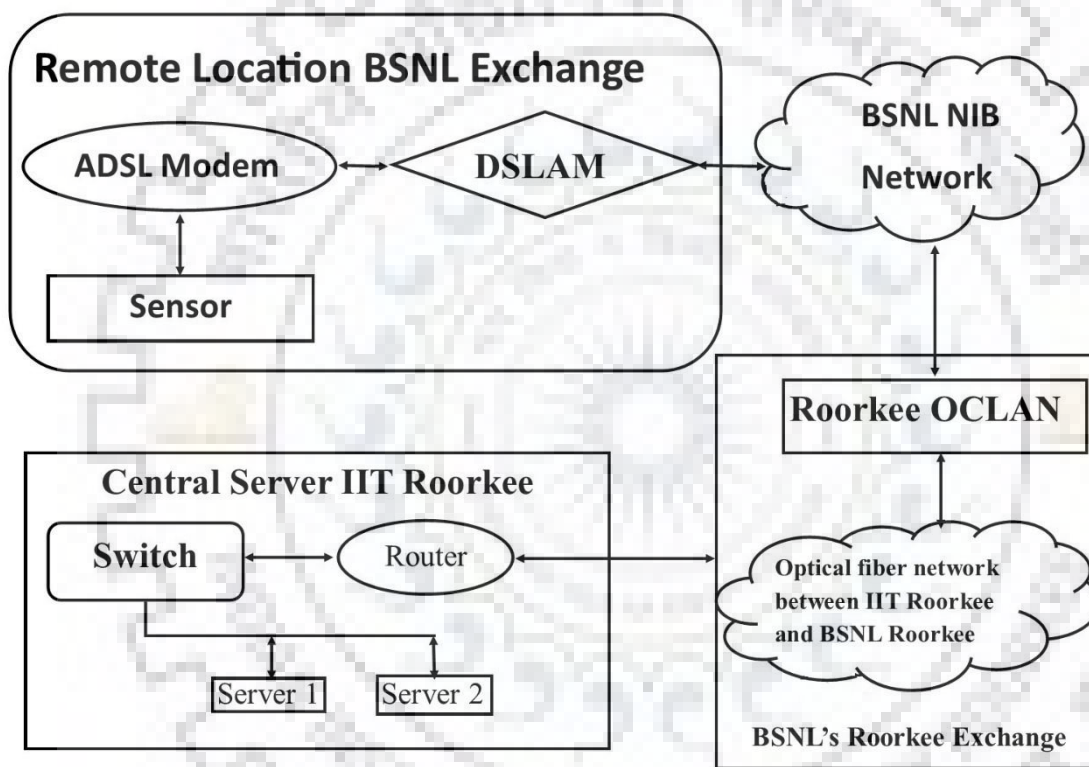


Figure 3.2: The figure shows in the sensor network created for the EEW for Uttarakhand, India.

To complete the connectivity with the central server at IIT Roorkee, 2 different circuits of Multi-Protocol Label Switching (MPLS) Virtual Private Network (VPN) of 2 Mbps have been installed connecting IIT Roorkee to Dehradun, and another for redundancy has been used for connecting IIT Roorkee to Haridwar. One major concern is latency in the transmission, and it was found during real-time analysis that BSNL VPNBB and SWAN both have negligible latency. We have verified several times and found that the delay in transmission was never more than 500 milliseconds. Hence, we can safely assume that the system has a latency of not more than 1.5 seconds. The basic schematic diagram of network connectivity is shown in Figure 3.3.



ADSL : Asymmetric digital subscriber line
 DSLAM : Digital Subscriber Line Access Multiplexer
 BSNL : Bharat Sanchar Nigam Limited
 NIB : National Internet Backbone

Figure 3.3: THE BASIC CONNECTIVITY DIAGRAM FOR VPNOBB (VIRTUAL PRIVATE NETWORK OVER BROADBAND) CIRCUIT FOR EEW NETWORK. (SOURCE BSNL)

Table 3.1: EEW stations in Garhwal Region of Uttarakhand installed at SWAN facility

S. No.	Station Code	Name	LATITUDE (°N)	LONGITUDE (°E)
1	AGMS	Augustmuni	30.38921	79.022160
2	BHLS	Bhilangana	30.387466	78.793618
3	BKTS	Barkot	30.80851	78.20489
4	CHMS	Chamoli	30.40565	79.331700
5	CLSS	Chinyalisour	30.57477	78.33123
6	CMBS	Chamba	30.345603	78.394577
7	DNDS	Dunda	30.70922	78.34746
8	DVLS	Deval	30.05533	79.58159
9	DVPS	Devprayag	30.14488	78.604650
10	GHTS	Ghat	30.26062	79.44861
11	GOPS	Gopeshwar	30.41200	79.320500
12	HDKS	Hindolakhali	30.23185	78.60634
13	JKLS	Jakholi	30.38939	78.89825
14	JSMS	Joshimath	30.55581	79.558640
15	KOTS	Kot	30.14903	78.69557
16	KRPS	Karanprayag	30.25628	79.217060
17	NGNS	Naugaon	30.79321	78.1488
18	PKRS	Pokhri	30.34236	79.19962
19	PORS	Pauri	30.15005	78.776440
20	PRLS	Purola	30.87922	78.08595
21	PTNS	Pratapnagar	30.516371	78.492953
22	RDPS	Rudraprayag	30.30644	79.002720
23	SRNS	Srinagar	30.21578	78.769540
24	TEHS	Tehri	30.37549	78.42968
25	TRLS	Tharali	30.06428	79.51466
26	UKMS	Ukhimath	30.51326	79.0948
27	UTKS	Uttarkashi	30.73039	78.44449

Table 3.2: EEW stations in Kumaon Region of Uttarakhand installed at SWAN facility.

S. No.	Station Code	Name	LATITUDE (°N)	LONGITUDE (°E)
1	ALMS	Almora (DHQ)	29.59648	79.65726
2	BGSS	Bageshwer (DHQ)	29.82619	79.77247
3	BHKS	Bhikiyasen (BHQ)	29.6976	79.26638
4	BMTS	Bhimtal	29.56361111	79.60388889

5	BNLS	Bhanoli(THQ)	29.60229	79.83613
6	BRKS	Barakot	29.47002	80.07773
7	BRNS	Berinag (BHQ)	29.79669	80.04061
8	BTLS	Betalghat (THQ)	29.71805556	79.40611111
9	CHKS	Chaukhutia (BHQ)	30.10944444	79.51583333
10	CHPS	Champawat (DHQ)	29.34248	80.08773
11	DCLS	Dharchula (THQ)	29.84837	80.54541
12	DHLS	Dhauladevi (BHQ)	29.78777778	80.06416667
13	DHTS	Dwarahat (BHQ)	29.82277778	79.5325
14	DIDS	Didihat (THQ)	29.80297	80.24859
15	DLCS	Dhaulachina (THQ)	29.78027778	79.93222222
16	DRIS	Dhari (THQ)	29.3918	79.63657
17	GNGS	Gangolihat (BHQ)	29.67649	80.09852
18	GRRS	Garur (BHQ)	29.93527778	79.6975
19	HLDS	Haldwani (THQ)	29.22111111	79.71972222
20	HWBS	Hawal Bagh	29.80583333	79.87861111
21	JNTS	Jainti(BHQ)	29.48255	79.8242
22	KFLS	Kafligair (THQ)	29.75358	79.77444
23	KKLS	Kosia Katoli (THQ)	29.57555556	79.66527778
24	KNDS	Kanda (THQ)	29.82684	79.88181
25	KNLS	Kanalichina (BHQ)	29.6713	80.27096
26	KPKS	Kapkot (BHQ)	30.09694444	79.915
27	KTBS	Kotabagh (BHQ)	29.64305556	79.55944444
28	LGHS	Lohaghat (BHQ)	29.40406	80.08475
29	LMGS	Lamgara	29.62111111	80.00138889
30	MNKS	Munakot (BHQ)	29.56653	80.28912
31	MNSS	Munsiari	30.0663	80.2373
32	NTLS	Nainital (DHQ)	29.54416667	79.47
33	OKKS	Okhal Kanda (BHQ)	29.45416667	79.97527778
34	PTIS	Pati	29.4068	79.93801
35	PTRS	Pithoragarh (DEOC)	29.57876	80.20777
36	RMGS	Ramgarh (BHQ)	29.63916667	79.55018611
37	RNKS	Ranikhet (THQ)	29.64354	79.428
38	SLTS	Sult (BHQ)	29.83833333	79.15166667
39	SMSS	Someshwer (THQ)	29.96222222	79.83194444
40	SYLS	Syaldey (BHQ)	29.82009	79.20989
41	TRKS	Tarikhhet (BHQ)	29.61308	79.40224
42	VKBS	Vikas Bhawan (BHQ)	29.60679	79.64514

Table 3.3: EEW stations in Garhwal Region of Uttarakhand installed at BSNL base transceiver station.

S. No.	Station Code	Name	LATITUDE (°N)	LONGITUDE (°E)
1	ADIB	Adibadri	30.15881	79.22606
2	AGMB	Augustmuni	30.39938	79.037240
3	AULB	Auli	30.59547	79.569210
4	BHIB	Bhiri	30.46723	79.07929
5	BMKB	Bharamkhal	30.69592	78.30321
6	CDPB	Chandrapuri	30.42578	79.068910
7	CHHB	Chhaam	30.50235	78.37616667
8	CMBB	Chamba	30.34683333	78.39213333
9	CMLB	Chamiyala	30.47476667	78.632298
10	CNKB	Chhinka	30.41173	79.36522
11	CYSB	Chinyalisour	30.57867	78.32616
12	DLTB	Dhanaulti	30.4233504	78.24725
13	DNTB	Dhauntri	30.60465	78.5166
14	DUNB	Dunda	30.71356	78.34896
15	GAZB	Gaza	30.27053333	78.42193333
16	GCRB	Gaucher	30.28836	79.158520
17	GDRB	Ghurdauri	30.18274	78.69388
18	GLMB	Gwaldom	30.00471	79.57015
19	GLTB	Gholteer	30.30016	79.10103
20	GNSB	Ghansali	30.4259333	78.664598
21	GOPB	Gopeshwar	30.41617	79.321400
22	GRSB	Gairsain	30.05466	79.28992
23	GYNB	Gyanshu	30.73206	78.42115
24	JKDB	Jhaknidhar	30.33567	78.51143
25	JMKB	Jamnikhhal	30.27085	78.60953
26	JMTB	Joshimath	30.55751	79.555930
27	KDLB	Kandikhhal	30.4353	78.408768
28	KNKB	Khankra	30.24518	78.91754
29	KNPB	Karanprayag	30.26104	79.215190
30	KNTB	Kanatal	30.4015	78.35225
31	KRKB	Kherakhhal	30.21816	78.915790
32	KRSB	Khirsu	30.17131	78.867840
33	KSTB	Kanskhet	30.04343	78.71263

34	KTSB	Koteshwar	30.2609	78.4898
35	LNGB	Langasu	30.29052	79.277100
36	MDLB	Mandal	30.46039	79.27483
37	MHDB	Mahidanda	30.75653	78.42993
38	MNRB	Maneri	30.74035	78.52931
39	MORB	Mori	31.01936	78.04545
40	MTLB	Matli	30.73962	78.37076
41	NGNB	Naugaon	30.78865	78.1389
42	NNPB	Nandprayag	30.33191	79.319870
43	NRBB	Narainbagar	30.14576	79.37637
44	NTYB	Nauti	30.20576	79.207070
45	PLKB	Pipalkoti	30.42883	79.427500
46	PRLB	Purola	30.8787	78.0819
47	PTHB	Paithani	30.14855	78.9854
48	PTNB	Pratap Nagar	30.4535	78.4872
49	RCRB	Ranichauri	30.3143	78.407868
50	SKTB	Srikot	30.22297	78.813350
51	SMLB	Simli	30.23256	79.255440
52	STKB	Saterakhal	30.31956	79.00459
53	THTB	Thatyur	30.4953	78.16403
54	TLWB	Tilwara	30.34307	78.974780
55	UKMB	Ukhimath	30.51229	79.09376

Table 3.4: EEW stations in Kumaon Region of Uttarakhand installed at BSNL BASE TRANSCIEVER STATION.

S. No.	Station Code	Name	LATITUDE (°N)	LONGITUDE (°E)
1	ARTB	Artola	29.87222	80.05361
2	BGSB	Bageshwar	29.84036	79.76943
3	BHWB	Bhawali	29.44639	79.60111
4	BJNB	Bajjnath	29.90001	79.61366
5	BKSB	Bhikiasain	29.69441	79.266
6	BLKB	Baluakot	29.80227	80.43027
7	BRCB	Barecheena	29.64217	79.74789
8	BRNB	Berinag	29.77448	80.05641
9	BSLB	Basoli	29.7013	79.70272
10	BTKB	Bhatrojkhan	29.75917	79.31861
11	BTLB	Betalghat	30.07611	79.65083
12	CBTB	Chaubatia	29.61032	79.45936

13	CHLB	Chillianaula	29.88556	79.34778
14	DGTB	Deghat	29.89835	79.22474
15	DIDB	Didihat	29.80004	80.25415
16	DNYB	Danya	29.57022	79.92536
17	DOLB	Dol	29.4885	79.75965
18	DVDB	Devidhura	29.41232	79.86496
19	DWTB	Dwarahat	29.77592	79.43246
20	GGLB	Ganai Gangoli	29.65483	80.04089
21	GNIB	Ganai	29.89191	79.35604
22	GRMB	Garampani	29.48272	79.47822
23	HWLB	Hawalbagh	29.78278	79.645
24	JJDB	Jhajjardeval	29.70278	80.23528
25	JRSB	Jaurasi	29.87945	79.27456
26	KFGB	Kafligair	29.77012	79.74629
27	KNLB	Kanalicheena	29.68713	80.27138
28	KPKB	Kapkot	29.94835	79.90192
29	KRBB	Karbala	29.5845	79.64166
30	KSNB	Kausani	29.84077	79.60422
31	LXMB	Laxmeshwar	29.70611	79.92139
32	MCRB	Machor	29.77139	79.46444
33	MKLB	Majkhali	29.865	79.76889
34	MKTB	Mukteshwar	29.58694	79.66278
35	MNLB	Manila	29.73834	79.20134
36	MNSB	Munsiari	30.07029	80.23955
37	PDGB	Pandey Gaon	29.58357	80.20271
38	RMGB	Ramgarh	29.94639	79.94361
39	SMSB	Someshwar	29.77645	79.60468
40	SYLB	Syaldey	29.83239	79.20038
41	THLB	Thal	29.83669	80.14658
42	TRKB	Tarikhet	29.61426	79.20316
43	WDDB	Wadda	29.56612	80.27734

3.4. Network Time Protocol

One of the important parameters for any successful EEW system sensor network is that all the components should be in sync in terms of time as calculation estimation as well as estimation of

depth and location is directly impacted by the accuracy of the time stamp of ground motion time history received from sensors. Therefore, all the sensors in the network must have their clocks synched with the EEW server. In order to achieve this, a network time protocol server (NTP) has been installed in one of the computers in the VPN network. Clocks of all the sensors as well as of the EEW server are updated from this NTP server every 10 minutes. Thus, ensuring that all the components, sensors, and servers, share the same time and there is no deviation in time. The decision not to use INTERNET time was taken primarily to ensure a secured network and server in terms of cyber security. Also, it was one of the agreed-upon conditions with the government to keep the network not accessible from the internet.



Chapter 4 Sensor Selection and its Dynamic Range

The selection of sensors for establishing a dense sensor network is one of the most crucial components of a successful EEW project. Since a large number of sensors need to be installed to create an optimized grid, the cost of the sensor plays a very important role. Apart from economic consideration, sensors must have some mandatory features, such as:

- Built-in facility for network connectivity,
- The sensor must be a single unit and easy to install and maintain,
- Sensors should have less power requirement as sometimes in remote locations it may need to run on battery.
- Packet size for data transmission must be small, as it helps in two important ways,
 - firstly with smaller data packet size, chances of data lost in transmission reduce in a substantial way,
 - secondly, smaller packet sizes are created faster as well as communicated faster, thus reducing latency of the system, which is of paramount importance for the EEW system.
- The dynamic range of the sensor should be such that minimum information is lost.

The price of a sensor is, most of the time, governed by its dynamic range. Hence, it becomes necessary to identify an optimum dynamic range required for the development of a network when hundreds of sensors need to be installed. In this study, the effect of dynamic range on different earthquake early warning parameters and strong motion characteristics has been studied.

4.1 Methodology and Procedure:

It is an established fact that as the dynamic range of the sensor increases, its price as well as operational cost increases. Also, for the EEW network, a large number of sensors need to be installed, which means that the economic feasibility of the project will play an important role in taking it through. This is the reason why a lot of studies have been going around the world about the suitability and testing of low-cost MEMS-based accelerometers. Some of these studies have been discussed in chapter 1, section 3. A number of EEW systems are either operational or under development based upon low-cost accelerometers. This provides the motivation to perform a study to test the optimum sensor dynamic range, which is required so that maximum information could be extracted from time history data from the sensor. The idea behind this study was to

theoretically analyze the possibility of an EEW network using low-cost MEMS sensors as well as to test the suitability of valuable strong-motion ground data to be received through such instrumentation.

To perform this study, earthquake records from Kik-Net and the K-net database of Japan have been used. In Kik-net & K-net database, data is available in the form of numerical counts as received from the ADC. A scale factor is provided, multiplying which to the counts gives the acceleration value. The numerator of the scale factor represents the full-scale range of the instrument, whereas the denominator represents the maximum count that can be obtained from ADC. As an example, for a 24-bit ADC maximum count that could be obtained is 2^{23} , which is equal to 8388608. To obtain value in acceleration unit (gal), the scale factor is multiplied by the numerical count. If this sensor's maximum scale range is +/- 2000 gal (or 2g), then this scale factor would be 2000/8388608. This means the resolution of this sensor would be 2.3842×10^{-4} gal. Now, if this sensor ADC is converted to 23 bit, ADC means the denominator will become 2^{22} (or 4194304), and the scale factor will be 2000/4194304. This gives a resolution of 4.7684×10^{-4} gal. It can be seen from this example that a reduction of 1 bit in ADC causes a reduction of resolution by half of the original value. Following the same logic, a 16-bit sensor would provide a resolution of 0.0610 gals. The 24-bit data from the Japanese dataset has been used in this study. The earthquake records available from the dataset were modified by reducing the resolution of ADC numerically and used for the analysis. The procedure used for reducing the resolution is explained as follows:

- In this study, it has been assumed that the counts coming from ADC only contains data (free from noise).
- In the first step, the value of the denominator is modified by a factor of 2 bits using a bit-shift operator in MATLAB thus converting it to 24 bit to 22 bit. This converts the scale factor from 2000/8388608 (i.e., 2.3842×10^{-4} gal) to 2000/2097152 (i.e., 9.5×10^{-4} gal), considering sensors scale range is 2000 gals.
- In the next step, the counts obtained from ADC, as time history, were modified by applying the same bit-shift operator by the factor of 2 bits.
- In this way, the scale factor and the data received are both now converted to 22 bit. Dynamic range is roughly approximated as 6-dB per bit; thus, a 24 bit ADC has a dynamic range of approximately 144-dB (6×24), and 22-bit ADC has a dynamic range of roughly equal to 132-dB.
- Now, multiplying the modified scale factor with modified time history (in counts) a new time history will be obtained in terms of gals, which will be approximately the same as the original history but with lesser resolution.

- Repeating the above steps again, multiple time histories can be obtained with different resolutions. For this study, the time histories used are 24 bit (original time history), 22 bit, 20 bit, 18 bit, 16 bit, 14 bit, 12 bit, and 10 bit.
- The EEW parameters and strong motion parameters were calculated using each time history and compared.

The Program for shifting bit and analysis is developed in MATLAB 2016A. Since MATLAB uses a big-endian schema to convert data from higher bit to lower bit, the right bit shift method is used.

Hence this study examines the impact of reduction of each bit from the ADC (or reduction in resolution of the sensor) on various EEW and strong motion parameters. The observations and outcomes of the study are discussed further in this chapter.

4.2 Effect on Magnitude using P_D or M_{PD}

P_D is defined as high pass filtered peak displacement for a predefined window length. For this study, P_D is calculated for a window length of 3 seconds. The data is high passed using a fourth-order Butterworth filter with a cut-off frequency at 0.075Hz.

To examine the impact of shifting bit on value of P_D , 8 different time histories of 24, 22, 20, 18, 16, 14, 12, and 10-Bit (Figure 4.1 to 4.8) were obtained from each time history of 24 bit by applying the method explained above.

P-phase in records was picked manually. The time histories were double integrated using the trapezoid method to obtain displacement time history. The maximum value or peak value of displacement of the first 3 seconds is then extracted, which is defined as P_D . M_{pd} was then calculated for all the cases, and error in magnitude estimation with respect to 24-bit record data is analyzed.

Following observations were made for 750 records for earthquakes having a magnitude greater than five and epicentral distance between 10 and 30 kilometers.

The Figure 4.1 and results detailed above indicate that as the resolution decreases, there is a definite drop in accuracy with which M_{PD} is estimated, but the difference is of the order of 0.01 up to 16 bit and then increased by one and more units when resolution is further decreased up to 10 Bit.

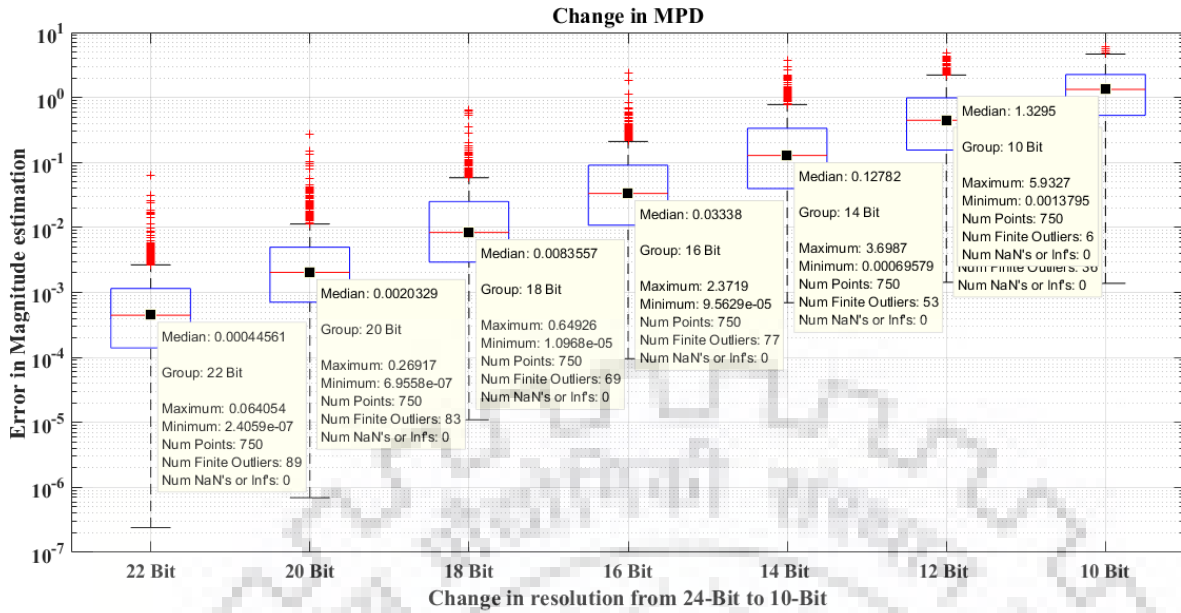


Figure 4.1 : Difference in magnitude estimation using P_D calculated for time histories at different ADC resolution varying from 22-Bit to 10-Bit with reference to original 24-Bit data.

Figure 4.2 to 4.8 shows the histogram for the difference in M_{PD} estimation for different resolution time histories.

For 22 Bit data or for P_D Calculated with 22-Bit data, the maximum difference in M_{PD} estimated is found to be 0.064 and minimum difference 2.4×10^{-7} , with a median at 0.000445. It is also observed that most of the estimations are well with in difference of -0.01 to 0.01.

Similarly, for 20 Bit data or for P_D calculated for 20-Bit time history, the maximum difference in M_{PD} estimation is around 0.269, and the minimum difference is 6.9×10^{-7} , with a median at 0.00203. The result, as can be seen in Figure 4.1, there is a very small or negligible difference between the estimated magnitude from 24-Bit and 20-Bit data time histories. It can be observed from figure 4.3 that most of the estimations are well with in difference of -0.05 to 0.05.

For P_D calculated for 18-Bit time history, the maximum difference in M_{PD} estimation is around 0.649, and the minimum difference is 1.09×10^{-5} , with a median at 0.0083. The result, as can be seen in Figure 4.1, there is a very small or negligible difference between the estimated magnitude from 24-bit and 18-bit data time histories. It can be observed from above Figure 4.4 that most of the estimations are well with in difference of -0.2 to 0.2.

For 16-Bit data or for P_D calculated for 16-Bit time history, the maximum difference in M_{PD} estimation is around 2.379, and the minimum difference is 9.56×10^{-5} , with a median at 0.0338. It can be observed from above Figure 4.5 that most of the estimations are well with in difference of -0.4 to 0.4.

Thus it can be safely assumed that for all practical purposes of EEW, the error up to 16-Bit data is quite suitable and thus can be safely used for the purpose of EEW.

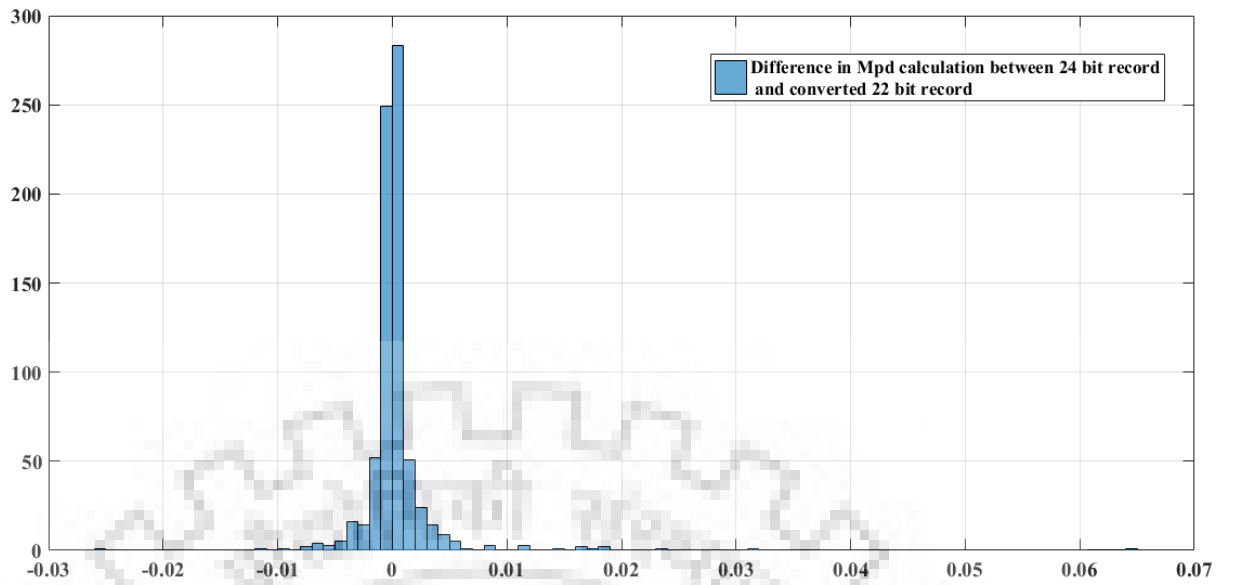


Figure 4.1: Number of records vs difference in M_{PD} estimation for 22 Bit converted record

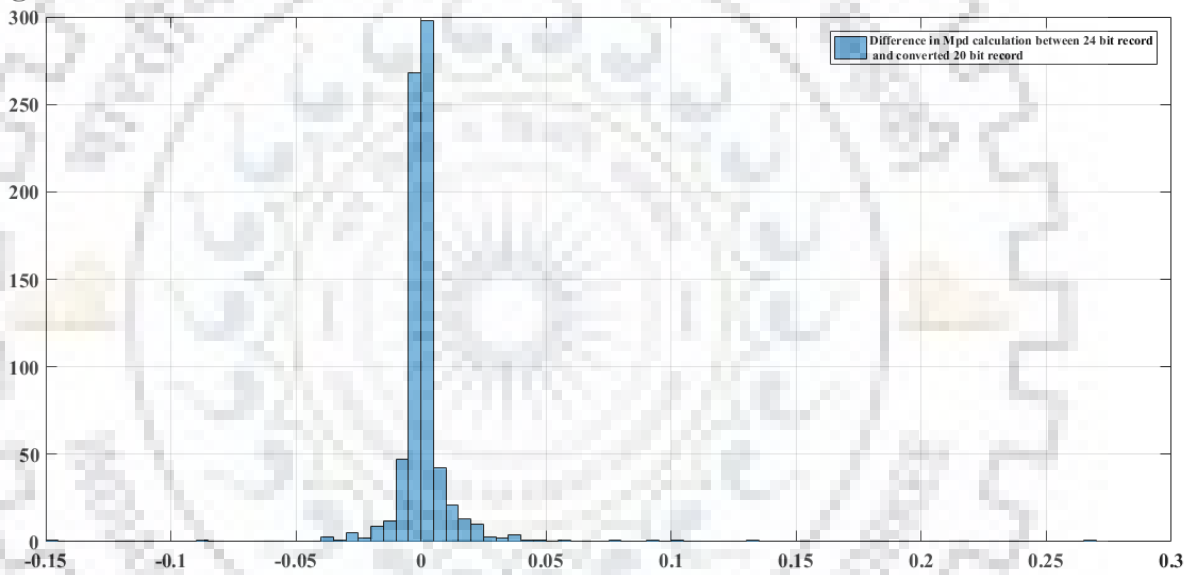


Figure 4.2: Number of records vs. change difference in M_{PD} estimation for 20 Bit converted record.

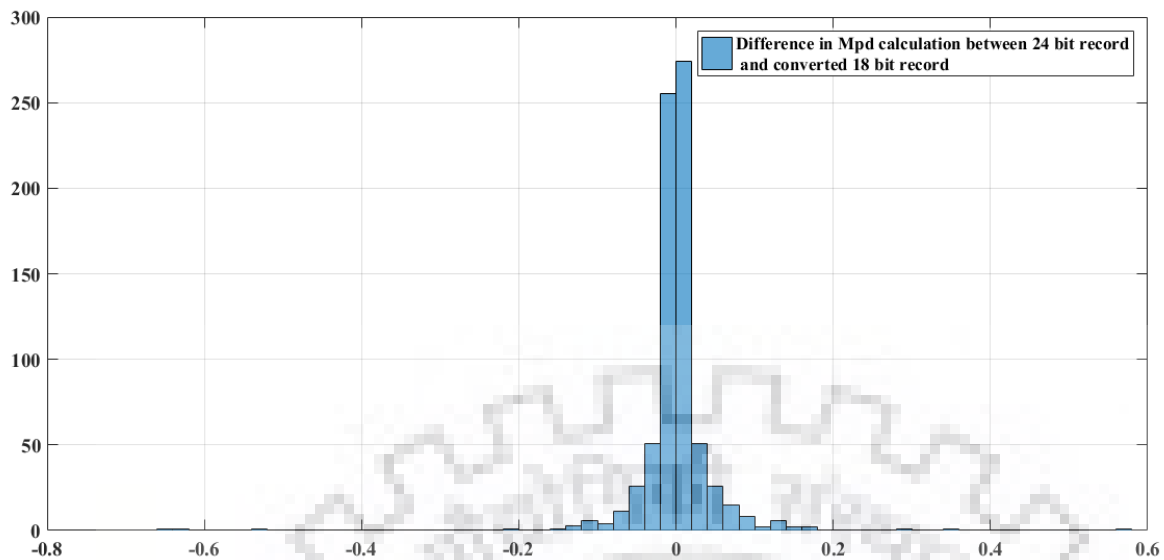


Figure 4.3: Number of records vs. difference in M_{PD} estimation for 18-Bit converted record.

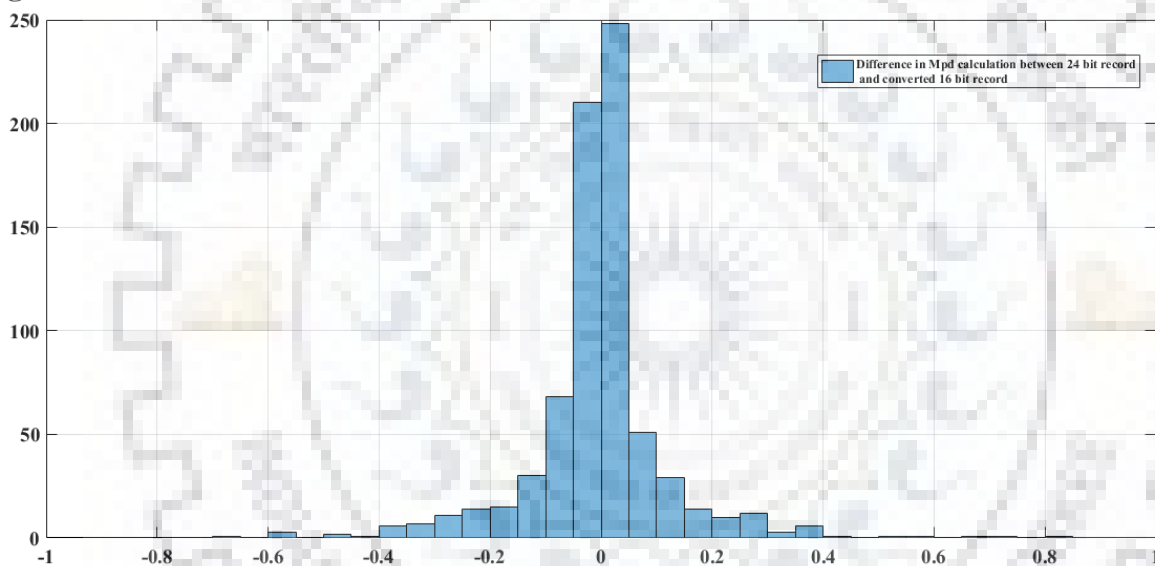


Figure4.4: Number of records vs. difference in M_{PD} estimation for 16-Bit converted record.

For 14-Bit data or for P_D calculated for 14-Bit time history, the maximum difference in M_{PD} estimation is around 3.69, and the minimum difference is 6.9×10^{-04} , with a median at 0.1278. It can be observed from above Figure 4.6 that most of the estimations have an error of the order difference of -1 to 1.

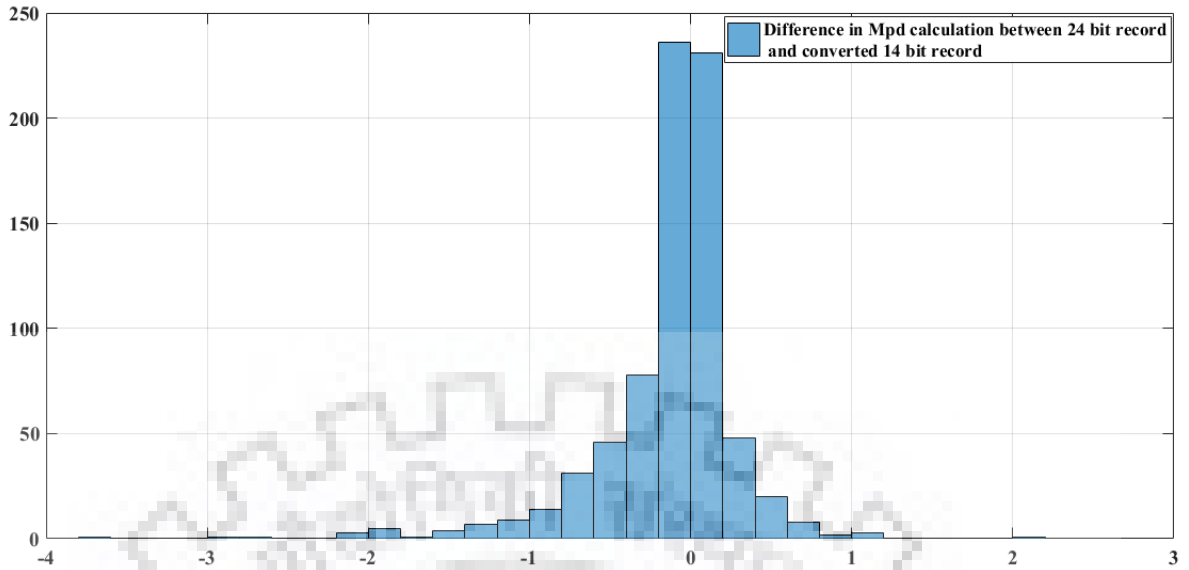


Figure 4.5: Number of records vs. change difference in M_{PD} estimation for 14-Bit converted record.

For 12 Bit data or for P_D calculated for 12 Bit time history, the maximum difference in M_{PD} estimation is around 4.915, and the minimum difference is 1.43×10^{-03} , with a median at 0.4458. It can be observed from the above Figure 4.7 that most of the estimations are well within a difference of -3 to 2. It would be appropriate to infer that the data beyond this limit is not at all suitable to be used for the purpose of EEW, as with this order of error, there are fair chances of false warning, and this will lead to a faulty system.

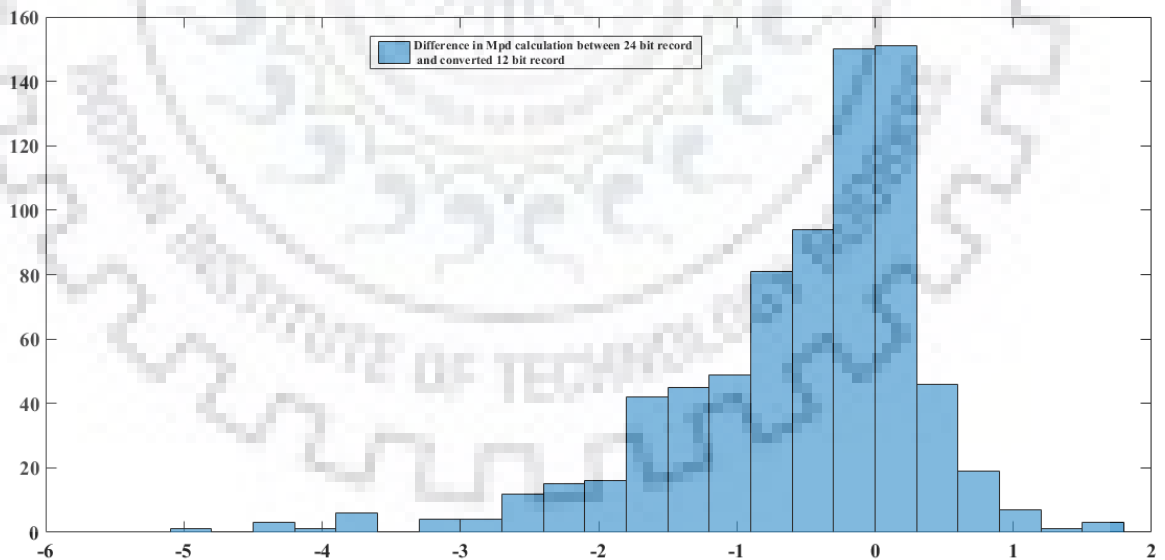


Figure 4.6: Number of records vs. change difference in M_{PD} estimation for 12 Bit converted record.

For 10-Bit data or for P_D calculated for 10 Bit time history, the maximum difference in M_{PD} estimation is around 5.9, and the minimum difference is 1.3×10^{-03} , with a median at 1.3295. It can be observed from figure 4.8 that most of the estimations are well within a difference of -5 to 1. This is almost certain at this stage that the data is not suitable for the purpose of EEW.

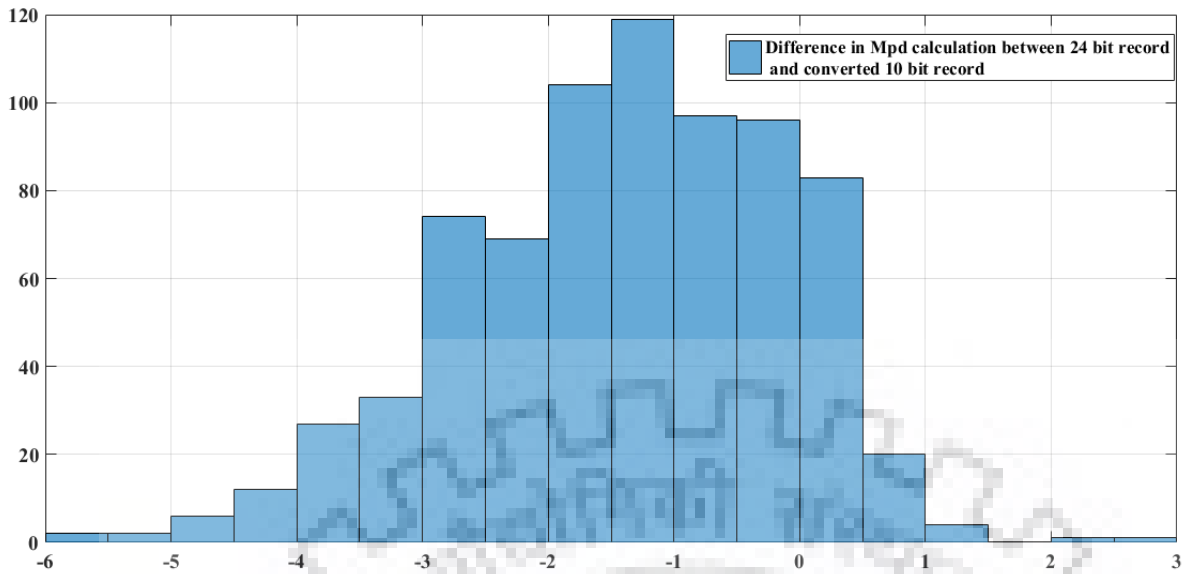


Figure 4.7: Number of records vs. change difference in M_{PD} estimation for 10 Bit converted record.

From figure 4.1 to 4.8, it can be inferred that up to 16-bit data, there is an acceptable error in magnitude estimation, whereas below 16 bit the error is too large, and thus the data below 16 bit is not suitable for EEW purposes. Thus with this study, it can be safely concluded that for M_{PD} estimation, the data beyond 16-Bit is not found suitable to be used for the EEW purpose.

4.3 Effect on magnitude estimation using τ_c

In figure 4.9, the error in magnitude estimation using τ_c (M_{τ_c}) has been shown. From the figure it can be seen that even up to 10-Bit data, the median error in the estimated M_{τ_c} values is of the order 1 Unit. However, the maximum value of median error is a little high even at 18-Bit or 16-Bit data. The data from figure 4.10 suggests that for 16-Bit data, the maximum error in magnitude estimation is as large as ~ 3 units, however, the median error is of the order 0.03 only. Thus it is evident from the figure that magnitude estimation using τ_c is quite sensitive as the resolution is decreased from 24-Bit to 16-Bit and further deteriorates as it reaches 10-Bit. It can also be

inferred that, as the resolution of data is reduced, the error is more distributed, and thus chances of false estimation are high.

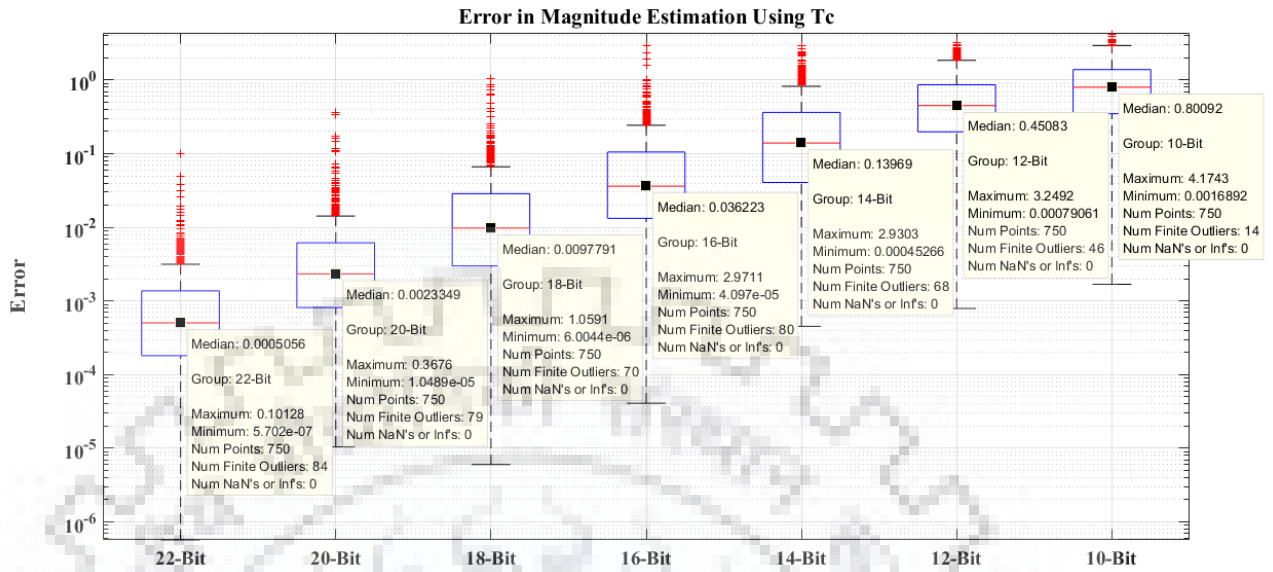


Figure 4.8: Difference in magnitude estimation using T_c , calculated for time histories at different ADC resolution varying from 22-Bit to 10-Bit with reference to original 24-Bit data.

From Figure 4.10, for 22-Bit converted data, it can be seen that the error in magnitude estimated is almost in the range of -0.02 to +0.02. The median error, as observed in Figure 4.9, is of the order 0.0005 unit only. Thus there is not much error in the estimation of magnitude

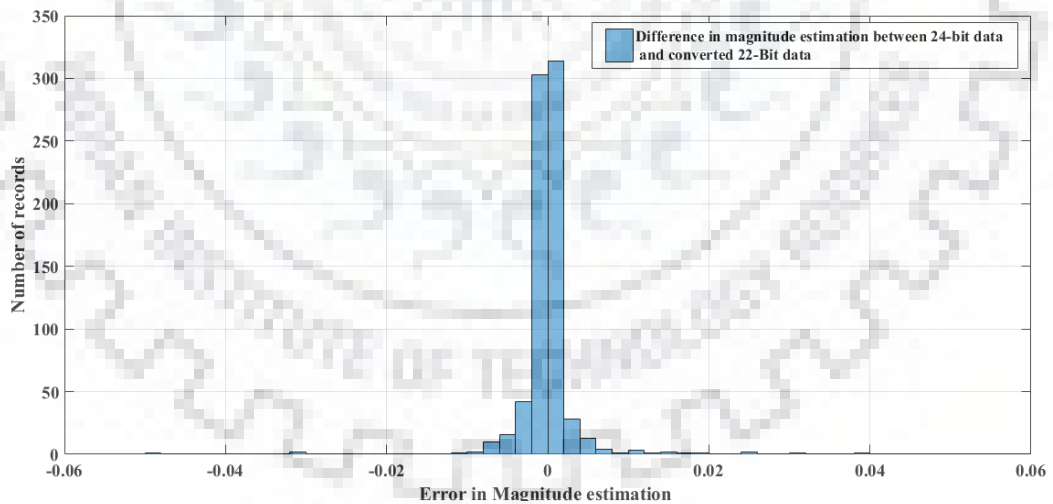


Figure 4.9: Number of records vs. change in M_{TC} estimation for 22-Bit converted record.

In figure 4.11, the error in magnitude estimation for 20-Bit converted data has been shown. It is evident from the figure that for most of the records, the error in estimation is well within -0.05 to +0.05 units. Also, the median error for the 20-Bit record is 0.0023 units only. Whereas, from figure 4.9, the maximum error is only 0.36 units.

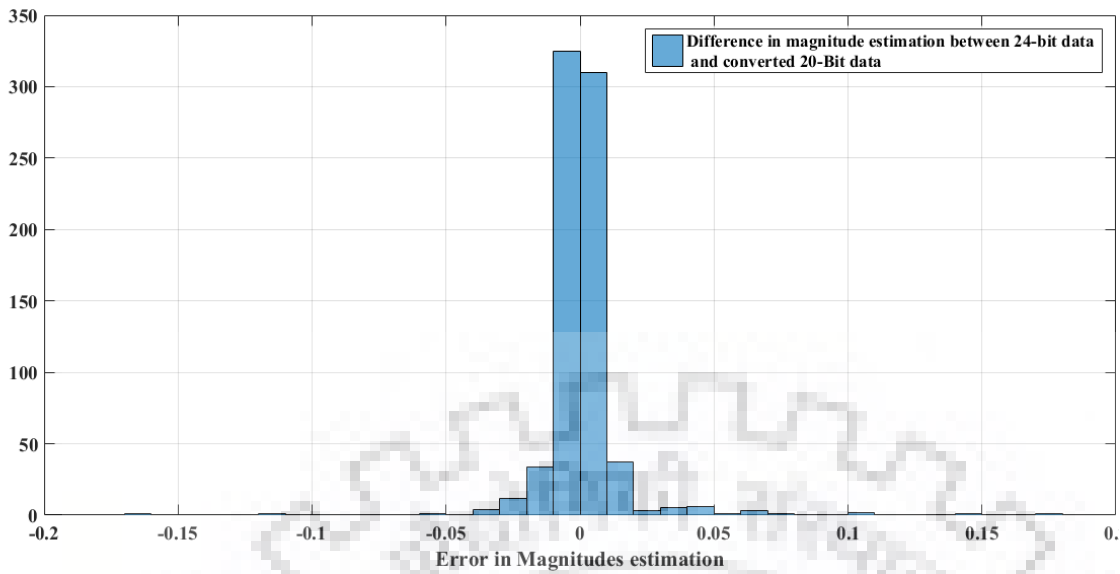


Figure 4.10: Number of records vs. change in M_{TC} estimation for 18-Bit converted record

In Figure 4.12 it can be seen that the error in magnitude estimation for 18-Bit converted data is almost in the order of 0.2 units only. The median error is also of the order 0.0097 units. However, the maximum error is one unit.

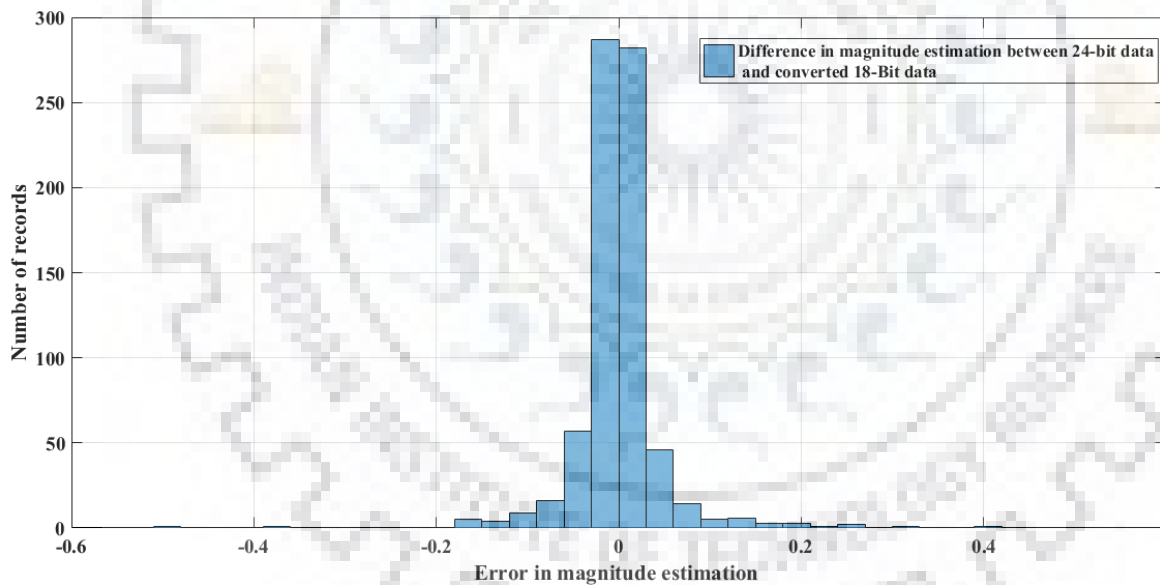


Figure 4.11: Number of records vs. change in M_{TC} estimation for 18-Bit converted record.

For 16-Bit records, the median error in magnitude estimation is of the order 0.036 units only. However, the maximum error is almost of the order of 3 units. This suggests that the error is now distributed to the large range. However, most of the errors are within the range of -0.5 to +0.5.

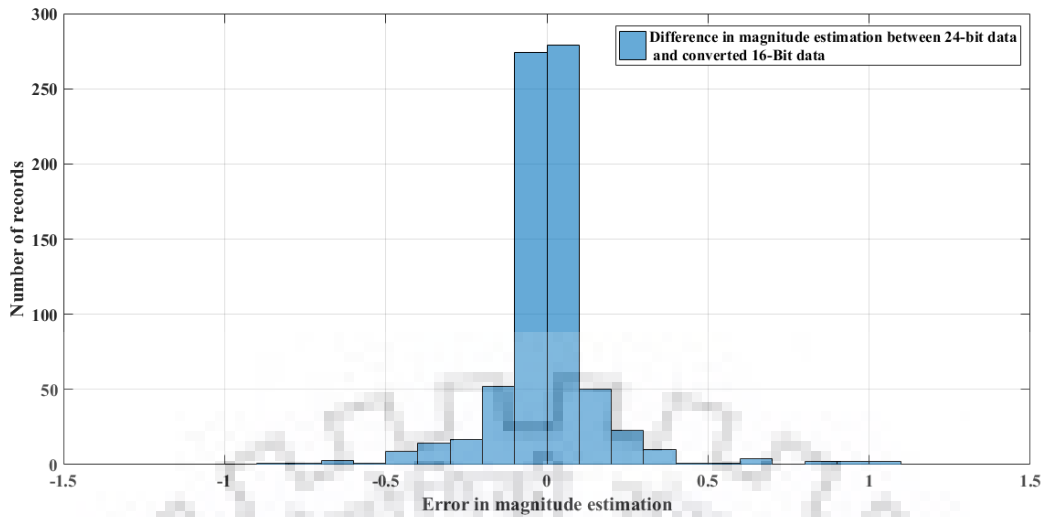


Figure 4.12: Number of records vs. change in M_{TC} estimation for 16-Bit converted record.

For 14-Bit converted data, as can be seen from figure 4.9 and figure 4.14, the error is more distributed, and it can be observed that most of the records have an error of the order one units, and also the distributed in a larger range. The median error is also of the order 0.139 units, and the maximum error is in the vicinity of 3 units. This clearly indicates that the T_c is quite sensitive as the data the ADC resolution is decreased. Thus it can be inferred that data below 16-Bit is not suitable for the EEW system if τ_c is to be used as a parameter.

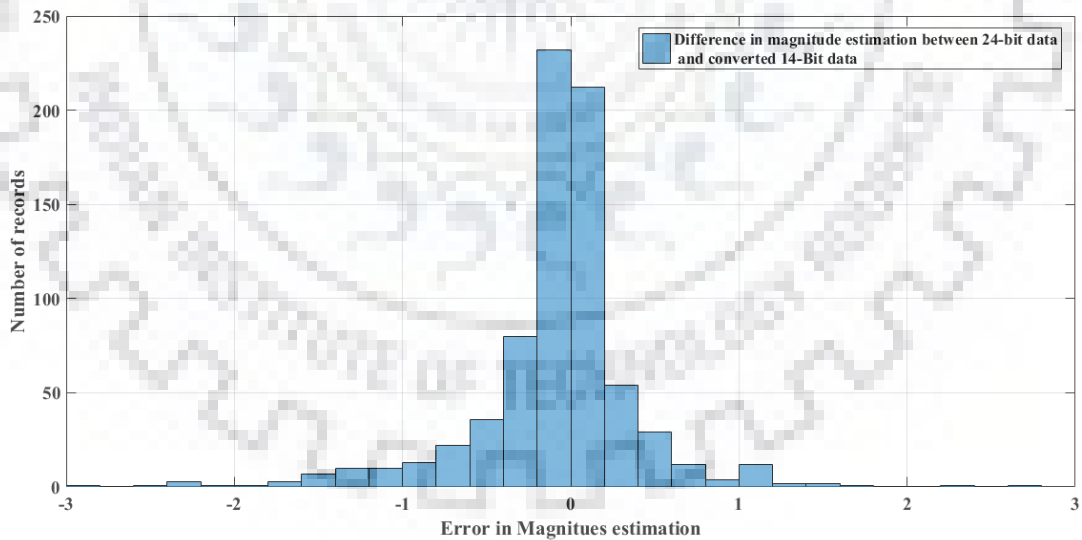


Figure 4.13: Number of records vs. change in M_{TC} estimation for 14-Bit converted record.

The error in magnitude estimation for 12-Bit and 10-Bit is discussed in Figure 4.15 and Figure 4.16, respectively. The error for 12-Bit converted data is even more distributed, and the error for most of the records is of the order two units. The error in 10-Bit converted data has median values

of 0.8. However, the error for most of the records is in the order of 3 units. Thus it can be concluded that the 12 or 10-Bit data is not at all suitable for EEW purposes.

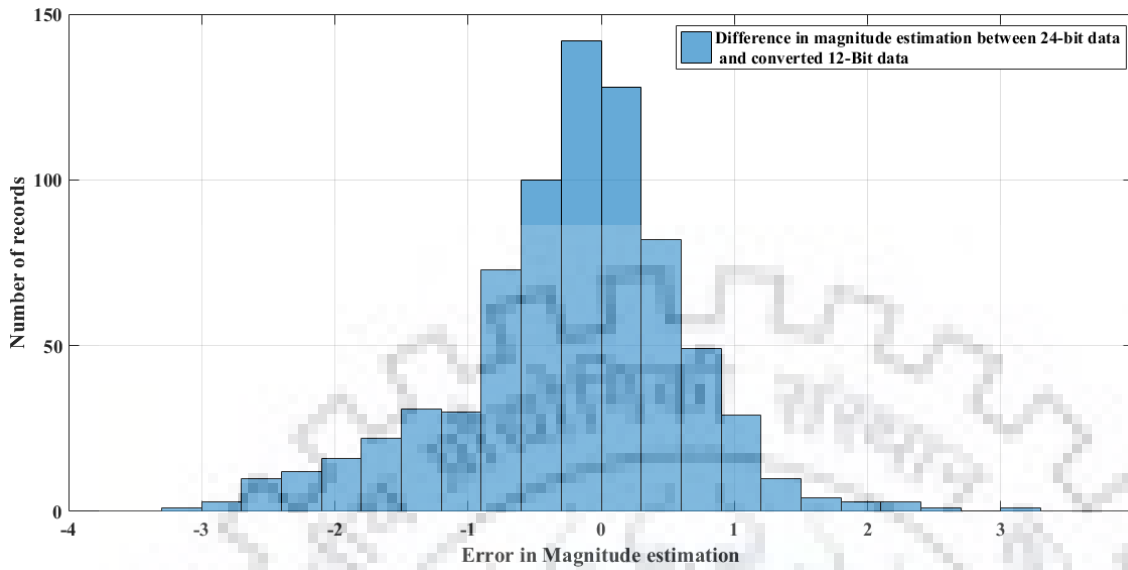


Figure 4.14: Number of records vs. change in M_{TC} estimation for 12-Bit converted record.

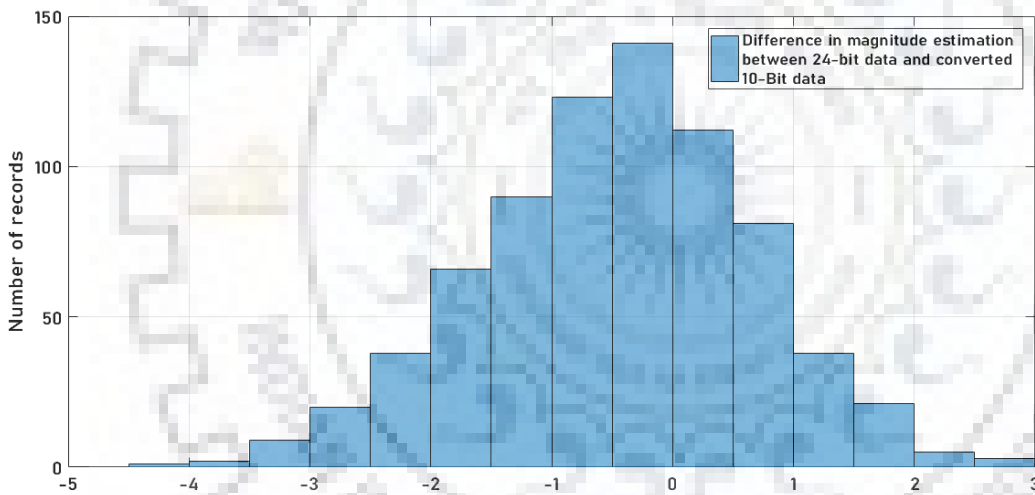


Figure 4.15: Number of records vs. change in M_{TC} estimation for 10-Bit converted record.

4.4 Effect on Spectral Acceleration:

Spectral acceleration is an important strong-motion parameter that has been used by researchers and academicians for quite a long time. It is also one of the most important parameters for structure engineers as, unlike Peak Ground Acceleration (PGA) or intensity of an earthquake at a place, the spectral acceleration relates to the actual acceleration as is felt by a structure corresponding to its natural frequency. Thus it is very useful and has found its inculcation in various standard codes for structure design(Freeman 2007).

The study on change in spectral acceleration is done because SPA is one of the most important parameters for structure point of view. Though spectral acceleration is not directly related to EEW. The network which is created for EEW serves another important purpose that is the collection of strong-motion data. Thus this study was performed to determine the suitability of

the strong motion data collected from the EEW network, comprising of low-cost MEMS sensors, for other engineering practices, especially structural engineering, as well.

Pseudo Acceleration Spectrum and Pseudo Velocity Spectrum have been calculated by solving the equation of motion for different periods and damping values using the Newmark Linear method. The method has been implemented using MATLAB.

To study the impact of lower bit data in spectral acceleration, time histories of actual 24-bit data and corresponding converted time histories have been used. For analysis of spectral acceleration, the following representative periods have been used. The periods were selected so that an analysis could be done for the presentative period. The periods are selected with an objective to have a well distributed and selected set of the period covering the whole spectrum.

Also, the most common damping values that are used by structure engineers viz 2%,5% and 10% have been used for the analysis. 2% damping corresponds to damping of steel, 5% for RCC and soil in general considered to has damping of 10 %.

Table 4.1 : Representative periods used for the analysis of Spectral Acceleration values

Periods used														
0(PGA)	0.03	0.05	0.1	0.2	0.3	0.5	0.74	1	2	3	4	5	7	10

4.4.1. Effect on Spectral Acceleration for 5% damping

The results obtained are shown in the Figures from 4.17 to 4.23, represent a change in the spectral acceleration values for the converted time histories from 22-bit to 10 bit, with respect to 24-bit data. Results plotted in Figures 4.17 to 4.23 are corresponding to 5% damping, and values are represented in percentage change with respect to the value for 24-Bit actual time history value. Figure4.17 represents the spectral acceleration values for zero periods or PGA values.. As is evident from the figure, for 22-Bit converted data, there is a maximum variation of 0.0045 % with a median value of 0.00060. The 75th percentile value is at 0.0011, and the 25th percentile value of 0.00025. It is clearly indicated from the above values that there is practically no change in the values of SA for a zero period when data is converted from 24-Bit to 22-Bit.

It is also evident from Figure4.17, that as the data is converted from 24-Bit to 10-Bit, there is a definite increase in the error with respect to original data. But the error is very small, and it reaches a median value of just 2% for 10-Bit data. Thus it would be correct to infer that for measuring or estimating PGA, there with up to 12 or 10-Bit accuracy is also suitable.

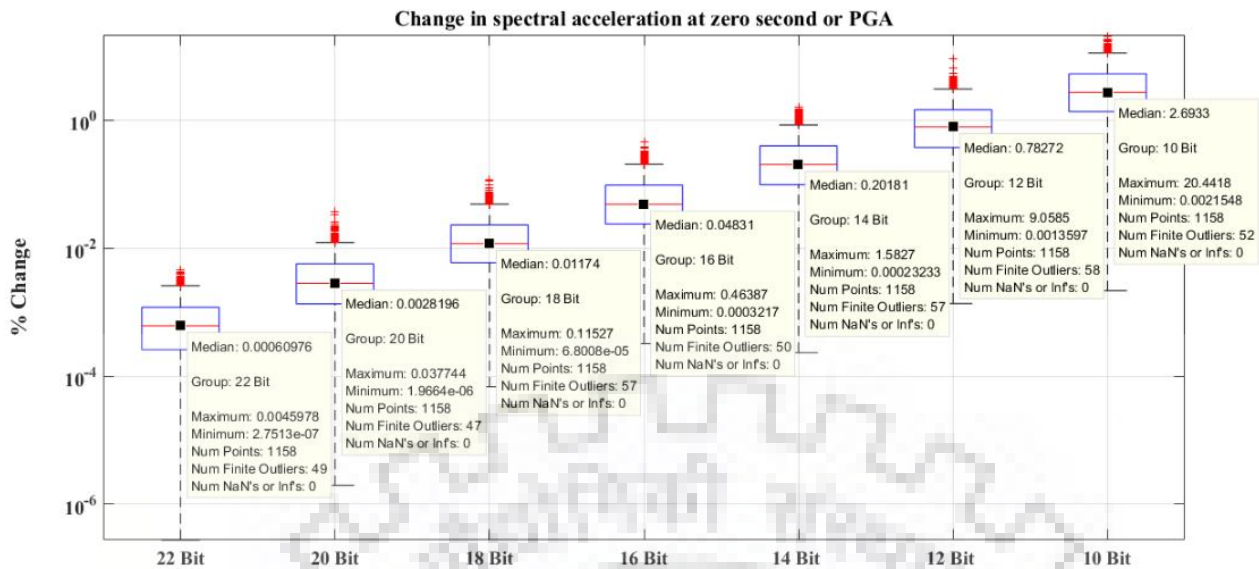


Figure 4.16: DIFFERENCE in Spectral Acceleration, calculated for time histories at different ADC resolution varying from 22-Bit to 10-Bit with reference to original 24-Bit data and Zero period or PGA.

The Figure4.18, explains the change in the error in SA for 0.03 second and 5% damping, with a decrease in Bit from 24-10Bit. Here also, it can be seen that the maximum error in the estimation of SA value when the bit is reduced from 24-Bit to 22-Bit is 0.0039 %, with a median value at 0.00075. The 75th percentile value is 0.00178, and the 25th percentile is at 0.00029.

For 0.03 second period also the median value for 10-Bit data is only 2.7 %. It can be inferred that a lot of information could be retrieved for this period also even if ADC resolution is as low as 10-Bit.

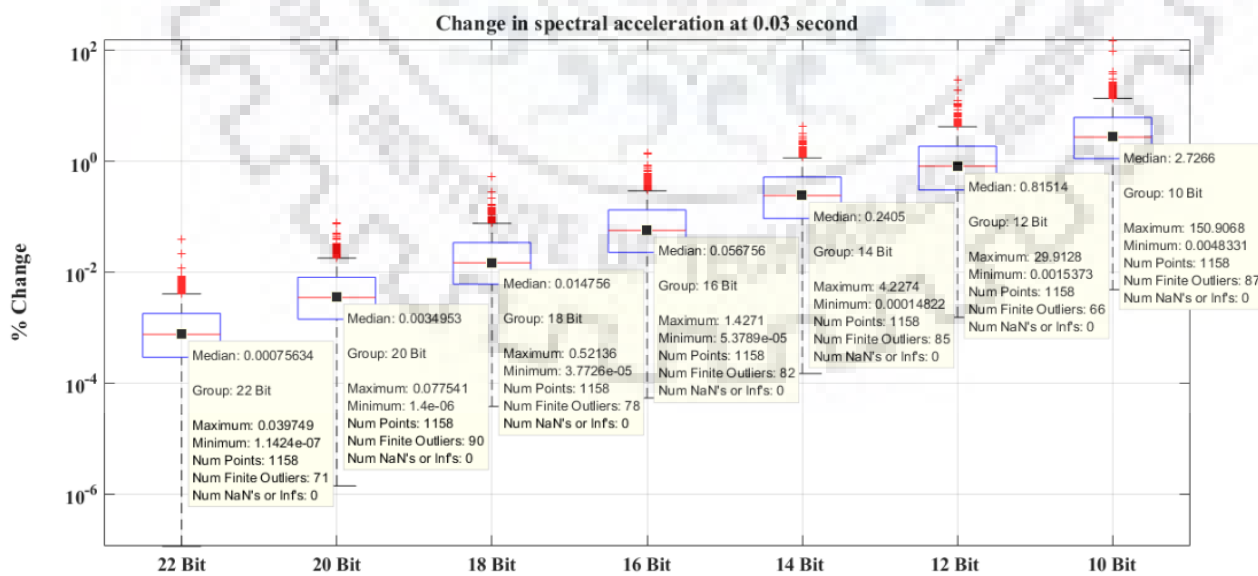


Figure 4.17: Difference in Spectral Acceleration, calculated for time histories at different ADC resolution varying from 22-Bit to 10-Bit with reference to original 24-Bit data and 0.03 second period.

Figure 4.19, explain the change in SA value for 0.05 second period and 5% damping. The median value for 22-Bit is 0.000843 with the maximum value of 0.0144. The 75th percentile value is 0.00178 and 25th percentile value is 0.000379. It can also be seen from the figure that up to 12-Bit the error in SA value is less than 1%.

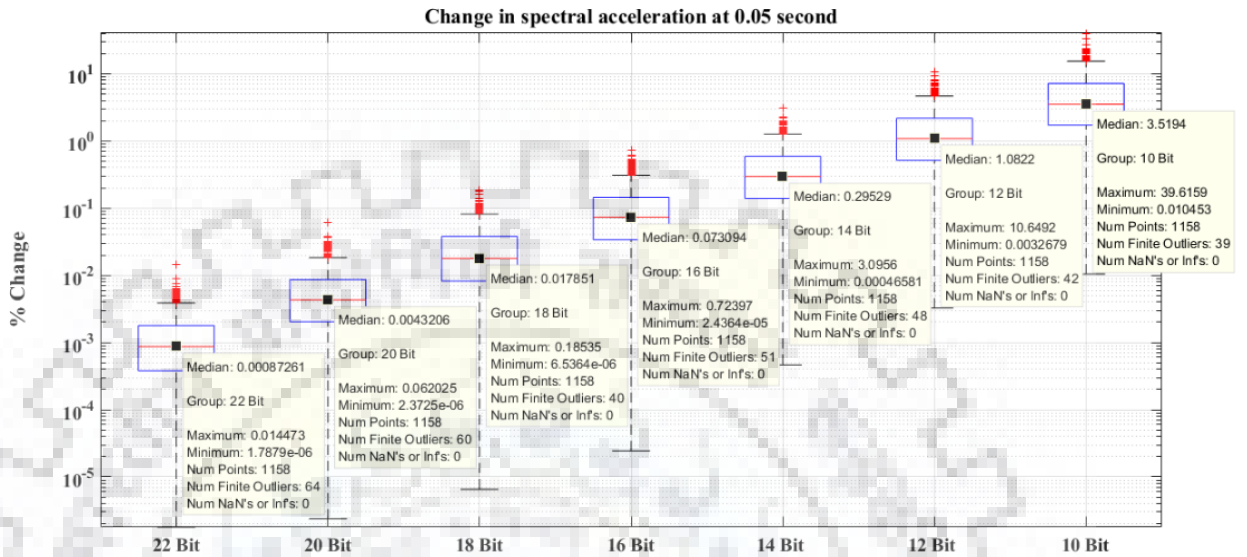


Figure 4.18: Difference in Spectral Acceleration, calculated for time histories at different ADC resolutions varying from 22-Bit to 10-Bit with reference to original 24-Bit data and 0.05 second period.

Figure 4.20, explain the change in SA value for 0.1 second period and 5% damping. For 22-Bit data, the maximum error is 0.0135%, and the median value is 0.0010. It is also evident from the figure that up to 12-Bit, the error is of the order 1% only.

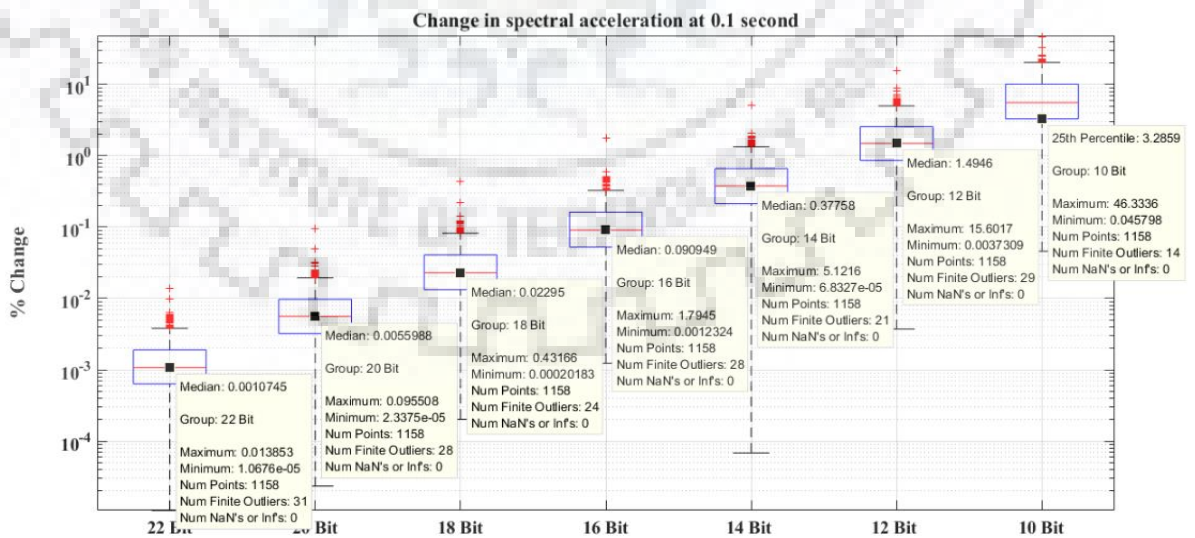


Figure 4.19: Difference in Spectral Acceleration, calculated for time histories at different ADC resolution varying from 22-Bit to 10-Bit with reference to original 24-Bit data and 0.1 second period.

In Figure 4.21, the error in percentage for 0.2 second period is explained. It is evident from the Figure that for 22-Bit data, the maximum error is 0.0127% whereas, the median value is at 0.0011. The 75th percentile value is at 0.0021, and the 25th percentile is at 0.00067. It is also evident that up to 14-Bit, the error is of the order 1% only.

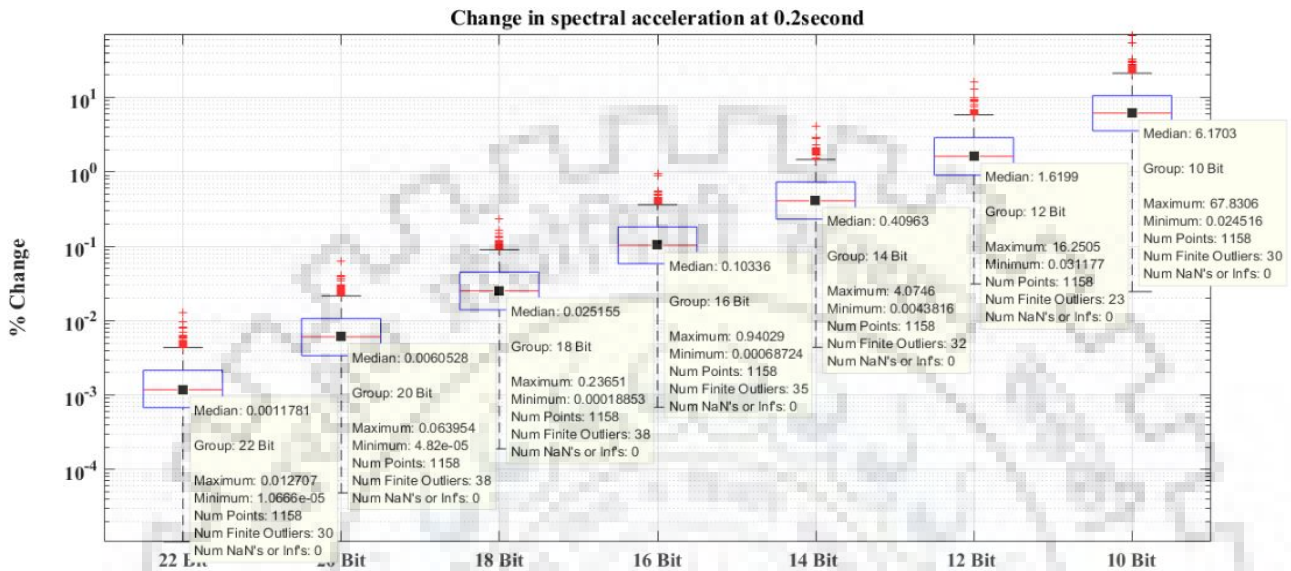


Figure 4.20: Difference in Spectral Acceleration, calculated for time histories at different ADC resolution varying from 22-Bit to 10-Bit with reference to original 24-Bit data and 0.2 second period.

Figure 4.22, explains the change in error for 0.3 second period. For 22-Bit data the maximum error is 0.021%, and the median value is at 0.00134%. The 75th percentile is at 0.0024, and the 25th percentile is at 0.00068%. It is also evident that up to 12-Bit, the error is of the order 1~2%.

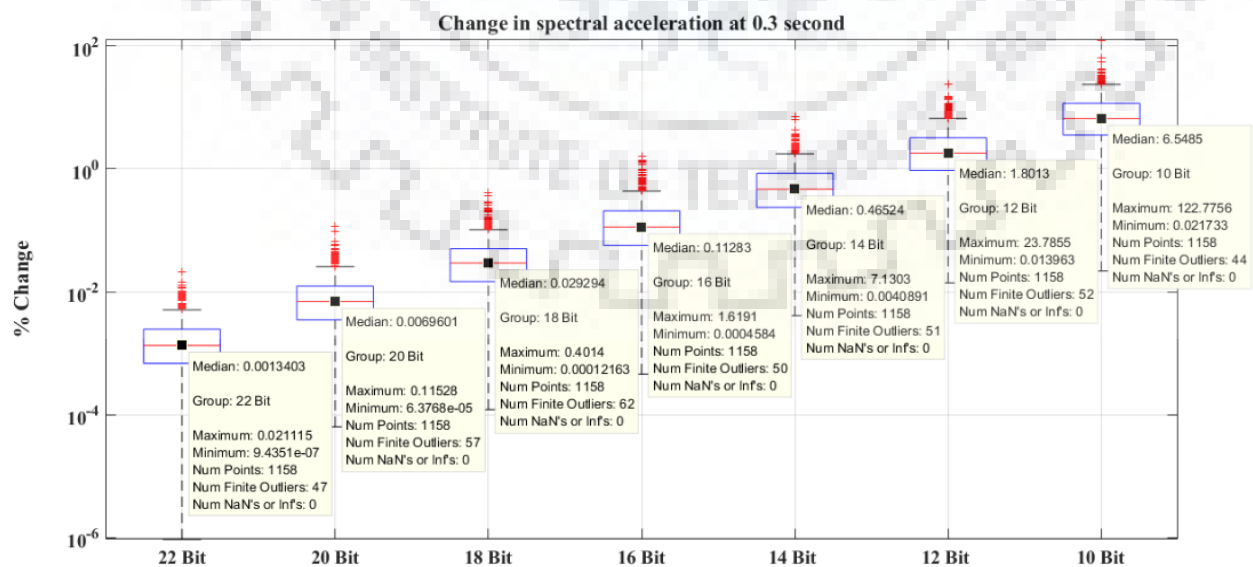


Figure 4.21: Difference in Spectral Acceleration, calculated for time histories at different ADC resolution varying from 22-Bit to 10-Bit with reference to original 24-Bit data and 0.3 second period.

Figure 4.23, explains the error in SA values for 0.5 second period and 5% damping. The maximum error is 0.052%, and the median is 0.0015. The 75th percentile is at 0.00329, and the 25th percentile is at 0.00074%. It is also evident that for up to 12-Bit data, the error is of the order 1~2% only.

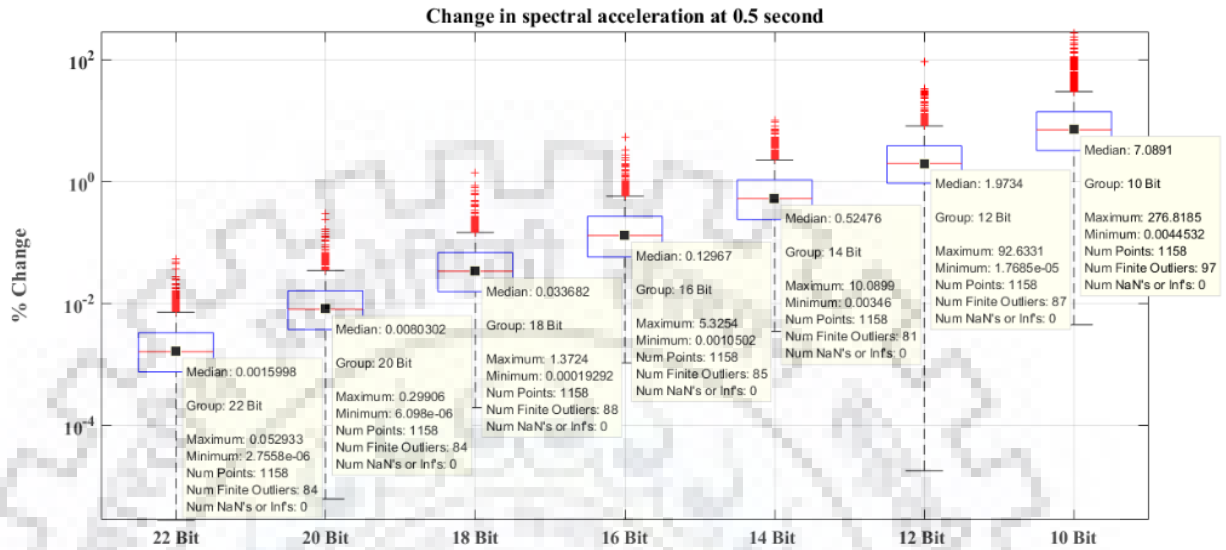


Figure 4.22: Difference in Spectral Acceleration, calculated for time histories at different ADC resolution varying from 22-Bit to 10-Bit with reference to original 24-Bit data and 0.5 second period.

Figure 4.24 demonstrates the error in SA values for 0.74 second period. The maximum value of error is 0.0914%, and the median value is 0.0021%. The 75th percentile is at 0.0047, and the 25th percentile value is at 0.00086%. Up to 12-Bit data, the error is in the range of 1~2%.

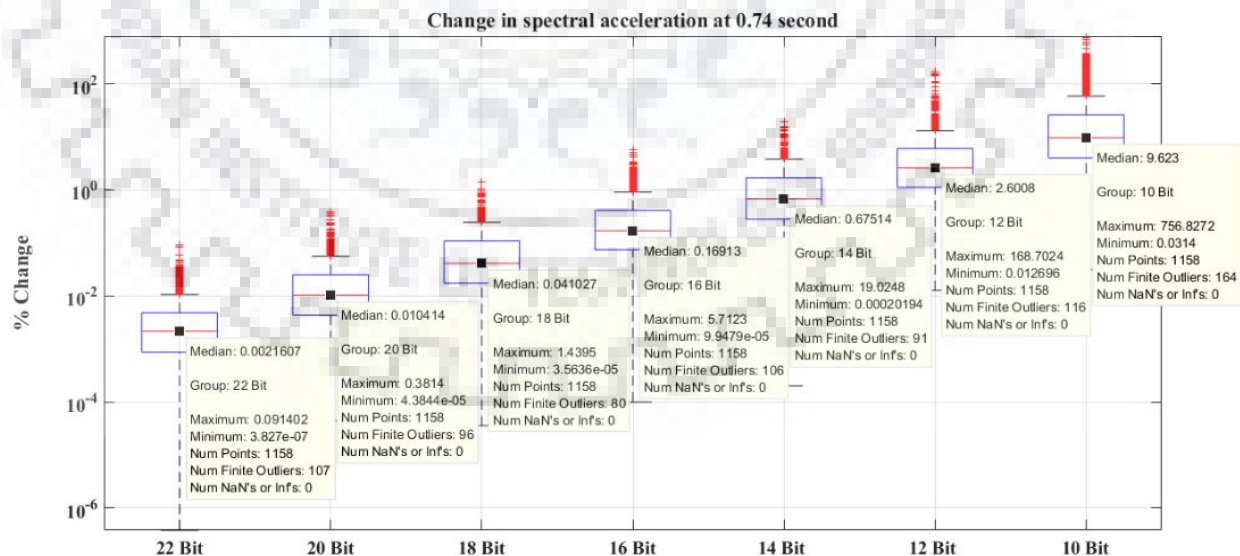


Figure 4.23: Difference in Spectral Acceleration, calculated for time histories at different ADC resolution varying from 22-Bit to 10-Bit with reference to original 24-Bit data and 0.74 second period.

Figure 4.25, demonstrates the error in the SA value for 1 second period. The maximum error is 0.215%, and the median value is at 0.0026%. The 75th percentile is at 0.007, and the 25th percentile is at 0.001%. For up to 14-Bit data the errors are less than 1%, whereas, for 10-Bit data also the error is of the order 10% only.

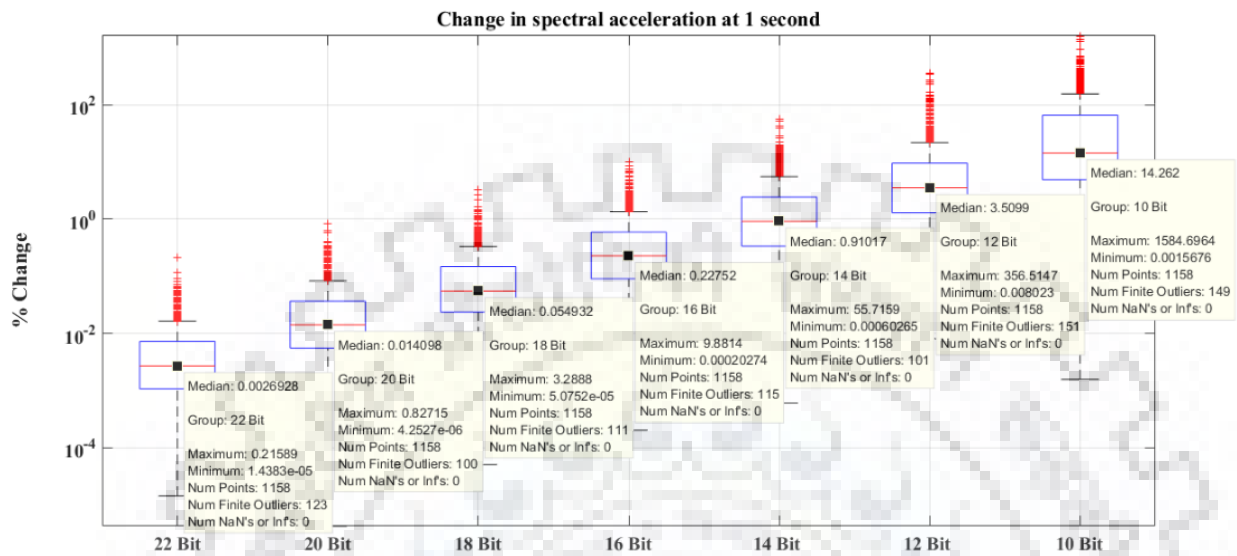


Figure 4.24: Difference in Spectral Acceleration, calculated for time histories at different ADC resolution varying from 22-Bit to 10-Bit with reference to original 24-Bit data and 1 second period.

Figure 4.26, explains the error in SA value for 5% damping and for period of 2 seconds. The maximum error for 22-Bit data is 0.438%, and the median value is at 0.0058. It is also evident from the figure that for up to 14-Bit, the error is of the order 1% only. However, the 10-Bit data has an error with a median value of 77%.

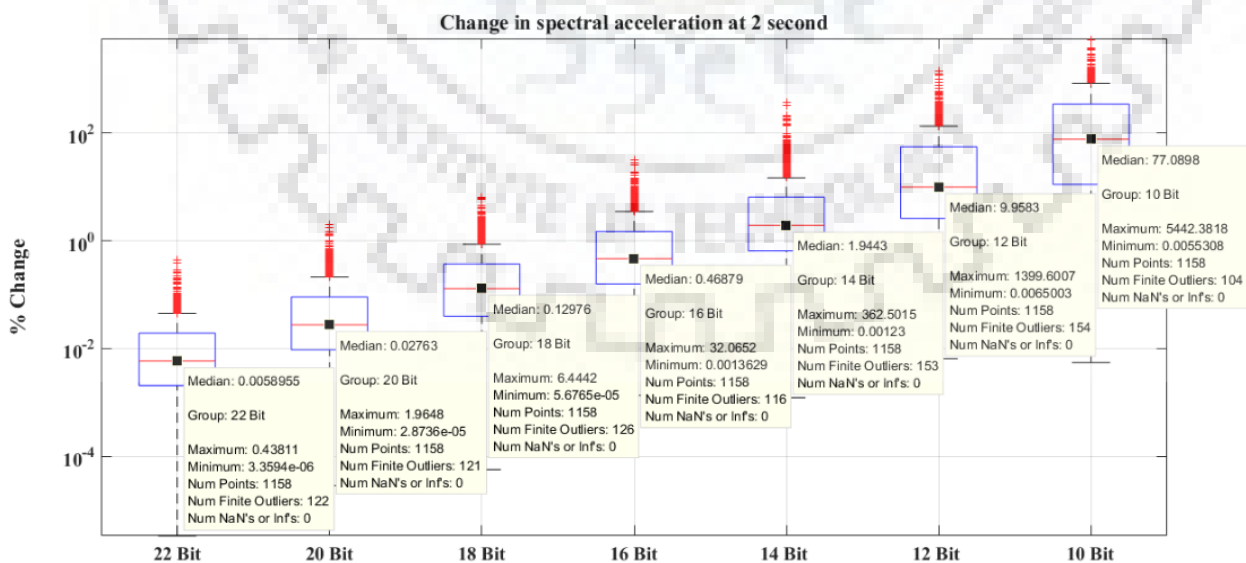


Figure 4.25: Difference in Spectral Acceleration, calculated for time histories at different ADC resolution varying from 22-Bit to 10-Bit with reference to original 24-Bit data and 2 second period.

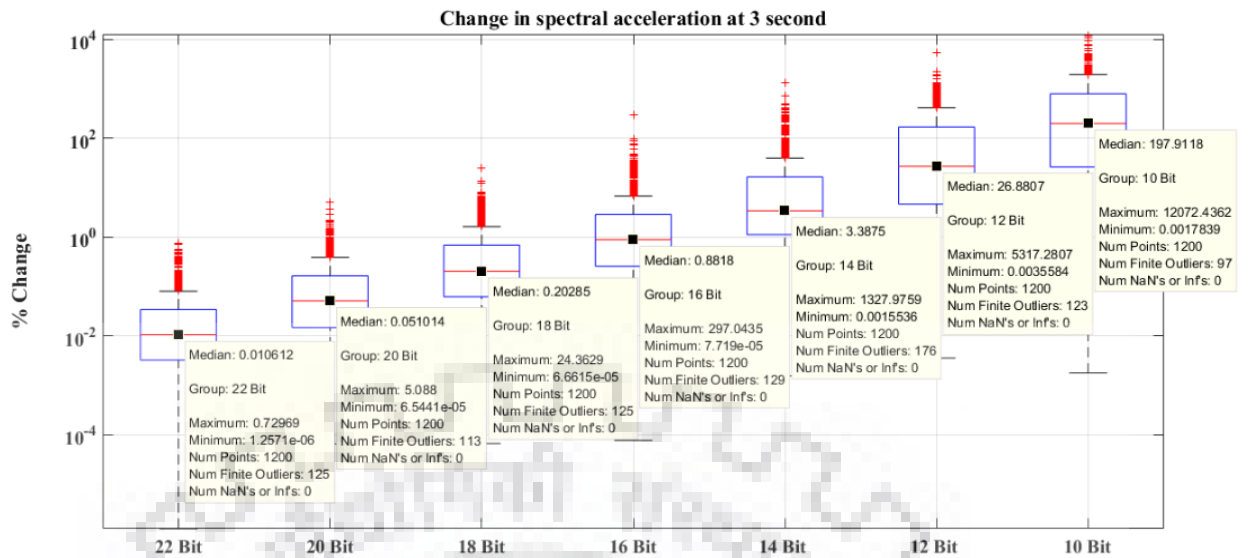


Figure 4.26: Difference in Spectral Acceleration, calculated for time histories at different ADC resolution varying from 22-Bit to 10-Bit with reference to original 24-Bit data and 3 second period.

Figure 4.27, explains the error in SA value for 3 second period and 5% damping. It is evident from the figure that for up to 14-Bit data, the error is of the order 1~3 percent only. However, errors in 12 and 10-Bit data with median values of 25 and 197%.

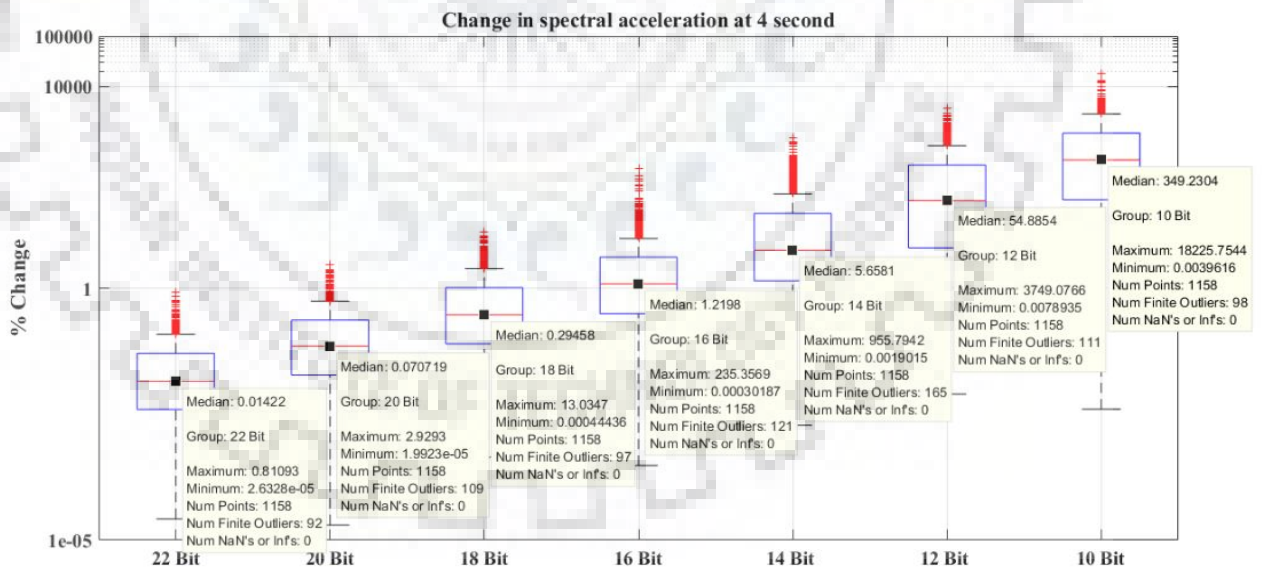


Figure 4.27: Difference in Spectral Acceleration, calculated for time histories at different ADC resolution varying from 22-Bit to 10-Bit with reference to original 24-Bit data and 4 second period.

Figure 4.28, explains the error in SA values with respect to actual 24-Bit data for 5% damping and for 4 second periods. Here it is seen that up to 14-Bit of data, the error is of order 4-5% and less than 1% for data up to 16-Bit. However, beyond 14-Bit, the error is too large.

Figure 4.29 explains the error in SA values for 5% damping and 5 second period. Here also, it is evident that for up to 14-Bit, the error is about 10%, but the median error is of order 1.7% for 16-Bit data.

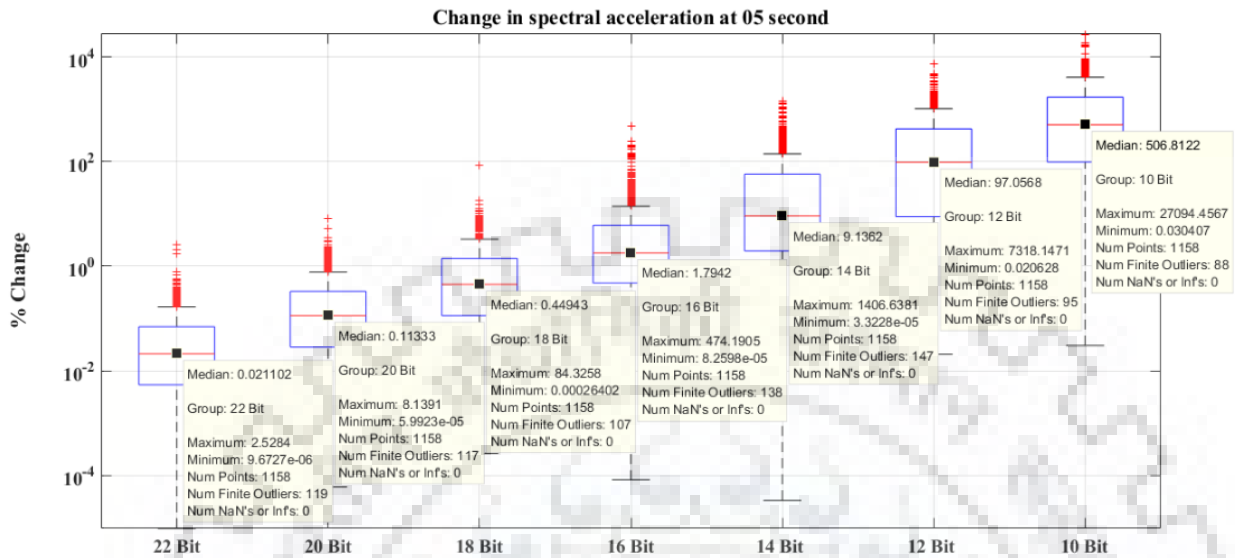


Figure 4.28: Difference in Spectral Acceleration, calculated for time histories at different ADC resolution varying from 22-Bit to 10-Bit with reference to original 24-Bit data and 5 second period.

Figure 4.30 shows error for 5% damping and 7 second period. It can be inferred from the figure that for up to 16-Bit data, the error is well within 2~3 %. However, for 12 and 10-bit data, the error is substantially of higher order. Which perhaps makes it not suitable to be used for such a large period.

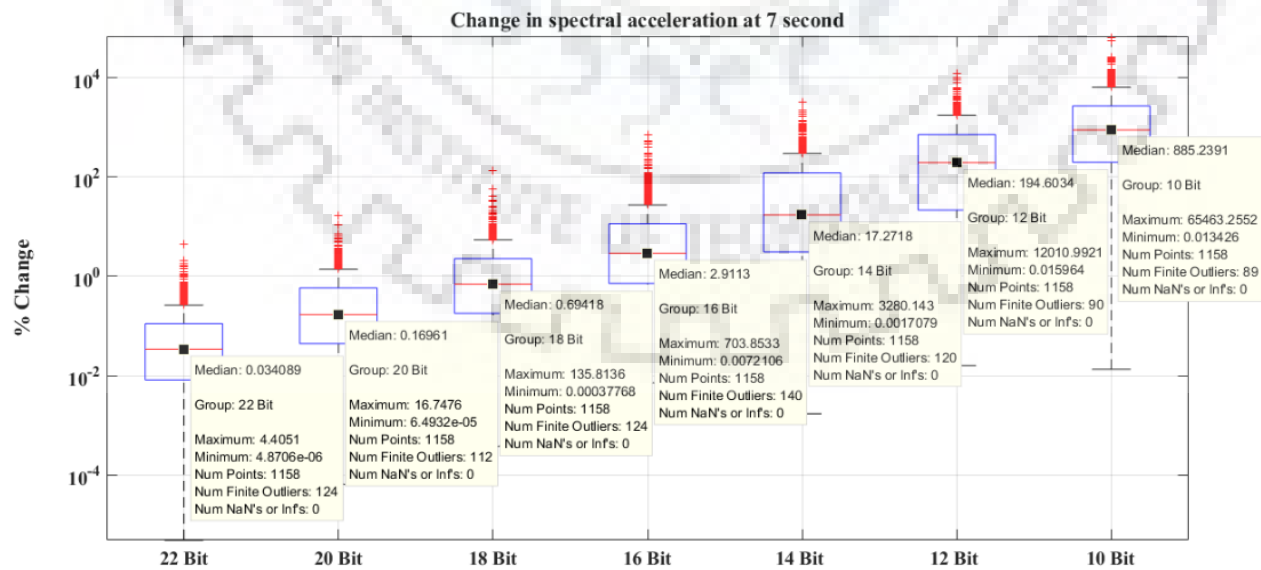


Figure 4.29: Difference in Spectral Acceleration, calculated for time histories at different ADC resolution varying from 22-Bit to 10-Bit with reference to original 24-Bit data and 7 second period.

Figure 4.31, shows an error for 5% damping and a period of 10 seconds. It is observed that for 10 second period, the error in data up to 16-Bit is of the order of 5-6%. However, the error is 14-Bit and above is too large and would not be good enough for extracting useful information

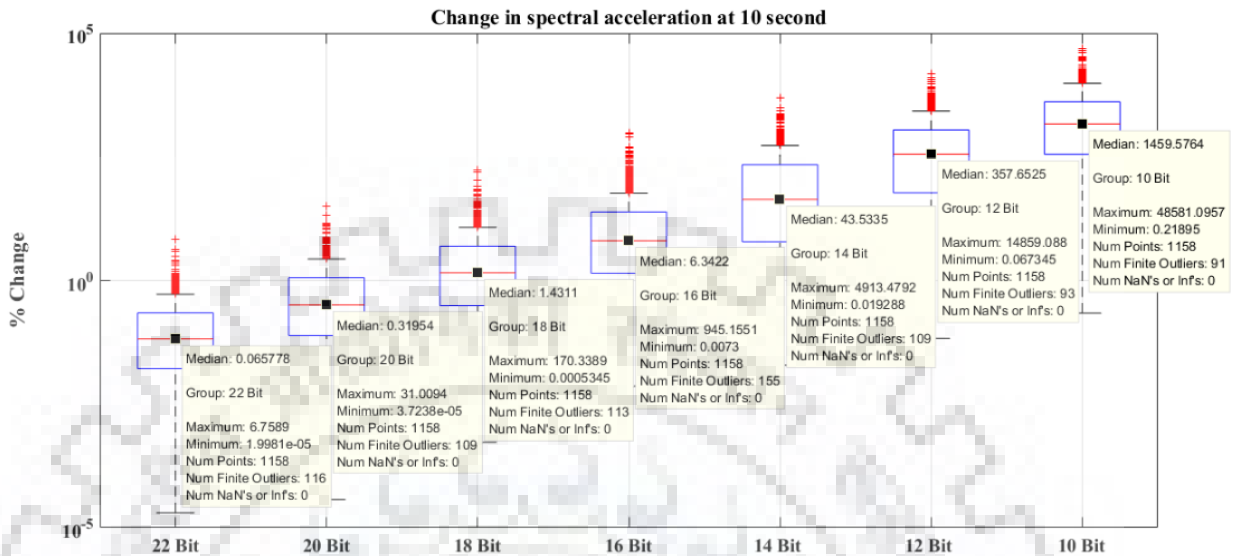


Figure 4.30: Difference in Spectral Acceleration, calculated for time histories at different ADC resolution varying from 22-Bit to 10-Bit with reference to original 24-Bit data and 10 second period.

4.4.2. Effect on Spectral Acceleration for 2% damping

Figure 4.32, shows change in spectral acceleration at 2% damping and for period zero or PGA. It is evident from the figure that for upto 10-Bit data the median error is 2.7%. Whereas up to 16 bit the error is well below 2%.

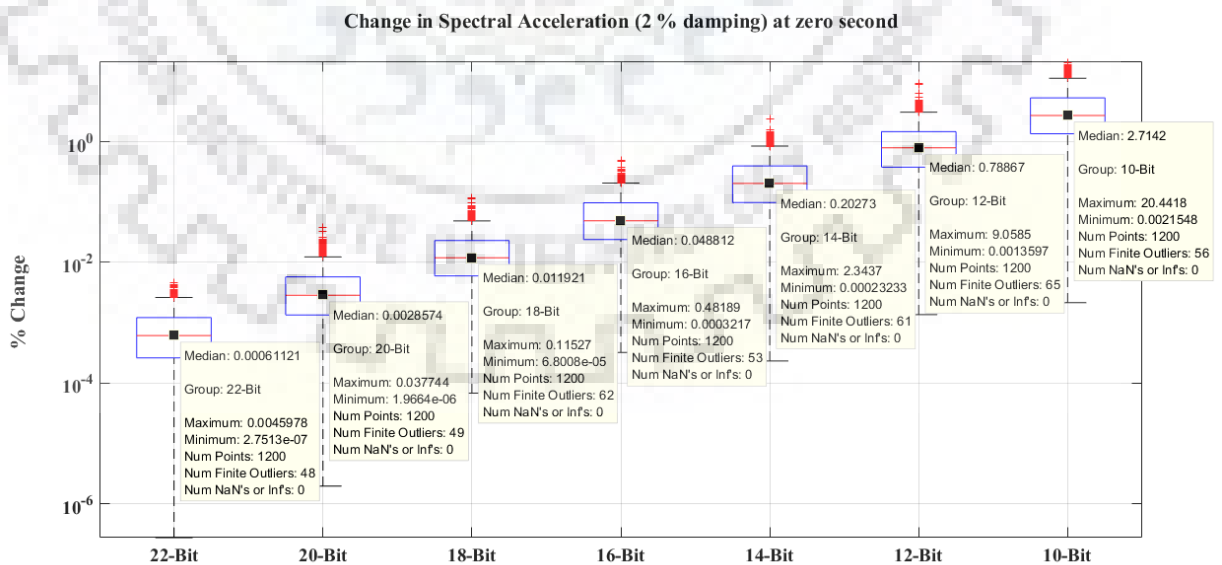


Figure 4.31: Difference in Spectral Acceleration at 2% damping, calculated for time histories at different ADC resolution varying from 22-Bit to 10-Bit with reference to original 24-Bit data and Zero period

Figure 4.33, demonstrates the error in SA values for period 0.03 and damping 2%. Here it is evident from the figure that the error is of the order 5% for 10-Bit data. Whereas, below 10-Bit data, the error is minimal and is of the order of less than 2%. For 16-Bit and more, the error is well below 0.08%.

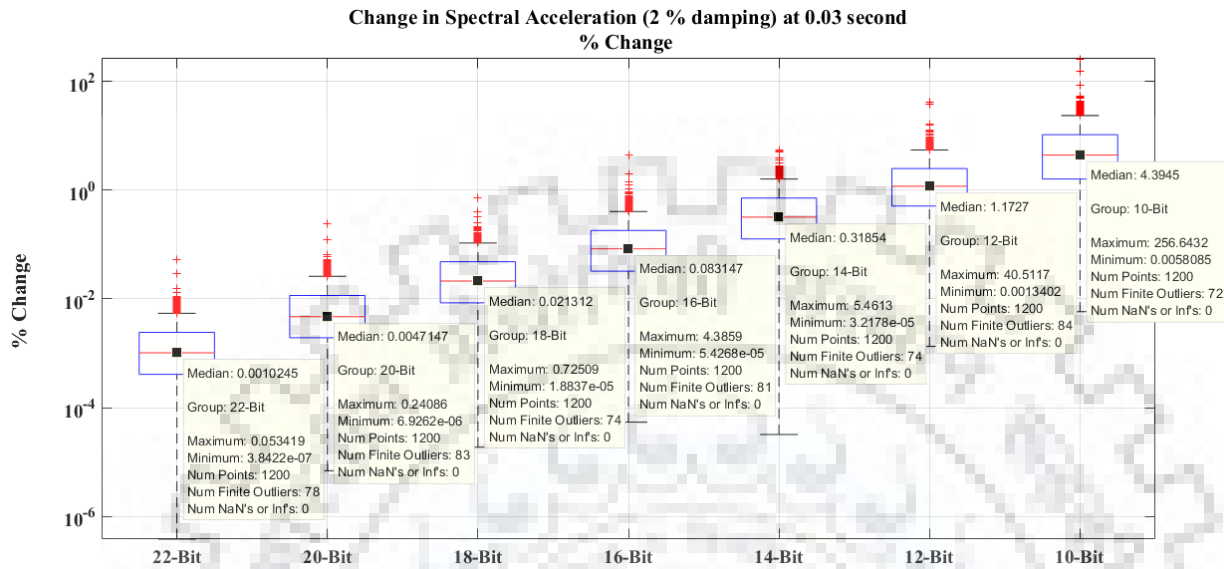


Figure 4.32: Difference in Spectral Acceleration at 2% damping, calculated for time histories at different ADC resolution varying from 22-Bit to 10-Bit with reference to original 24-Bit data and 0.03 period

Figure 4.34 shows error in SA values for 0.05 second period with respect to the 24-Bit data. Here it is evident from the figure that for 10-Bit data, the median error is less than 5%. Whereas, for 16-Bit data, the error is very small or negligible

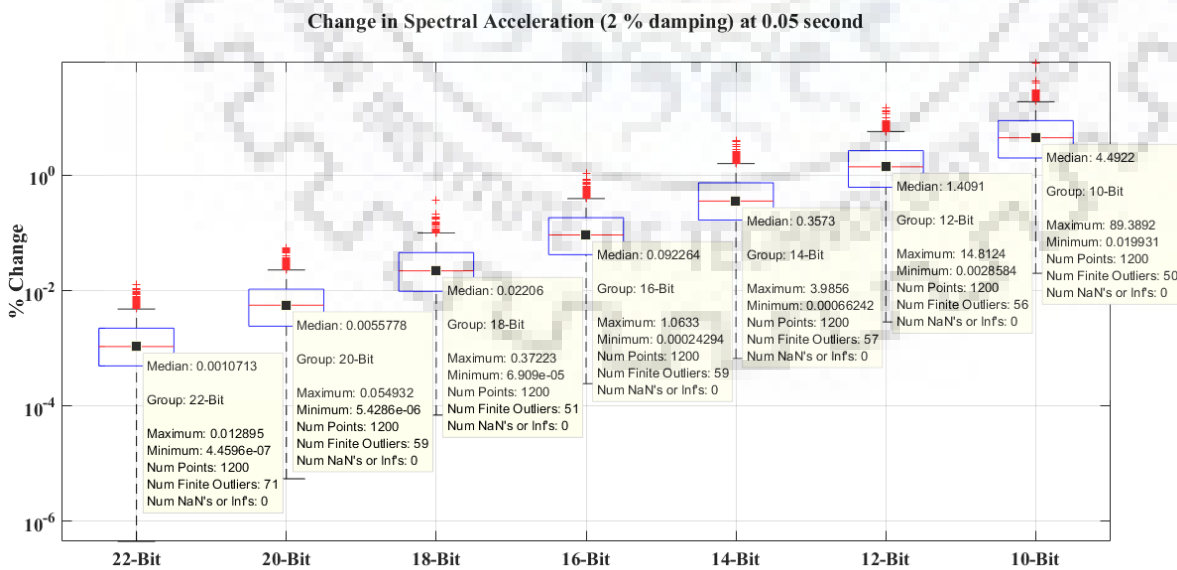


Figure 4.33: Difference in Spectral Acceleration at 2% damping, calculated for time histories at different ADC resolution varying from 22-Bit to 10-Bit with reference to original 24-Bit data and 0.05 period

Figure 4.35, explain the effect of SA values for 0.1 second period and 2 % damping. It is evident from the figure that error is well within 2% for data less than 12-Bit. For 16-Bit data, the error is less than 0.1%.

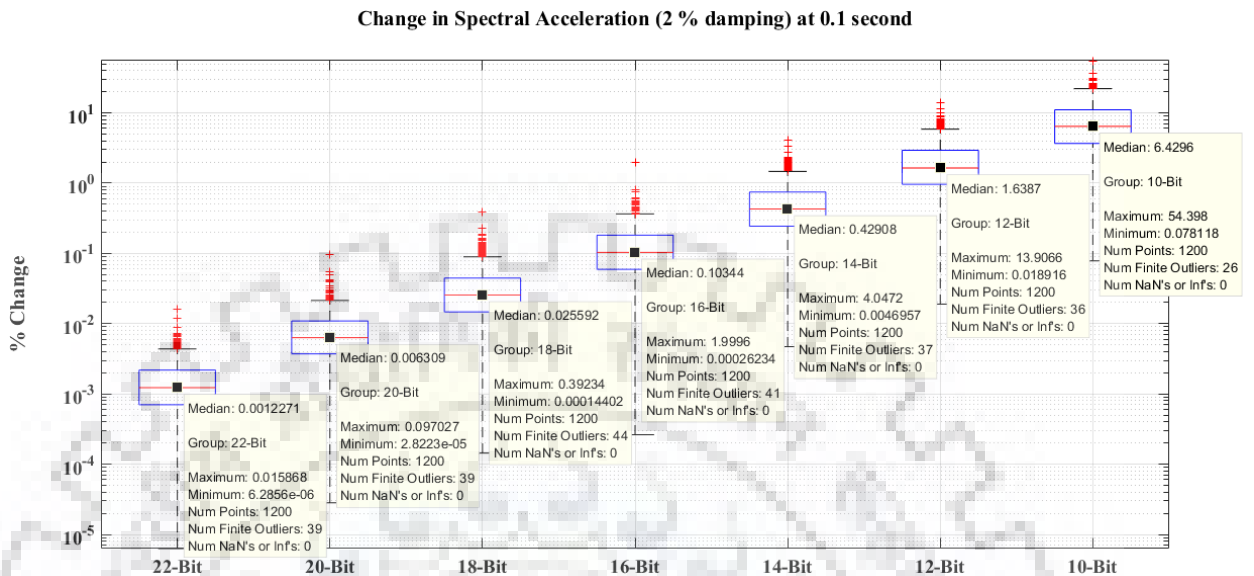


Figure 4.34: Difference in Spectral Acceleration at 2% damping, calculated for time histories at different ADC resolution varying from 22-Bit to 10-Bit with reference to original 24-Bit data and 0.1 second period

Figure 4.36, explain the error for 0.2 second period and 2% damping. It is evident from the figure that the error is well within 2% for 12-Bit data. Even for 10-Bit data, the error is of the order ~6%. However, for 16-Bit, the error is less than 0.1%.

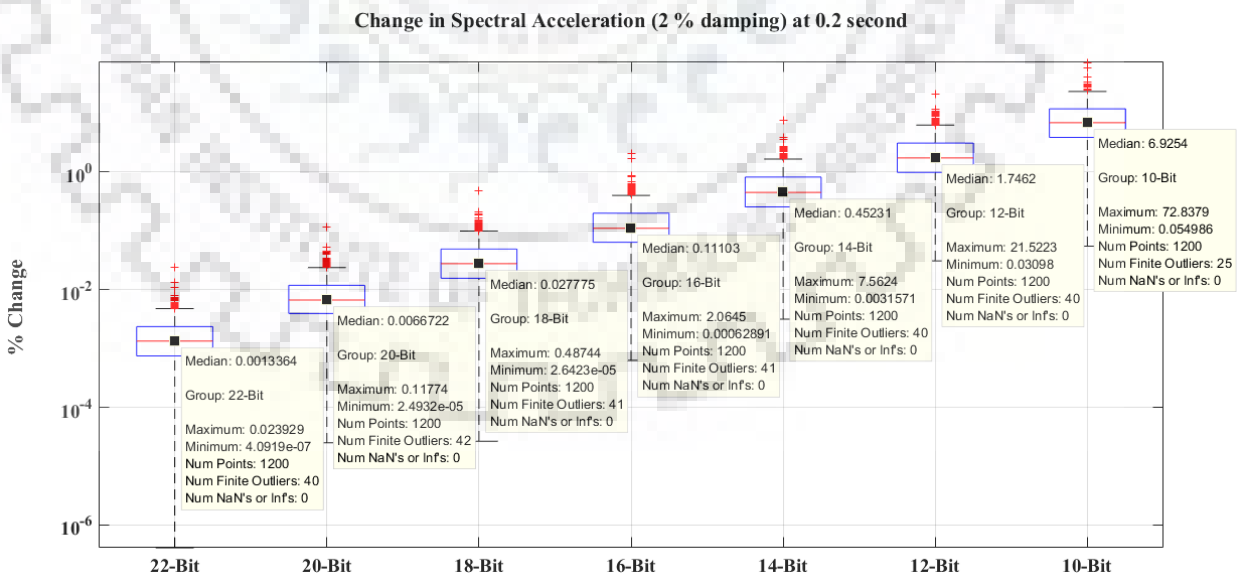


Figure 4.35: Difference in Spectral Acceleration at 2% damping, calculated for time histories at different ADC resolution varying from 22-Bit to 10-Bit with reference to original 24-Bit data and 0.2 second period

Figure 4.37, explain the error for 0.3 second period. As is evident from the figure, the error is less than 0.5% for 16-Bit data and above.

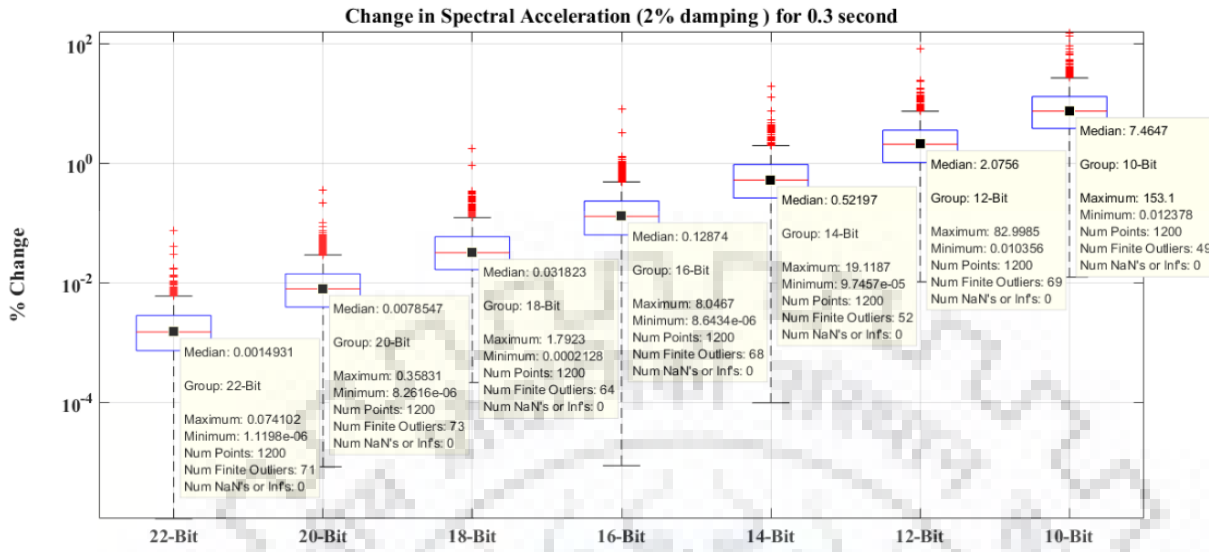


Figure 4.36: Difference in Spectral Acceleration at 2% damping, calculated for time histories at different ADC resolution varying from 22-Bit to 10-Bit with reference to original 24-Bit data and 0.3 second period

Figure 4.38, demonstrates the error in SA value for 0.5 second period and 5% damping. It can be inferred from the figure that for 12-Bit and more resolution data, the error is less than ~2% and is even less than 0.6% for 14-Bit and more.

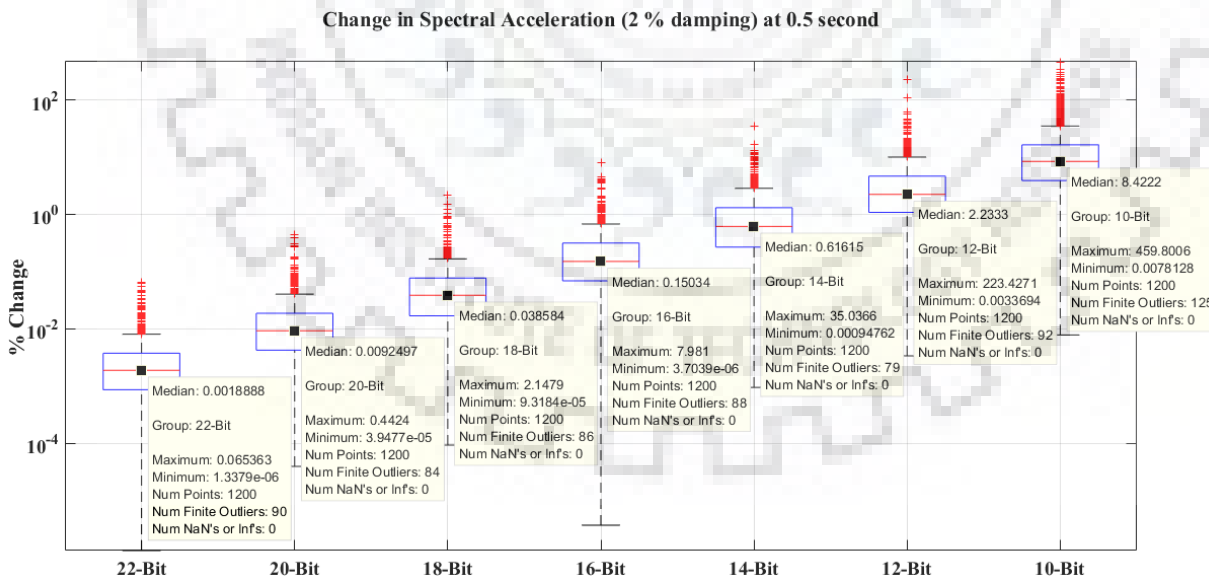


Figure 4.37: Difference in Spectral Acceleration at 2% damping, calculated for time histories at different ADC resolution varying from 22-Bit to 10-Bit with reference to original 24-Bit data and 0.5 second period

Figure 4.39, explains the error in the SA value for 0.74 seconds. It is evident that median error is even less than 0.8% for data more than 14-Bit resolution. For 16-Bit resolution, the median error is less than 0.2%.

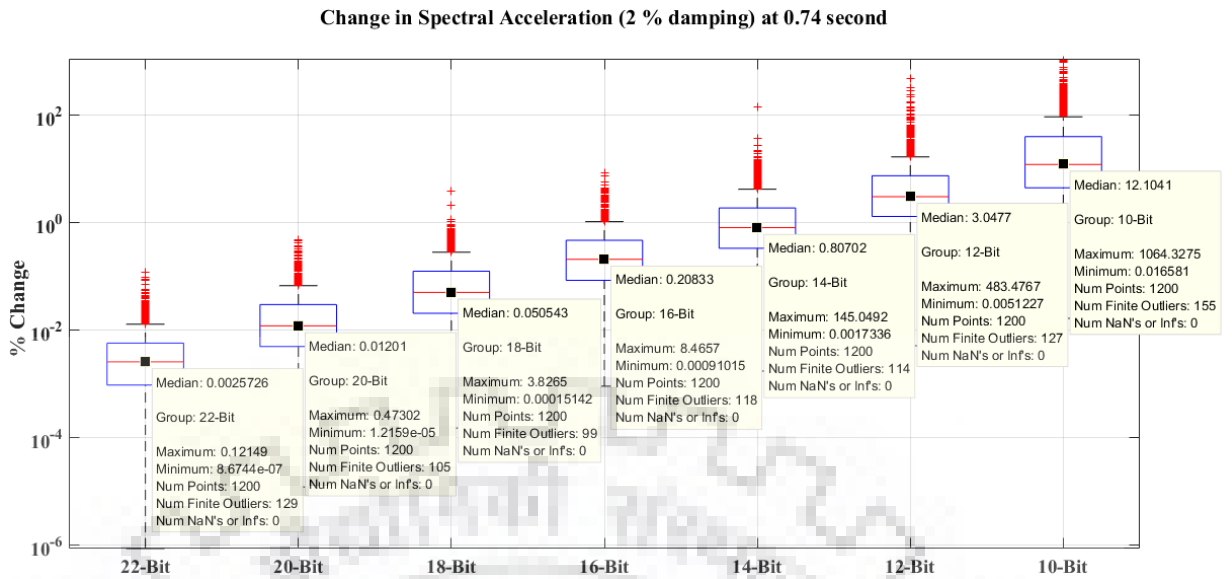


Figure 4.38: Difference in Spectral Acceleration at 2% damping, calculated for time histories at different ADC resolution varying from 22-Bit to 10-Bit with reference to original 24-Bit data and 0.74 second period

Figure 4.40, demonstrates the error in SA acceleration for 1 second period and 2% damping. It is evident from the figure that for 14-Bit and 16-Bit data, the median error is even less than 1% and 0.2%, respectively.

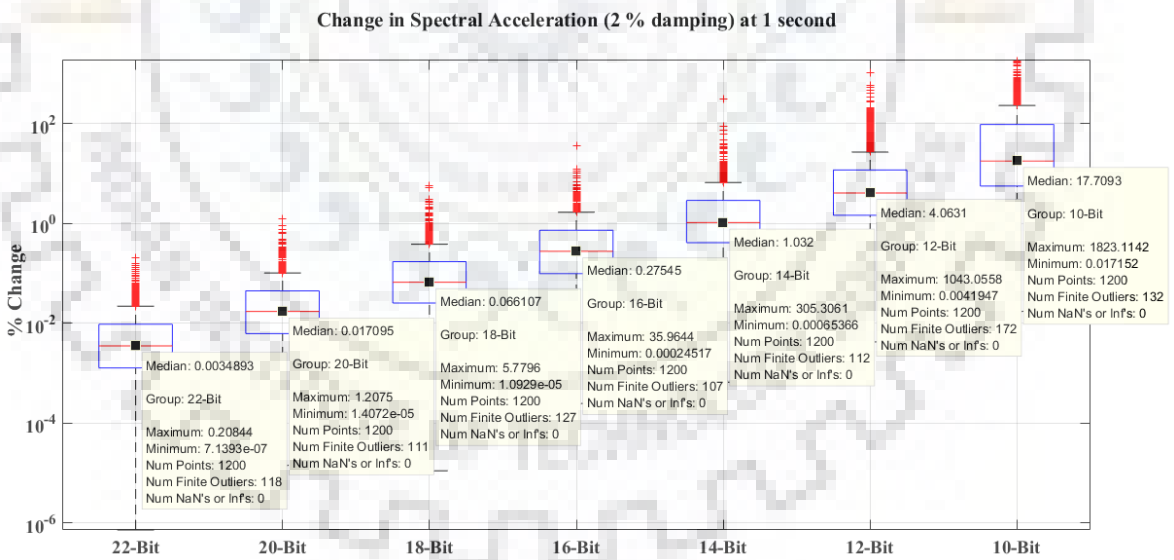


Figure 4.39: Difference in Spectral Acceleration at 2% damping, calculated for time histories at different ADC resolution varying from 22-Bit to 10-Bit with reference to original 24-Bit data and 1 second period

In Figure 4.41, it is evident that for a period of 2 seconds, the median error is of the order 2% for 14-Bit data and is even less than 0.5% for 16-Bit data.

Change in Spectral Acceleration (2 % damping) at 2 second

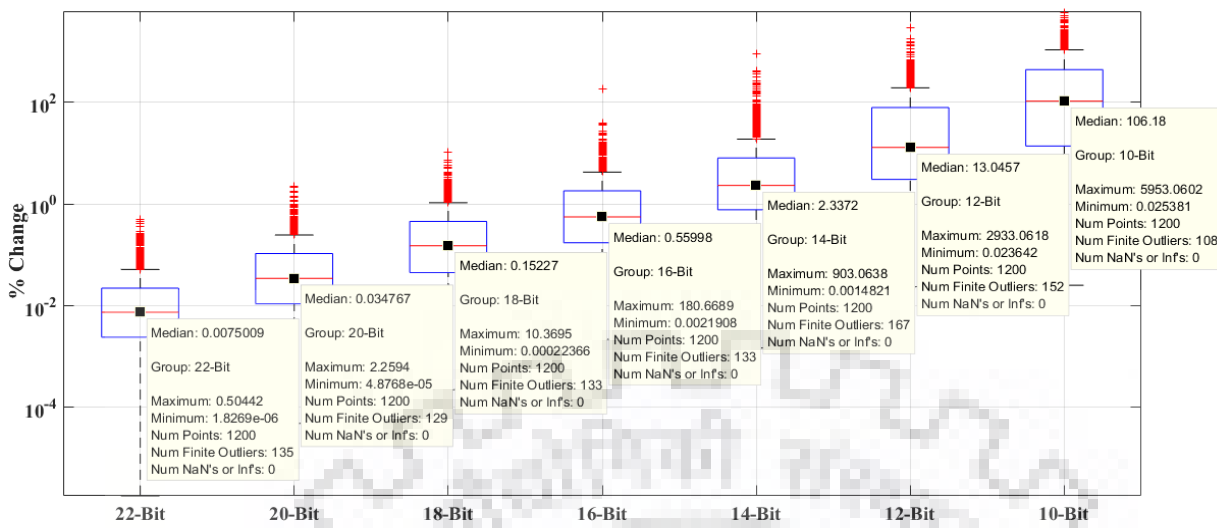


Figure 4.40: Difference in Spectral Acceleration at 2% damping, calculated for time histories at different ADC resolution varying from 22-Bit to 10-Bit with reference to original 24-Bit data and 2 second period

Figure 4.42 shows error in SA values for 3 second period and 2% damping. It is evident from the Figure that for 16-Bit data and above, the error is even less than 1%.

Change in Spectral Acceleration (2 % damping) at 3 second

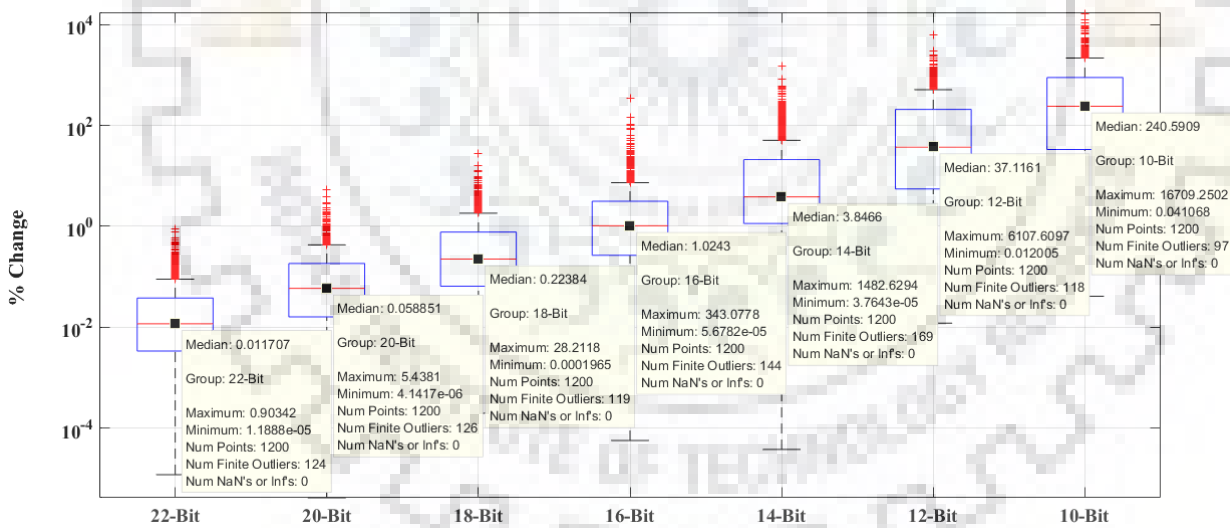


Figure 4.41: Difference in Spectral Acceleration at 2% damping, calculated for time histories at different ADC resolution varying from 22-Bit to 10-Bit with reference to original 24-Bit data and 3 second period

For 3 second period, there is a certain increase in error as Bit is further decreased beyond 14-Bit. However, for 16-Bit and more, the error is still less than ~1% (Figure 4.43).

From Figure 4.43, it can be inferred that data at 16-Bit has a median error of the order ~1%.

Whereas, for 12 and 10-Bit, the error is too large to be useful.

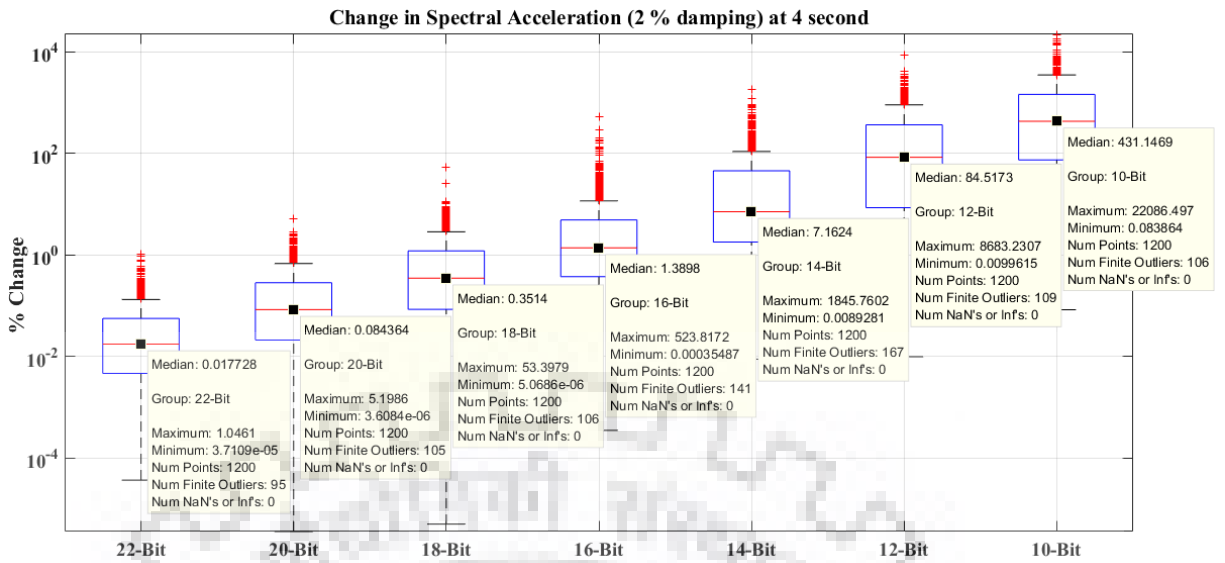


Figure 4.42: Difference in Spectral Acceleration at 2% damping, calculated for time histories at different ADC resolution varying from 22-Bit to 10-Bit with reference to original 24-Bit data and 3 second period

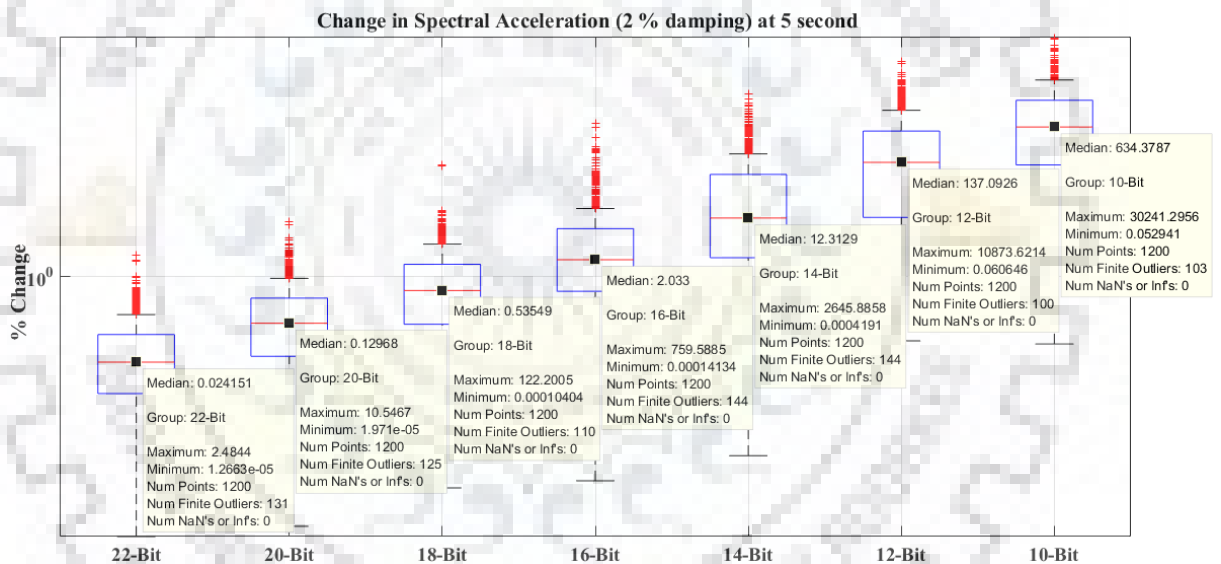


Figure 4.43: Difference in Spectral Acceleration at 2% damping, calculated for time histories at different ADC resolution varying from 22-Bit to 10-Bit with reference to original 24-Bit data and 5 second period

From figure 4.45, it can be inferred that for 7 second period, and 2% damping, the data for 16-Bit resolution and more still have an error of the order ~3%.

Change in Spectral Acceleration (2 % damping) at 7 second

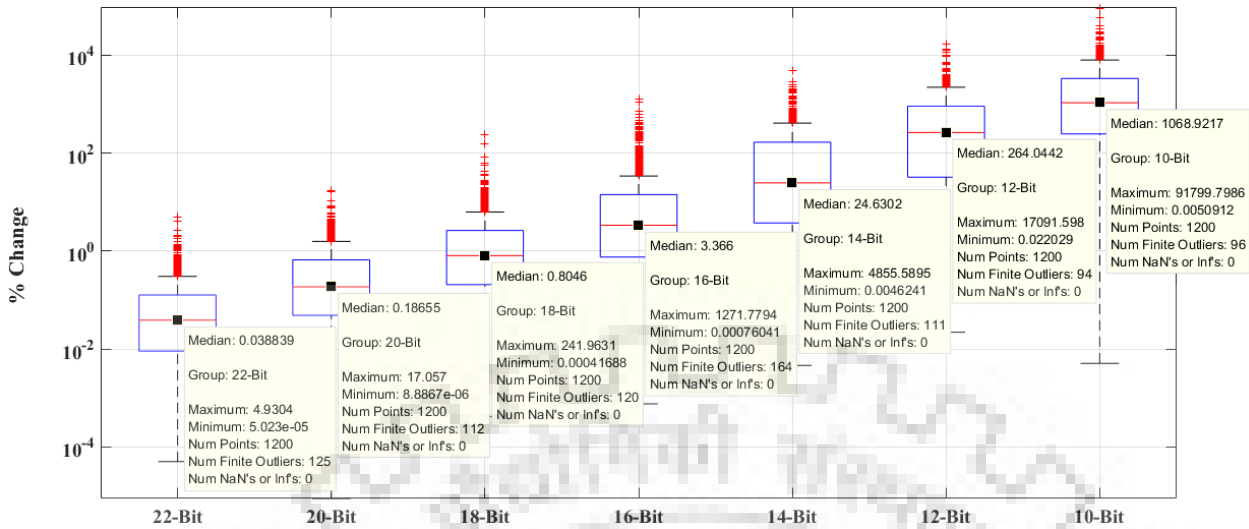


Figure 4.44: Difference in Spectral Acceleration at 2% damping, calculated for time histories at different ADC resolution varying from 22-Bit to 10-Bit with reference to original 24-Bit data and 7 second period

Figure 4.46, for data of 16-Bit resolution and more, the median error is still less than 7%

Change in Spectral Acceleration (2 % damping) at 10 second

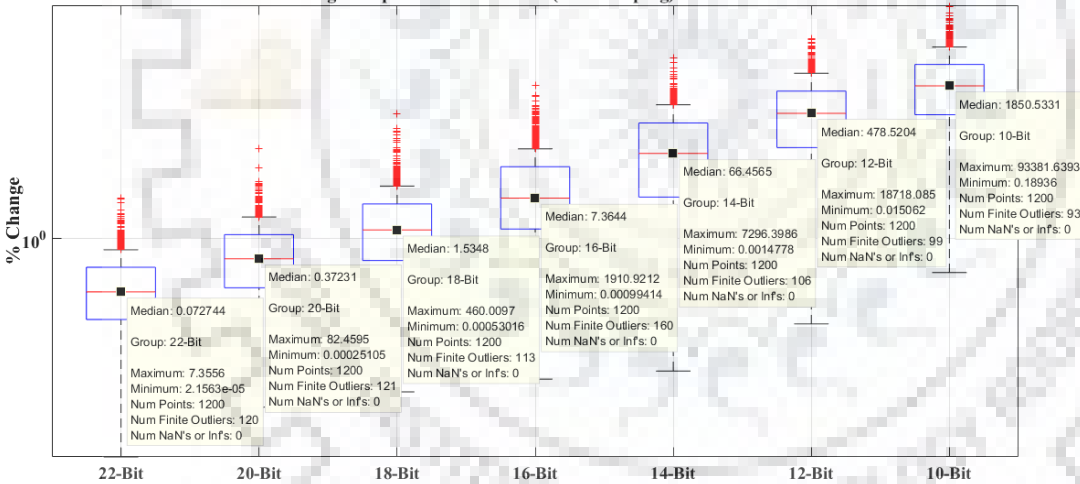


Figure 4.45: Difference in Spectral Acceleration at 2% damping, calculated for time histories at different ADC resolution varying from 22-Bit to 10-Bit with reference to original 24-Bit data and 10 second period

4.4.3. Effect on Spectral Acceleration for 10 % Damping.

In this section, the effect of lowering the Bit is discussed for 10 % damping.

In Figure 4.47, the change in SA values, for 10% damping and corresponding to zero period or PGA is discussed. All changes or errors are with respect to the 24-Bit original data and corresponding converted data to respective bits. It is evident from the figure that even for 10-Bit data, the median error is only of order 2%.

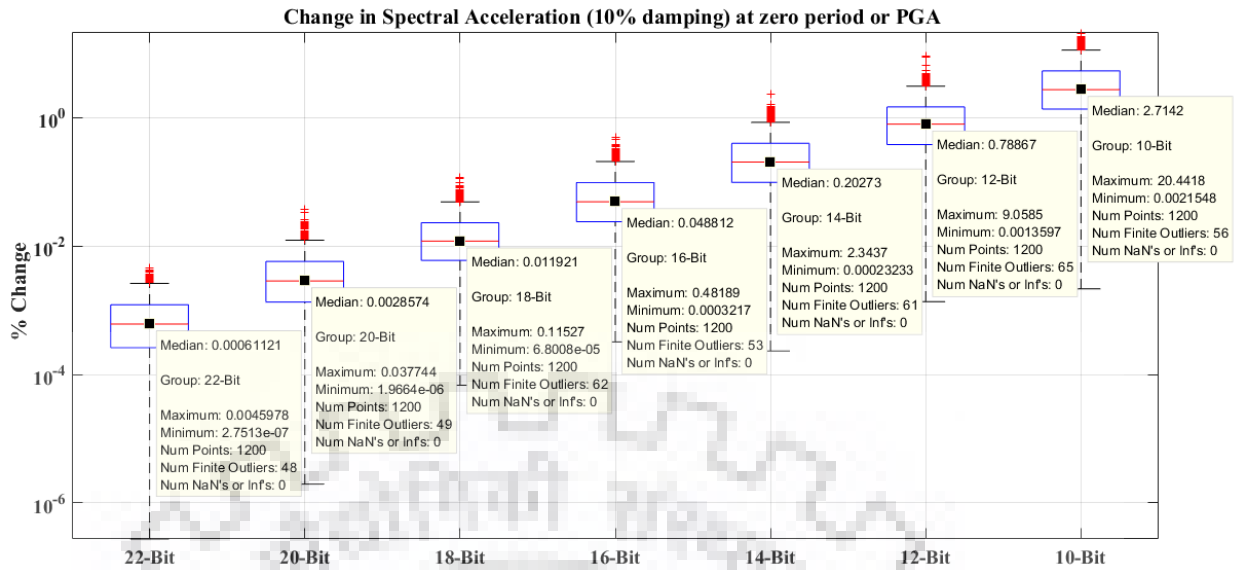


Figure 4.46: Difference in Spectral Acceleration at 10% damping, calculated for time histories at different ADC resolution varying from 22-Bit to 10-Bit with reference to original 24-Bit data and 0 second period

Figure 4.48 shows the error with respect to 0.03 seconds and 10% damping. All errors are with respect to 24-Bit unchanged actual time history. Here it is observed that for up to 10-Bit, the median error is only 2%. The median error for 216-Bit data is as low as 0.048%.

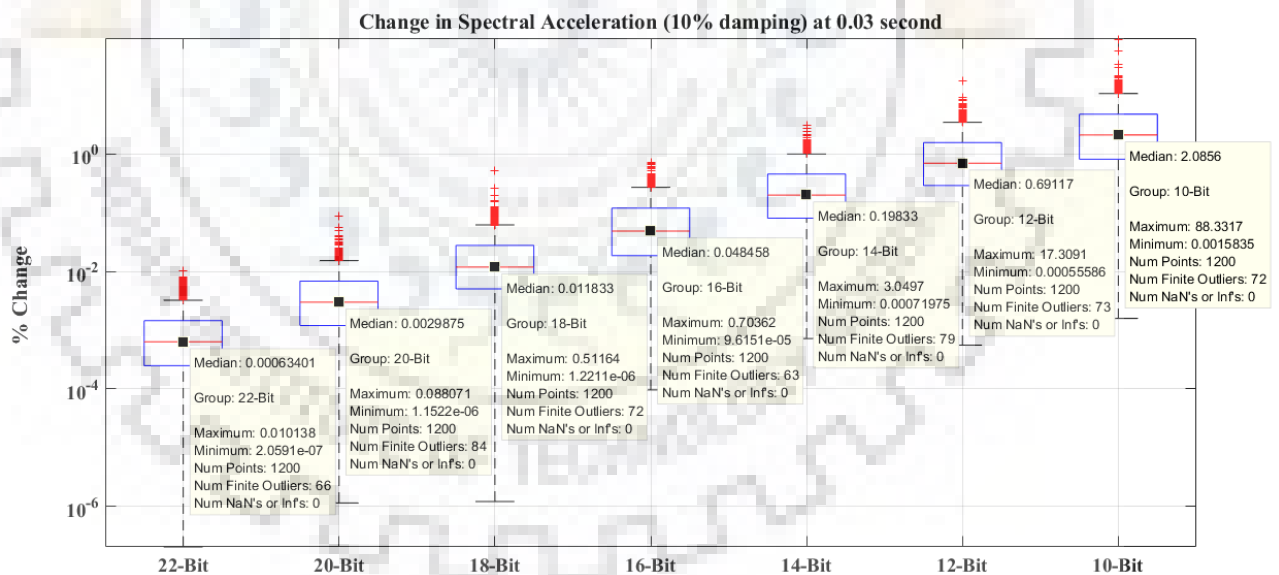


Figure 4.47: Difference in Spectral Acceleration at 10% damping, calculated for time histories at different ADC resolution varying from 22-Bit to 10-Bit with reference to original 24-Bit data and 0.03 second period

Figure 4.49 show the error for 0.05 second period and 10% damping. It is observed from the Figure that error up to 12-Bit data is nearly equal to ~1%. Whereas for 16-Bit data, the median error is as low as 0.063%.

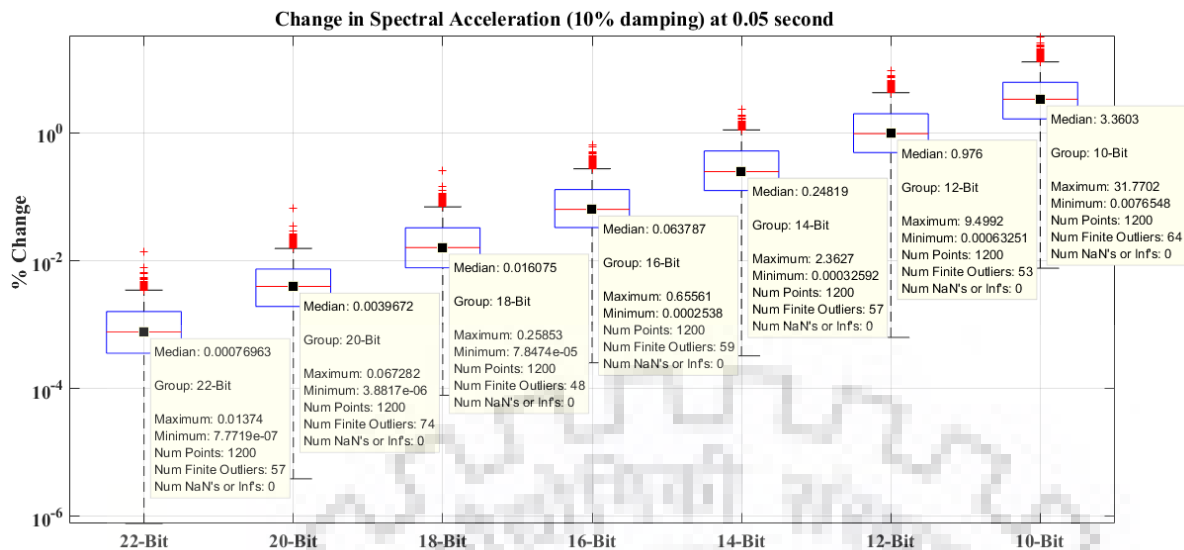


Figure 4.48: Difference in Spectral Acceleration at 10% damping, calculated for time histories at different ADC resolution varying from 22-Bit to 10-Bit with reference to original 24-Bit data and 0.05 second period

Figure 4.50, show the error for 0.2 second period and 10% damping. It is evident from the figure that for data up to 14-Bit, the median error is ~0.3%. For 16-Bit data, the median and maximum errors are 0.08% and 1.46%, respectively.

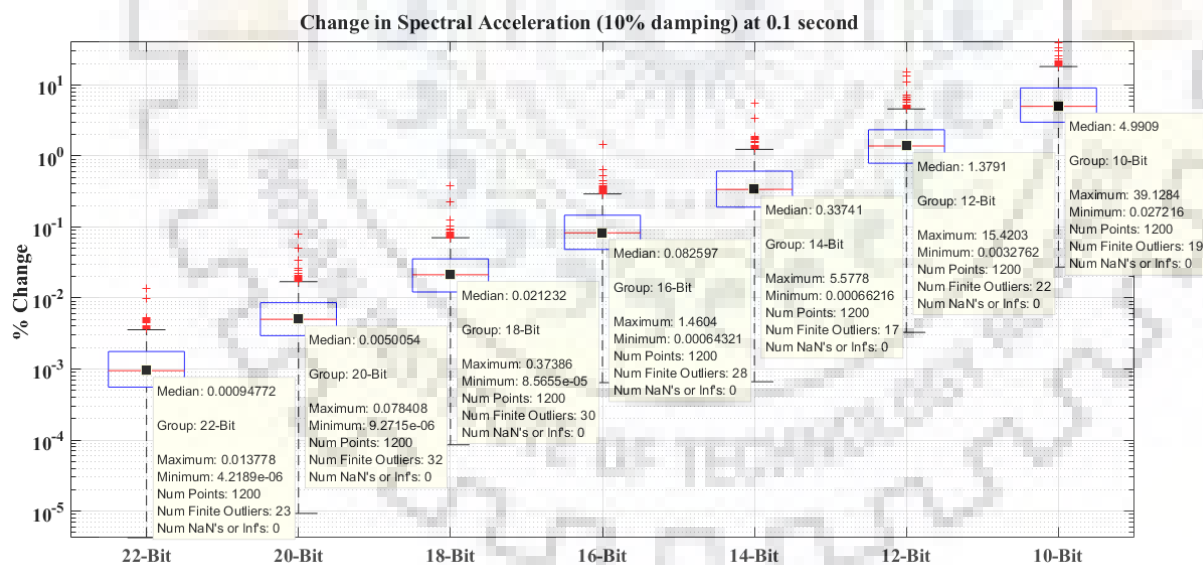


Figure 4.49: Difference in Spectral Acceleration at 10% damping, calculated for time histories at different ADC resolution varying from 22-Bit to 10-Bit with reference to original 24-Bit data and 0.1 second period

In Figure 4.51, the error for period 0.2 seconds and damping 10% is demonstrated. For up to 12-Bit, the median and maximum error are of the order ~1.4% and ~16%. Whereas for the 16-Bit record, the mean error is 0.09%, and the maximum is 0.25%.

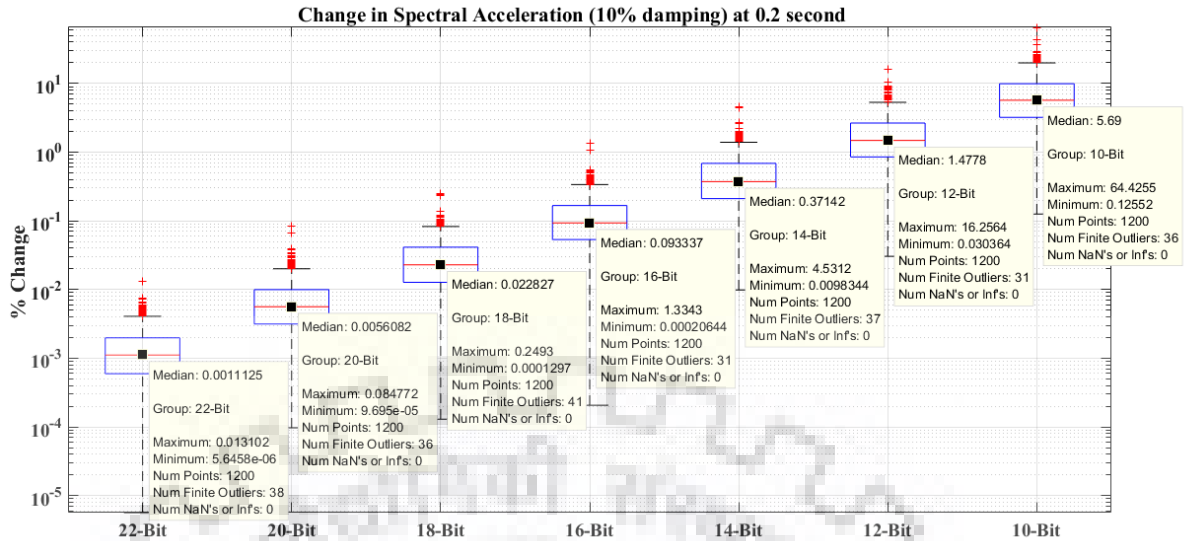


Figure 4.50: Difference in Spectral Acceleration at 10% damping, calculated for time histories at different ADC resolution varying from 22-Bit to 10-Bit with reference to original 24-Bit data and 0.2 second period

The Figure 4.52 shows the error in SA values for a 0.3 second period and 10% damping. All errors are with respect to original 24-Bit data. Here it is evident that for the 16-bit record, the mean error is 0.1 %, whereas the maximum error is 5.8%. The median and maximum error below 16-Bit data is a little over the higher side.

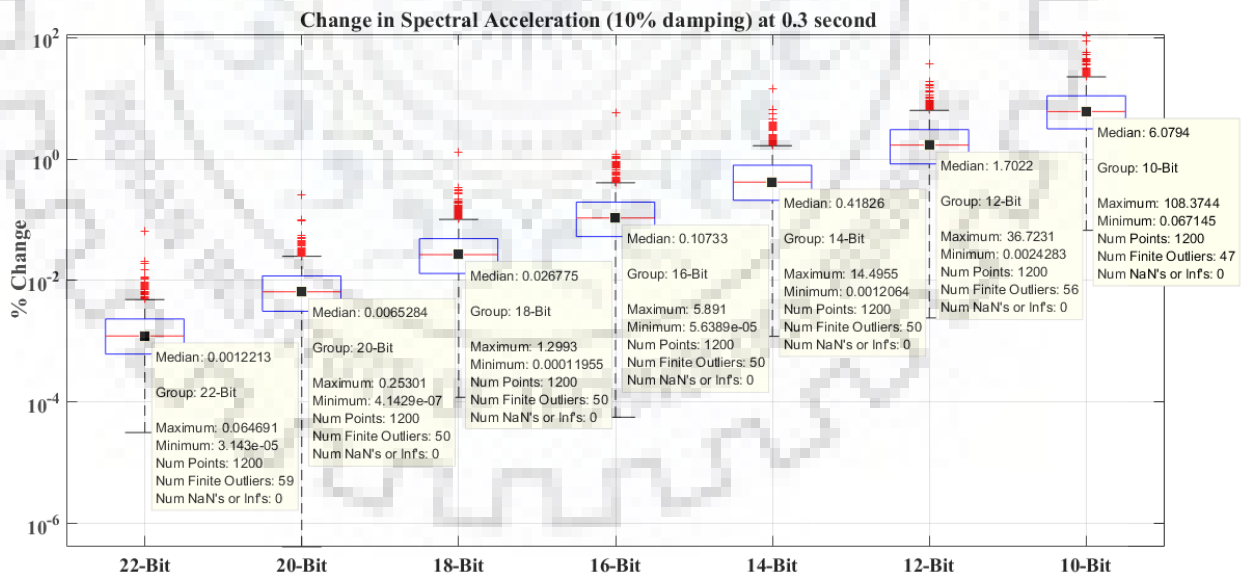


Figure 4.51: Difference in Spectral Acceleration at 10% damping, calculated for time histories at different ADC resolution varying from 22-Bit to 10-Bit with reference to original 24-Bit data and 0.3 second period

In Figure 4.53, the error is SA values for 0.5 second period, and 10% damping is compared with respect to original 24-Bit data. Here it is evident that for 16-Bit data, the median and maximum errors are 0.1% and 6.5%.

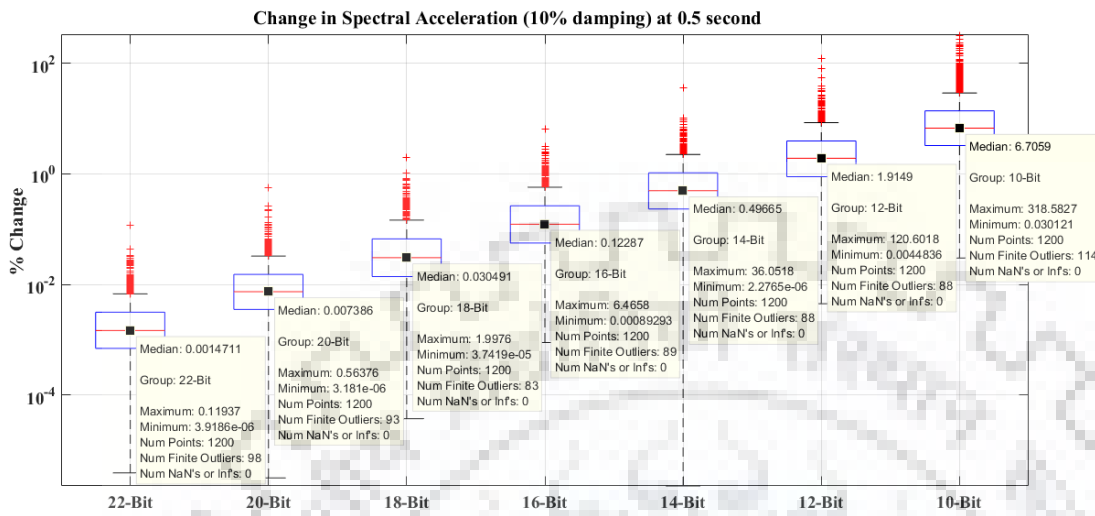


Figure 4.52: Difference in Spectral Acceleration at 10% damping, calculated for time histories at different ADC resolution varying from 22-Bit to 10-Bit with reference to original 24-Bit data and 0.5 second period

In Figure 4.54, the error in SA values for 0.74 second period is shown. Here also it is evident that for up to 16-Bit data, the median and maximum error are of the order 0.1% and 5% only. However, for 12-Bit and less, the median and maximum errors are both on the higher side.

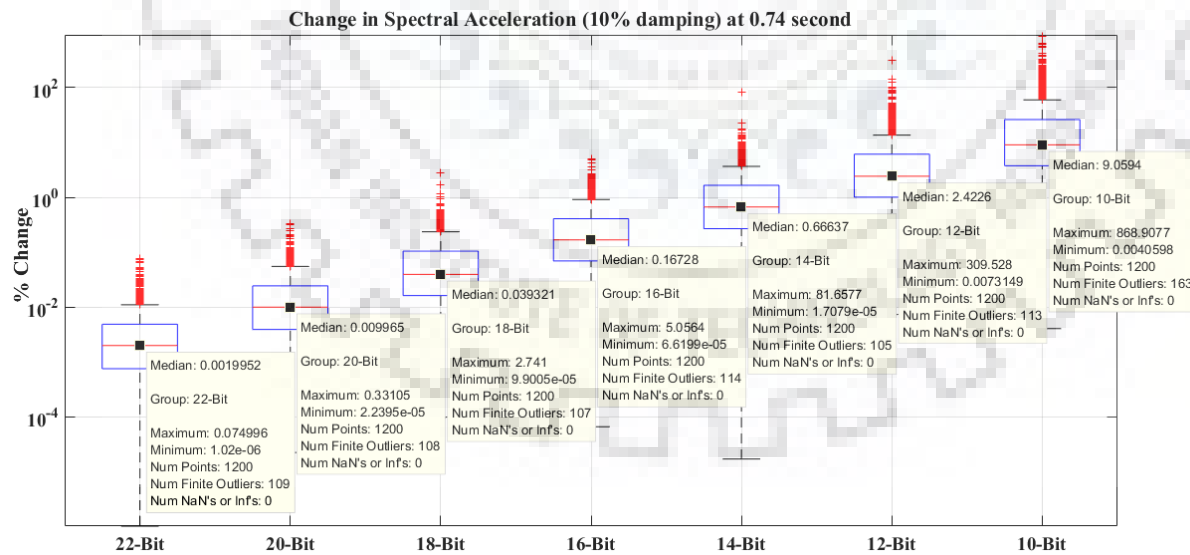


Figure 4.53: Difference in Spectral Acceleration at 10% damping, calculated for time histories at different ADC resolution varying from 22-Bit to 10-Bit with reference to original 24-Bit data and 0.74 second period

In Figure 4.55, the error in SA values for 1 second period is discussed. It is evident from the figure that for 1 second period, for up to 16-Bit data, the median and maximum error are of the order 0.2% and 15%

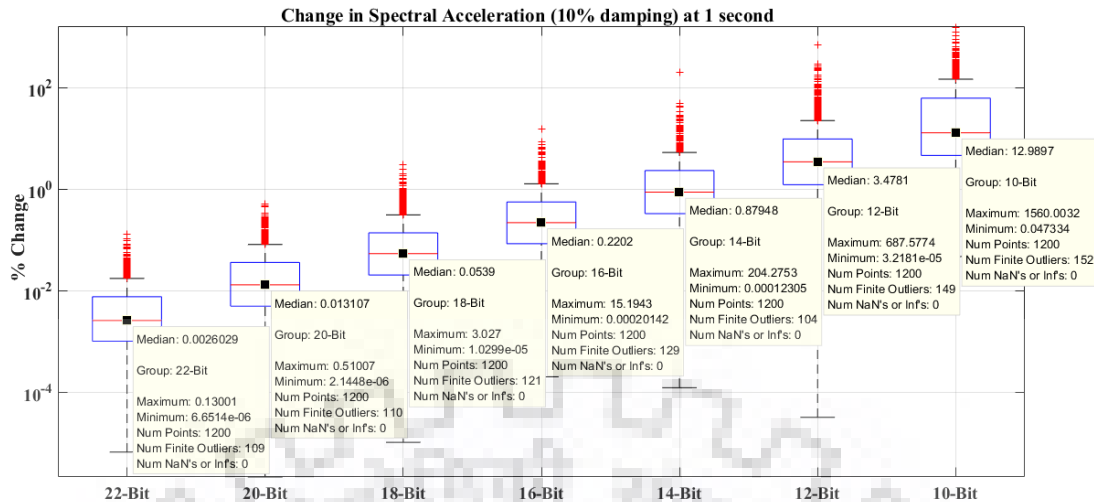


Figure 4.54: Difference in Spectral Acceleration at 10% damping, calculated for time histories at different ADC resolution varying from 22-Bit to 10-Bit with reference to original 24-Bit data and 1 second period

Figure 4.56 represents the change in SA values for 2 second period. It is evident from the figure that for 16-Bit data, the median error is still less than 0.45 %.

Figure 4.57 represents the error for 2 second period and damping 10%. Here also it is observed that the median error is less than ~ 1% for data more than 16-Bit.

Figure 4.58 shows the error in SA values for 4 second period. It is evident from the figure that for 16-Bit and more data, the median error is still of the order ~1%.

Figure 4.58 shows the error in SA values for 4 second period. It is evident from the figure that for 16-Bit and more data, the median error is still of the order ~1%.

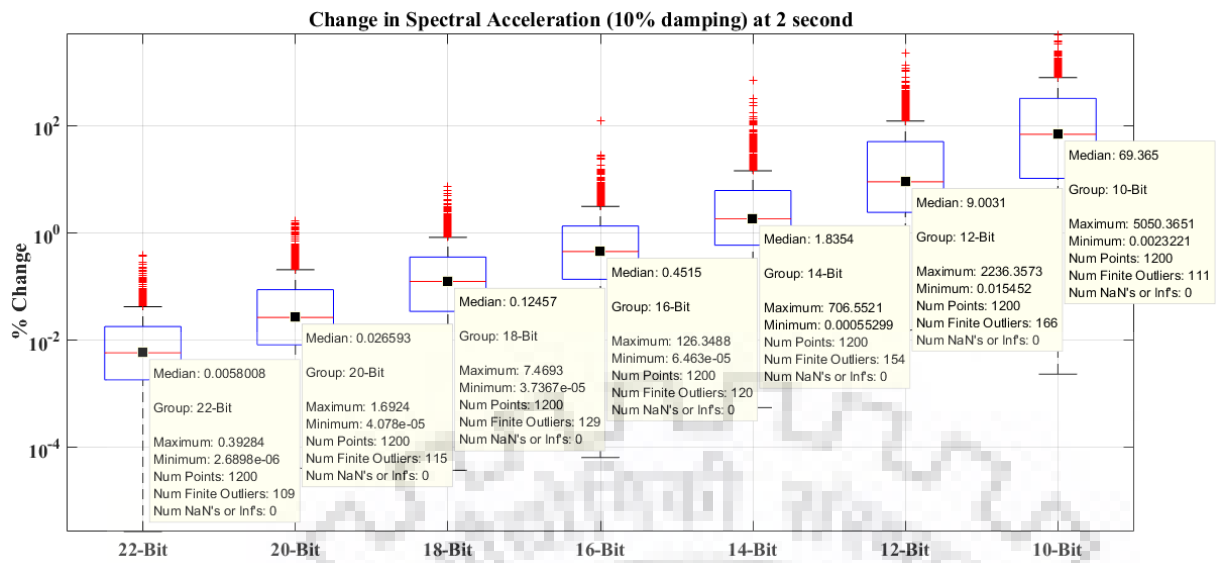


Figure 4.55: Difference in Spectral Acceleration at 10% damping, calculated for time histories at different ADC resolution varying from 22-Bit to 10-Bit with reference to original 24-Bit data and 2 second period

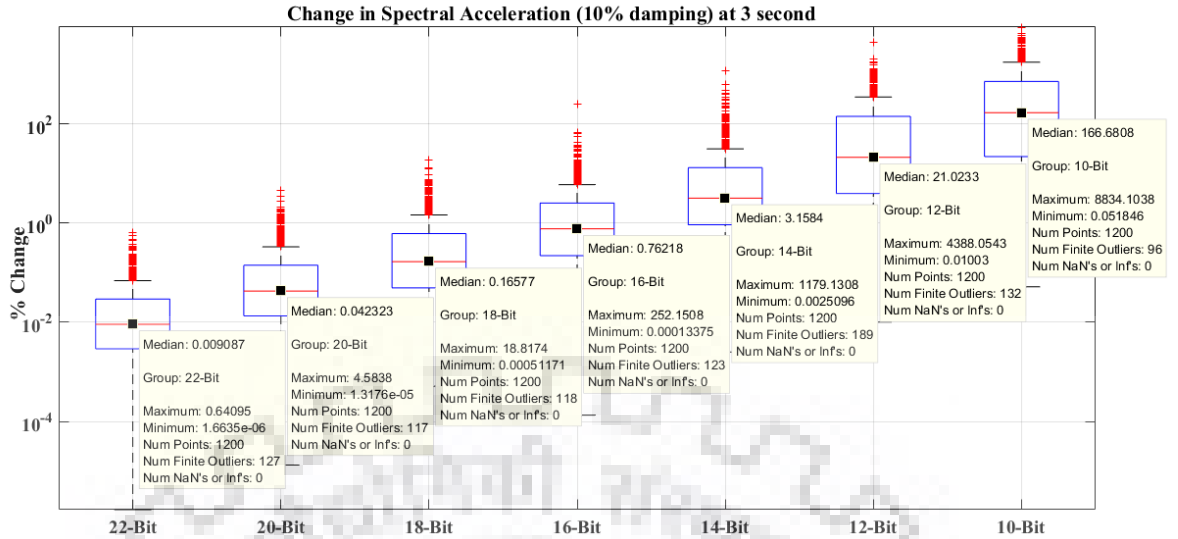


Figure 4.56: Difference in Spectral Acceleration at 10% damping, calculated for time histories at different ADC resolution varying from 22-Bit to 10-Bit with reference to original 24-Bit data and 3 second period

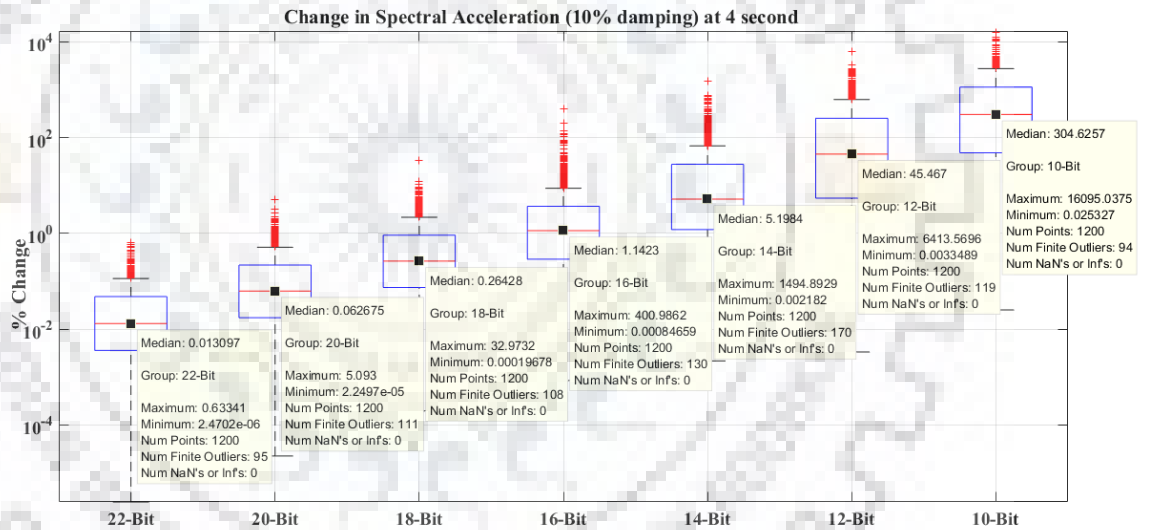


Figure 4.57: Difference in Spectral Acceleration at 10% damping, calculated for time histories at different ADC resolution varying from 22-Bit to 10-Bit with reference to original 24-Bit data and 4 second period

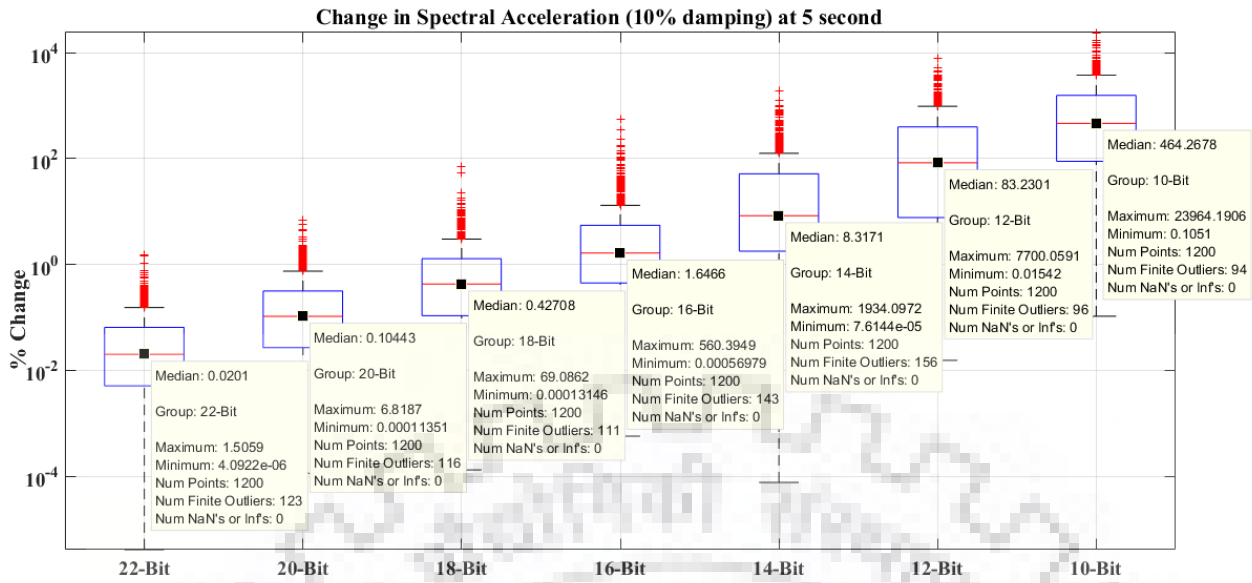


Figure 4.58: Difference in Spectral Acceleration at 10% damping, calculated for time histories at different ADC resolution varying from 22-Bit to 10-Bit with reference to original 24-Bit data and 5 second period

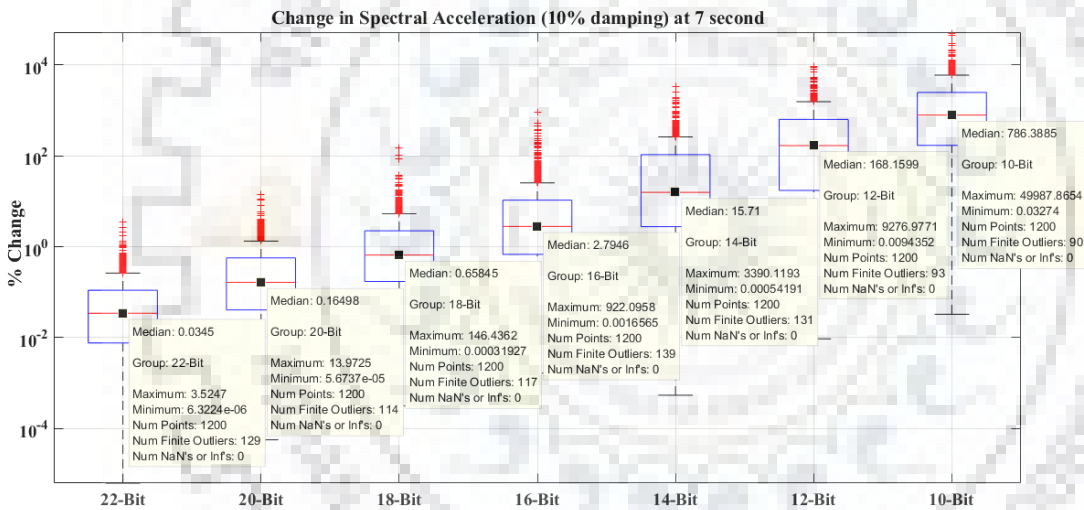


Figure 4.59: Difference in Spectral Acceleration at 10% damping, calculated for time histories at different ADC resolution varying from 22-Bit to 10-Bit with reference to original 24-Bit data and 7 second period

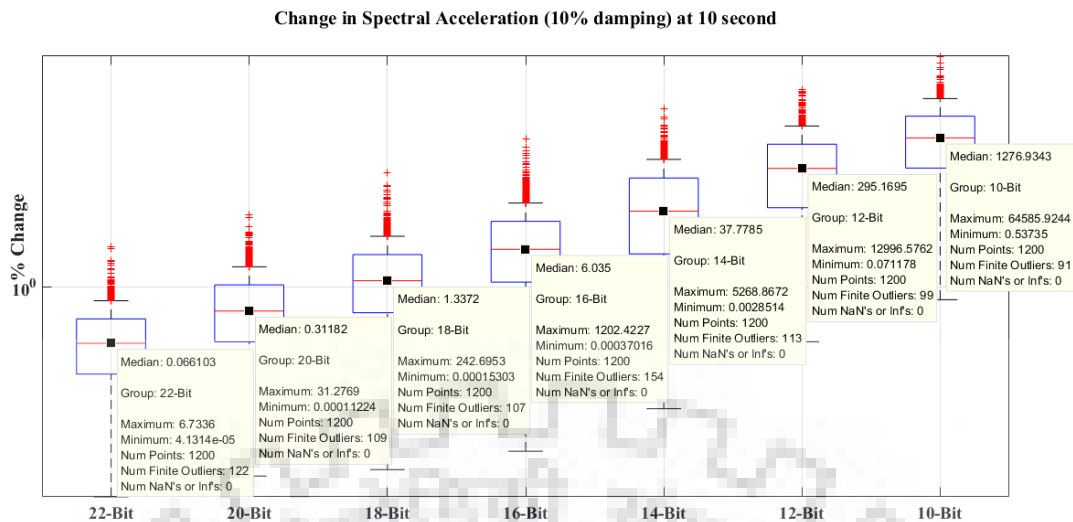


Figure 4.60: Difference in Spectral Acceleration at 10% damping, calculated for time histories at different ADC resolution varying from 22-Bit to 10-Bit with reference to original 24-Bit data and 10 second period

4.5 Effect on Fourier spectrum or Fourier amplitude.

For most engineering applications the earthquake data is converted from the time domain to Frequency-Domain. The method of converting data to an alternate frequency-domain is known as Fourier Transform. The Fourier transform is derived from the Fourier series, and it is established that all the periodic functions can be represented as the sum of sine and cosine functions. The Fourier transform is generally expressed in the form of a complex number for each frequency. The norm of the complex number is called amplitude for the corresponding frequency or Fourier spectrum. The square of Fourier spectrum is also known as power spectrum. In this analysis, the error in Fourier amplitude of converted time histories, with respect to original 24-Bit data, has been calculated. Important frequencies, shown in table 2, which have been derived from the important time periods from table 1 have been considered for analysis.

Table 4.2 Representative frequencies used for analysis of Fourier Amplitudes. The frequencies are corresponding to the periods used for spectral acceleration analysis

Frequency(Hz)													
25	20	10	5	3.33	2	1.35	1	.5	.33	.25	.2	.14	.1

4.5.4. Effect on Fourier amplitude

In Figure 4.62, Change in Fourier amplitude corresponding to the 25 Hz frequency has been shown for all seven groups of converted time histories viz. 22-Bit, 20-Bit, 18-Bit, 16-Bit, 14-Bit, 12-Bit and 10-Bit.

The median error for 22-Bit is 0.002%, and the maximum error is 0.139%. Also, the 75th percentile value is 0.004, and the 25th percentile value is 0.001 %.

Also, up to 16-Bit, the median error is of the order 0.179 %, and the maximum error is also 11.62%

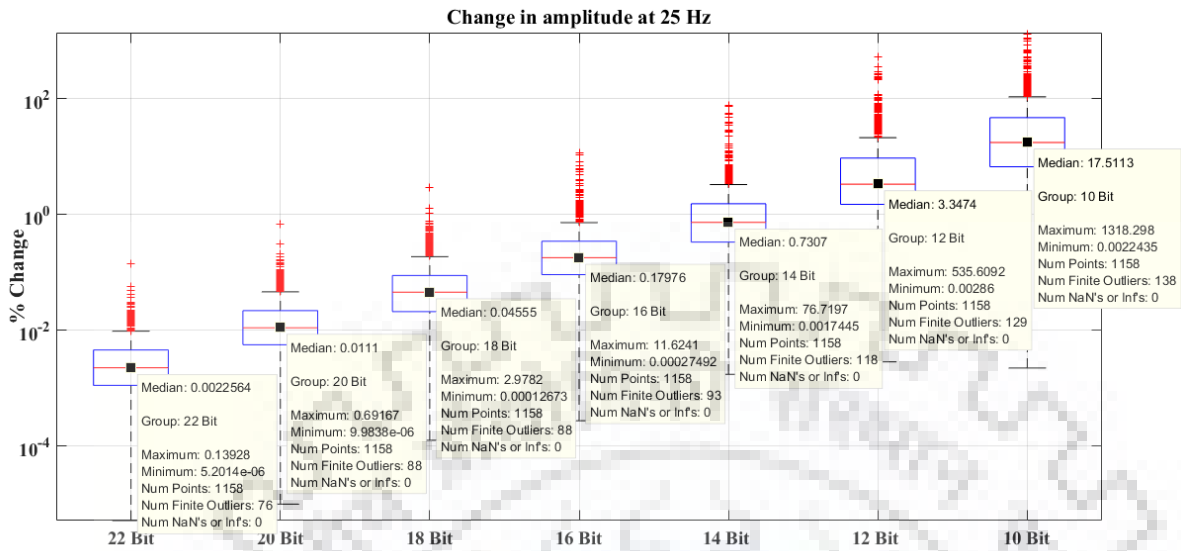


Figure 4.61: Difference in Fourier Amplitude, calculated for time histories at different ADC resolution varying from 22-Bit to 10-Bit with reference to original 24-Bit data and 25 Hz frequency.

Figure 4.63 show the error for 20 Hz data. It can be seen from the figure that the median error for 22-Bit data is 0.002%, whereas the maximum error is 0.139% only. The 75th and 35th percentile values are 0.0038 and 0.001 % only.

For 16-Bit data, the median error is 0.16% and has a maximum value of 11.49 %. The 75th and 25th percentile values are at 0.3 and 0.07%.

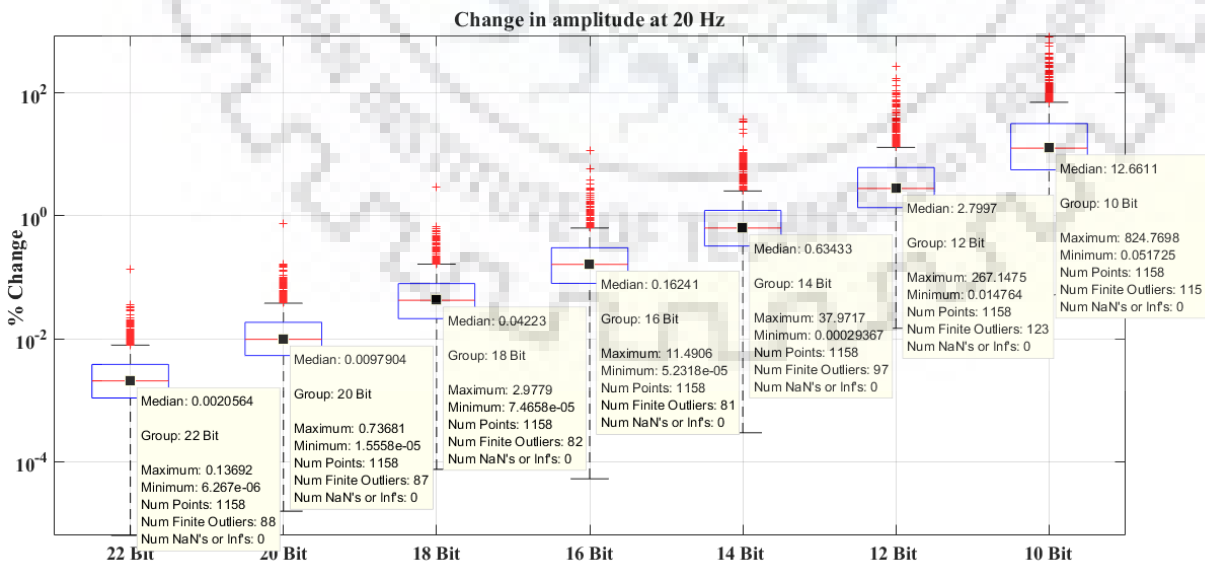


Figure 4.62: Difference in Fourier amplitude, calculated for time histories at different adc resolution varying from 22-bit to 10-bit with reference to original 24-bit data and 20 hz frequency.

In Figure 4.64, the error corresponding to frequency 10 Hz has been discussed. The median and maximum error for 22-Bit data are 0.002 and 0.07%, respectively. The 75th percentile error value is at 0.003, and the 25th percentile error value is at 0.001%.

For 16-Bit data, the median error is 0.16% and has maximum values of 4.8%. The 75th and 25th percentile values are at 0.29 and 0.09%.

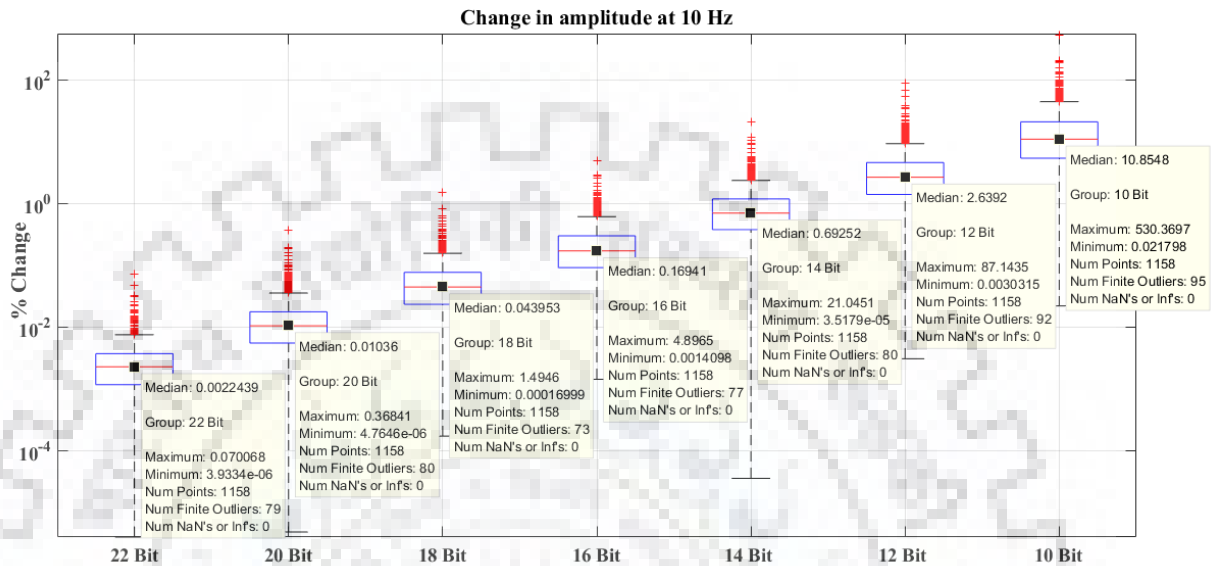


Figure 4.63: Difference in Fourier Amplitude, calculated for time histories at different ADC resolution varying from 22-Bit to 10-Bit with reference to original 24-Bit data and 10 Hz frequency.

Figure 4.65, the error in Fourier amplitude with respect to 5 Hz frequency are shown. Here the median error for 22-Bit data is 0.0022%, and the maximum error is 0.11%.

For 16-Bit data, the median error is 0.185% and has maximum values of 4.05%. The 75th and 25th percentile values are at 0.32 and 0.092%.

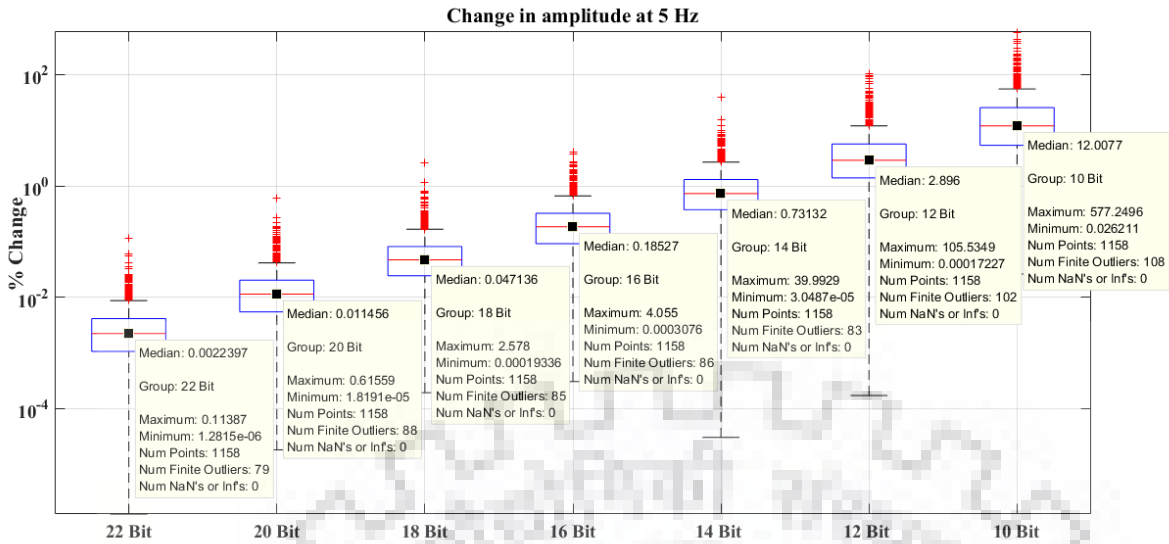


Figure 4.64: Difference in Fourier Amplitude, calculated for time histories at different ADC resolution varying from 22-Bit to 10-Bit with reference to original 24-Bit data and 5 Hz frequency.

In Figure 4.66, the error in Fourier amplitude for 3.33 Hz are shown. The median and maximum error corresponding to 22-Bit data are as 0.002 and 0.15% only.

For 16-Bit data, the median error is 0.2% and has maximum values of 7.3%. The 75th and 25th percentile values are at 0.39 and 0.09%.

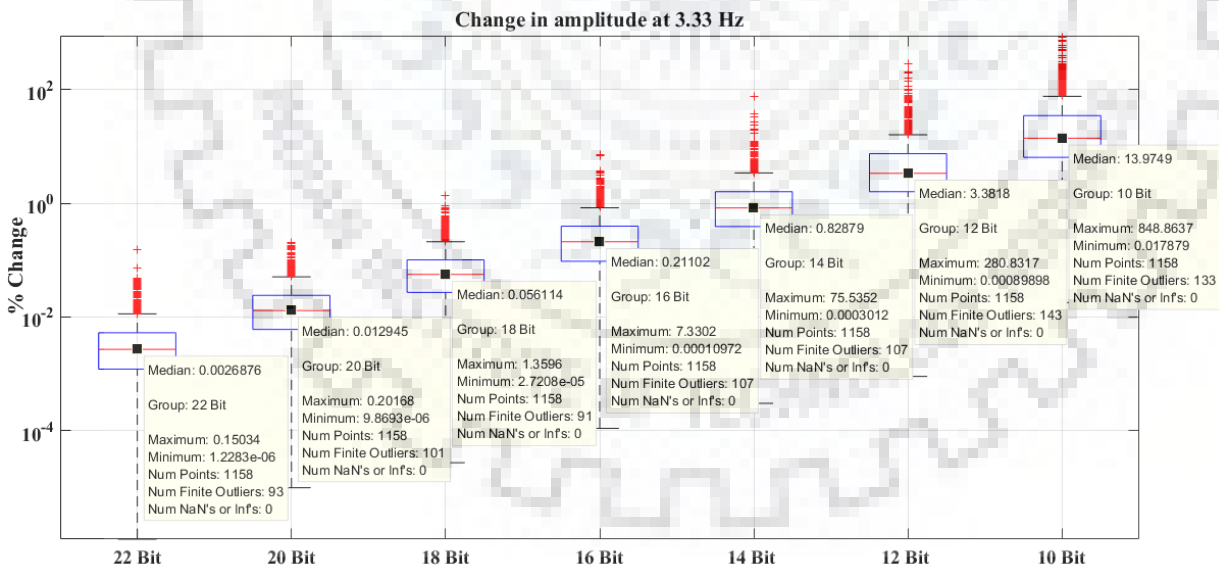


Figure 4.65: Difference in Fourier Amplitude, calculated for time histories at different ADC resolution varying from 22-Bit to 10-Bit with reference to original 24-Bit data and 3.33 Hz frequency.

In Figure 4.67, the error in Fourier amplitude for 2 Hz have been discussed. The median and maximum error corresponding to 22-Bit data are as 0.003 and 0.13% only.

For 16-Bit data the median error is 0.25% and has maximum values of 20.11%. The 75th and 25th percentile values are at 0.57 and 0.119%.

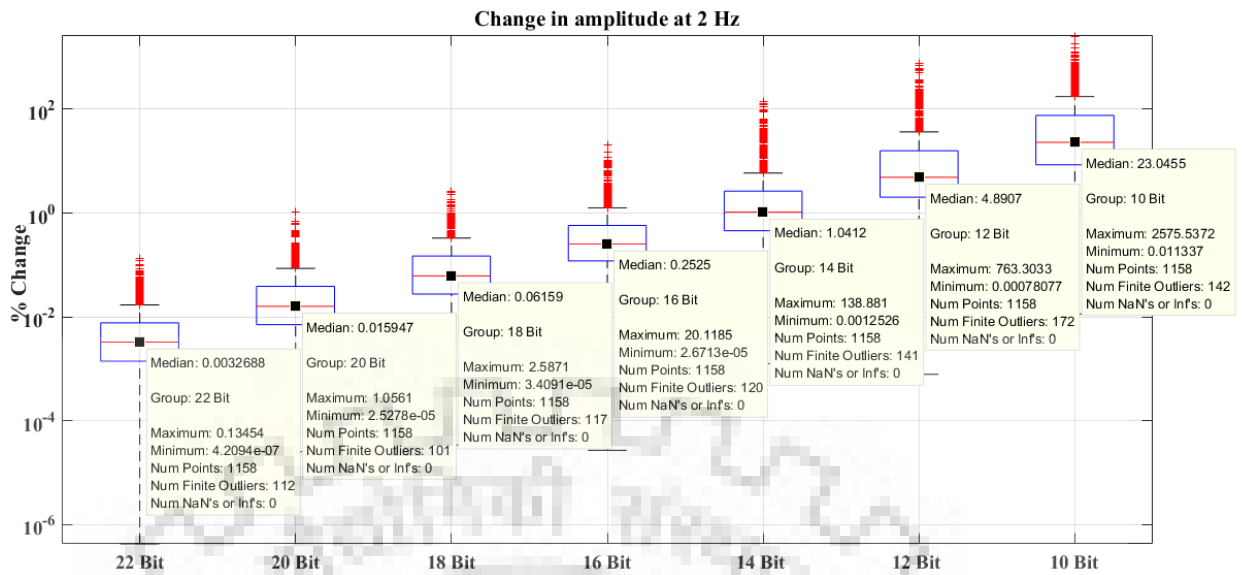


Figure 4.66: Difference in Fourier Amplitude, calculated for time histories at different ADC resolution varying from 22-Bit to 10-Bit with reference to original 24-Bit data and 2 Hz frequency.

In Figure 5.68, the error in Fourier amplitude for 1.35 Hz are shown. The median and maximum error corresponding to 22-Bit data are as 0.0043 and 0.43%, respectively.

For 16-Bit data the median error is 0.33%, and the 75th and 25th percentile values are at 1.01 and 0.13%.

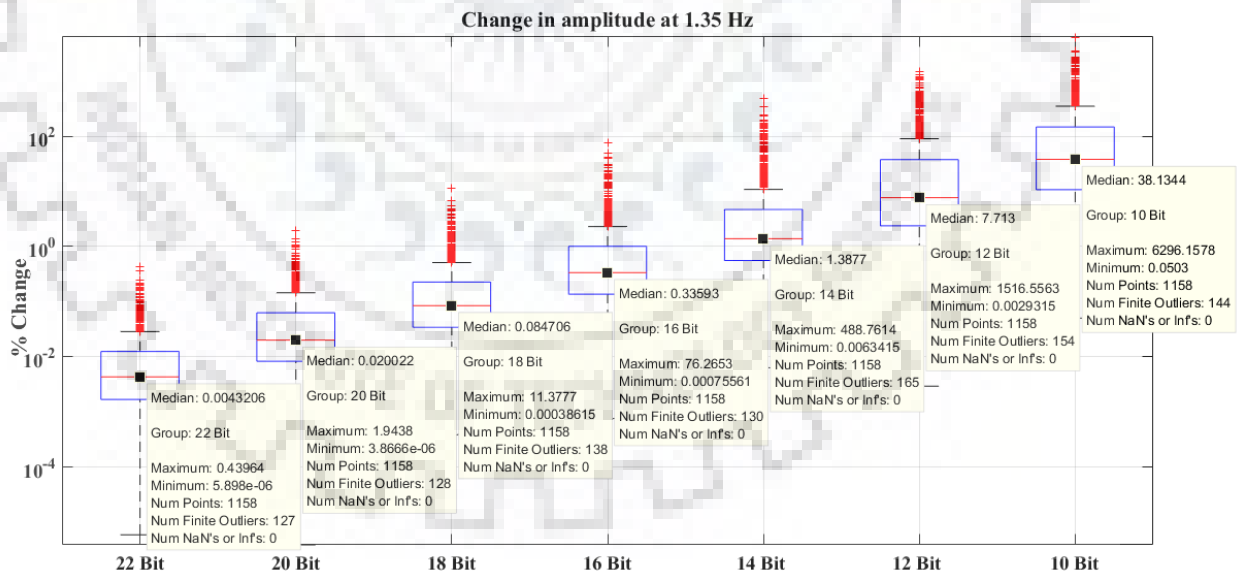


Figure 4.67: Difference in Fourier Amplitude, calculated for time histories at different ADC resolution varying from 22-Bit to 10-Bit with reference to original 24-Bit data and 1.35 Hz frequency.

The error corresponding to the 1 Hz frequency in Fourier amplitudes are given in Figure 4.69. It is observed that the median error corresponding to 22-bit data is 0.055 whereas the maximum error is 0.69%.

For 16-bit data, the median and maximum error are 0.44%, and the maximum values are at ~125%. The 75th percentile and 25th percentile values are 1.5 and 0.165%, only

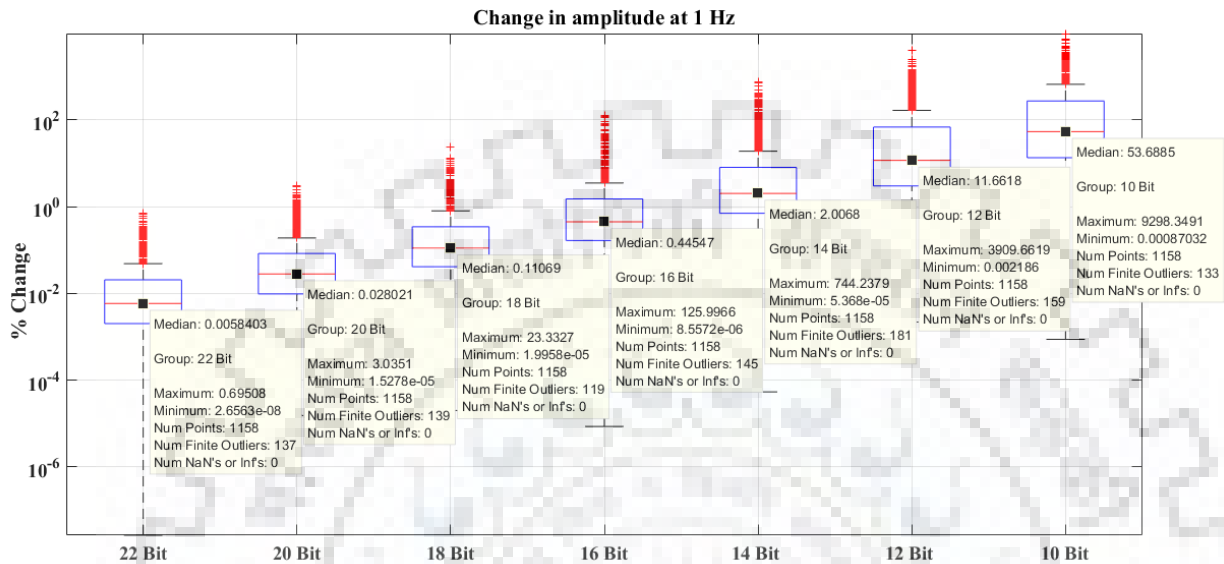


Figure 4.68: Difference in Fourier Amplitude, calculated for time histories at different ADC resolution varying from 22-Bit to 10-Bit with reference to original 24-Bit data and 1 Hz frequency.

In Figure 4.70, the error corresponding to frequency 0.5 Hz has been discussed. The median and maximum error for 22-bit data, are 0.06 and 2.8 %, respectively. The 75th percentile error value is at 0.06, and the 25th percentile error value is at 0.004%, respectively.

For 16-Bit data, the median error is 1.21%. The 75th and 25th percentile values are at 6.54 and 0.286.

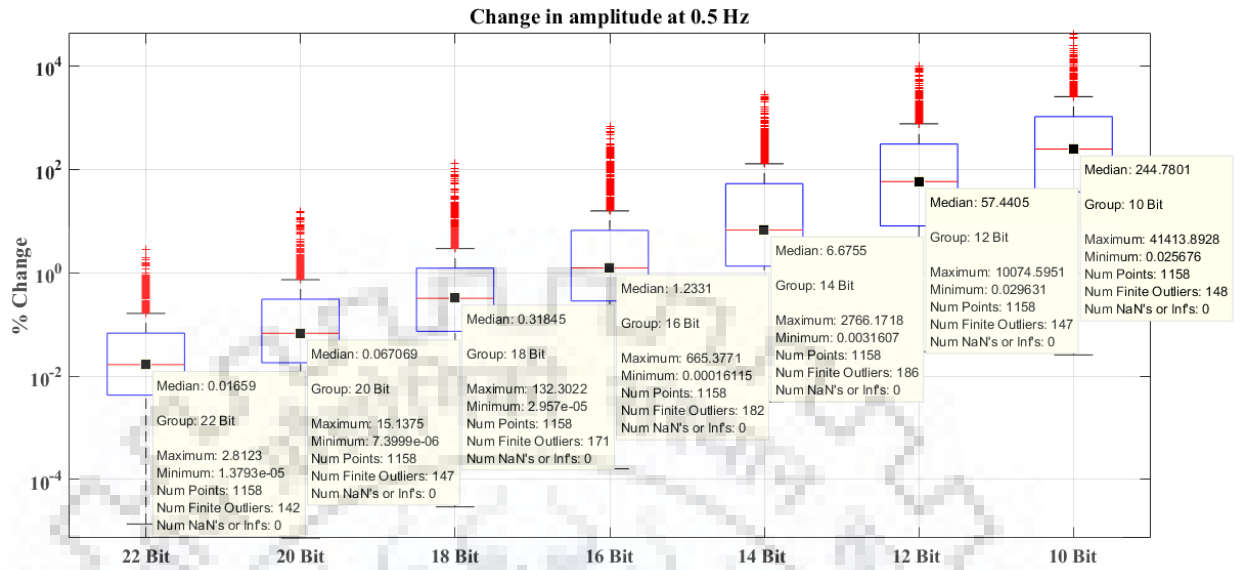


Figure 4.69: Difference in Fourier Amplitude, calculated for time histories at different ADC resolution varying from 22-Bit to 10-Bit with reference to original 24-Bit data and 0.5 Hz frequency.

The error corresponding to the 1 Hz frequency in Fourier amplitudes are given in Figure 4.71. It is observed that the median error corresponding to 22-bit data is 0.035% whereas the maximum error is ~10%.

In the case of 16-Bit data the median error is ~3%. The 75th and 25th percentile values are also 14.51 and 0.58%, respectively.

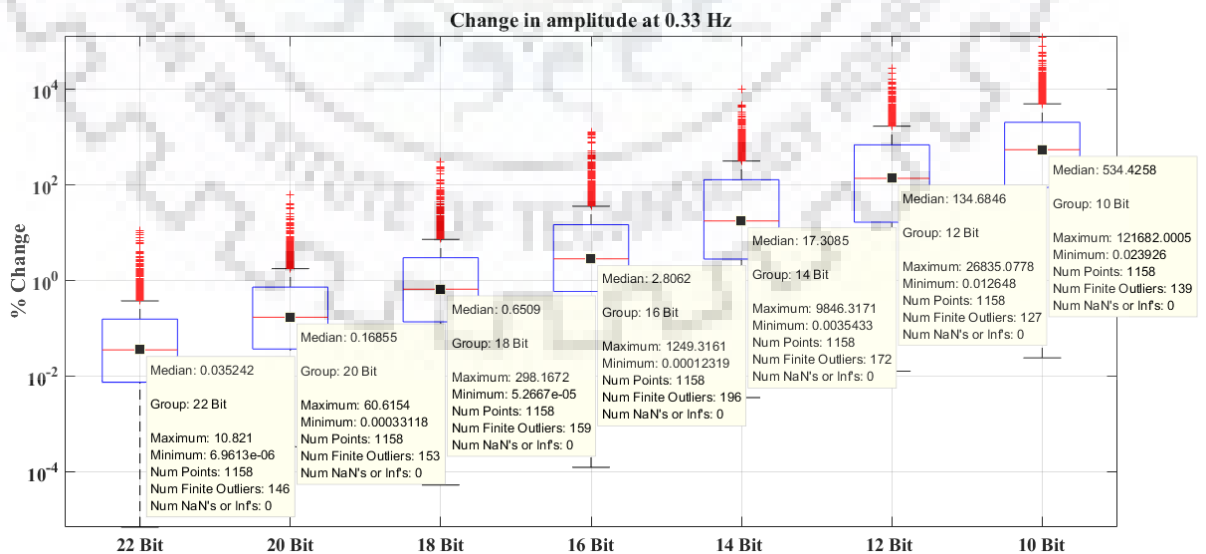


Figure 4.70: Difference in Fourier Amplitude, calculated for time histories at different ADC resolution varying from 22-Bit to 10-Bit with reference to original 24-Bit data and 0.33 Hz frequency.

The error corresponding to the 0.25 Hz frequency in Fourier amplitudes are given in Figure 4.72. It is observed that the median error corresponding to 22-bit data is 0.052 whereas the maximum error is 0.11.96%.

For 16-Bit data, the median and maximum error are ~5%, and the maximum values is at ~2000%. The 75th percentile and 25th percentile values are 25.30 and ~1%, respectively.

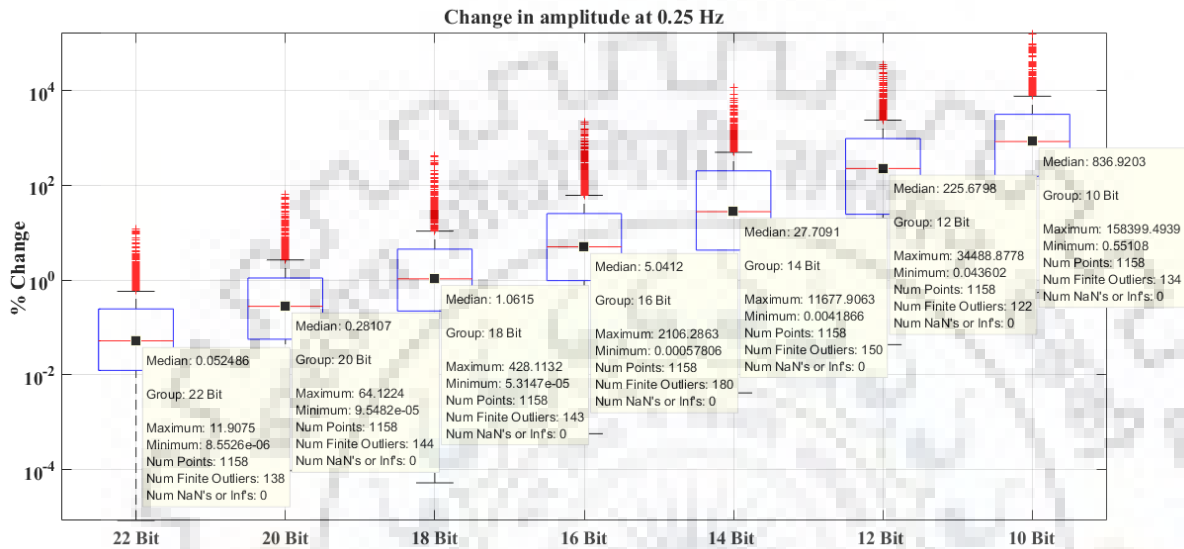


Figure 4.71: Difference in Fourier Amplitude, calculated for time histories at different ADC resolution varying from 22-Bit to 10-Bit with reference to original 24-Bit data and 0.25 Hz frequency.

For 0.2Hz Frequency, the following observations are made.

Median and maximum error corresponding to 22-Bit data are 0.084 and 26.6%, respectively.

For 16 Bit data, the median error is of the order ~7%, whereas 75th and 25th percentile values are 37.0 and 1.42%, respectively.

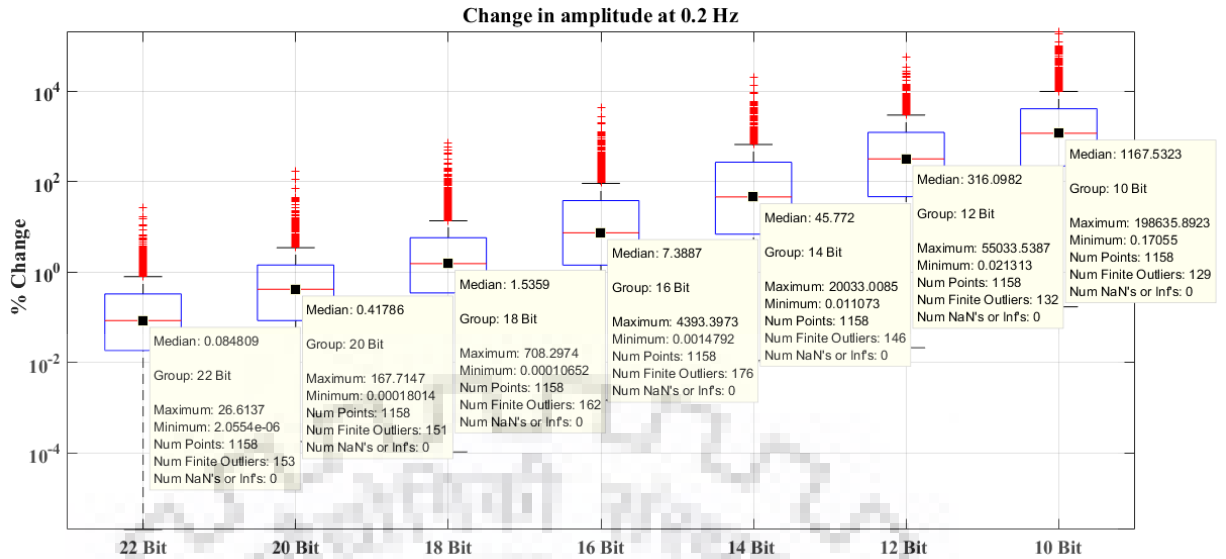


Figure 4.72: Difference in Fourier Amplitude, calculated for time histories at different ADC resolution varying from 22-Bit to 10-Bit with reference to original 24-Bit data and 0.2 Hz frequency.

For 0.14 Hz Frequency, the following observations are made.

Median and maximum error corresponding to 22-Bit data are 0.14 and 37.6%, respectively.

For 16 Bit data, the median error is of the order ~12%, whereas 75th and 25th percentile values are ~61 and 2.44%, respectively.

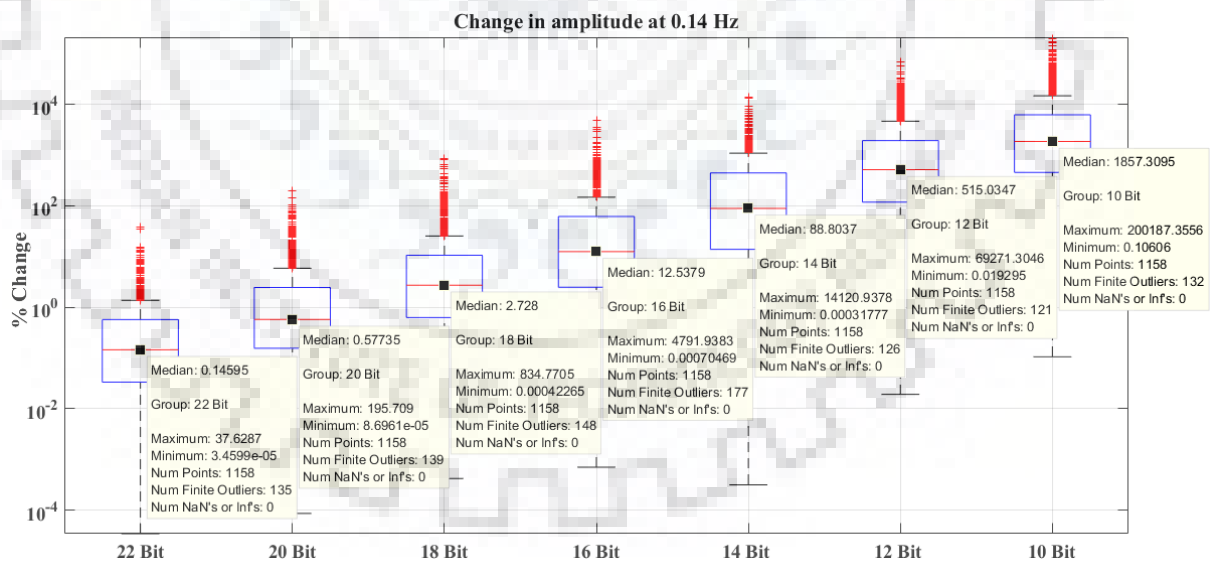


Figure 4.73: Difference in Fourier Amplitude, calculated for time histories at different ADC resolution varying from 22-Bit to 10-Bit with reference to original 24-Bit data and 0.14 Hz frequency.

Figure 4.75, the error for Fourier amplitudes with respect to 24-Bit original data has been discussed. It is evident from the Figure that for 16-Bit data, the median error is of the order 20%. The 75th percentile and 25th percentile are at 93.12 and 4.69 %, respectively.

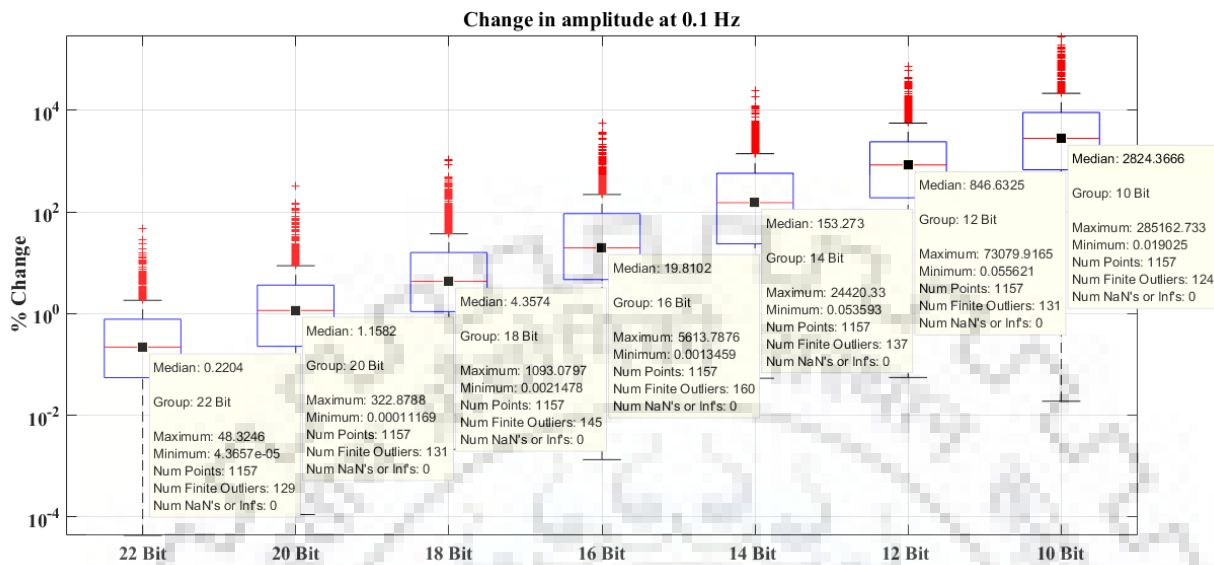


Figure 4.74: Difference in Fourier Amplitude, calculated for time histories at different ADC resolution varying from 22-Bit to 10-Bit with reference to original 24-Bit data and 0.75 Hz frequency.

From above analysis that now frequency noise is added as we keep on decreasing the sensor dynamic range. Thus it may be concluded that data for higher frequencies can be extracted with greater accuracy as compared to the low-frequency data.

Chapter 5 Central Processing unit

The central processing unit is the heart of the whole EEW system; this is an engine that performs all the tasks that are related to EEW. The main components of the central server are as follows;

- Hardware, which includes high computing workstation or server and networking equipment.
- A software program that can receive data from different sensors located at a remote location.
- Modules for picking of earthquake trace, in case of an event, from an otherwise continuous data stream
- Module for estimation of magnitude and location from the set of available triggered streams
- Module for taking decisions and dissemination of warnings to the target users

The central processing unit or earthquake early warning server comprises of high computing server, which should be able to handle data traffic from 100 plus sensors simultaneously. For the software part, it was decided to use EARTHWORM software. The earthworm is an open-source platform that is currently maintained by Instrumental Software Technologies, Inc. Earthworm serve is one of the most widely used worldwide for seismic data processing. Earthworm can be configured and compiled for most of the operating systems like Solaris, Centos, Macosx, Redhat, Ubuntu, and Windows. (Johnson et al. 1995)

(<https://isti.com/products/eq-monitoring-seismic-software/earthworm/>).

In this study point source approach has been used as following rupture or waiting for rupture could lead to loss of very important initial seconds and thus losing the cause of such system.(Minson et al. 2018). Though an event could be more characterized if the initial 10 seconds data is analyzed (Melgar and Hayes 2019).

This chapter deals with the details of the Earthworm software used for the development of the EEW system in India. The first section gives details of the central server and modules of Earthworm, which have been used for EEW, the second section deals with the Network used for communication of data from the sensor to the central server. In the third section, the details of the decision-making module have been discussed.

5.1. Central Processing Unit and Decision Making

All sensors have been connected to the central server located at IIT Roorkee by using the Earthworm platform through a Virtual private network over broadband (VPNBB). The Earthworm has been developed by USGS(Johnson et al. 1995) and is widely used for the real-time processing of seismic data. It is an open-source program where various modules have been

developed by a number of seismologists worldwide, and since the program is open source, need-based custom modules can be developed in-house. Using this functionality of Earthworm central server has been configured, and the EEW system for India has been developed by using and modifying the already available program as per our need and requirement.

The decision to choose Earthworm was taken considering the following main design criteria:

The modules developed for performing each task are independent and can function in isolation both in terms of hardware and software. This implies that different modules can be modified and more functionality can be added without affecting the overall system configuration and processing.

The modules in particular and Earthworm as a whole is system independent, which implies that different modules can be run in a different types of computer systems, and all these systems can be connected together, where they can act as a part of a whole integrated single system, in spite of having different software hardware and geographical location.

Another added advantage is that data acquisition modules, data formatting modules, data sharing modules are readily available. So even if in the future a variety of other sensors are needed to be added, the module performing the EEW task could run without any major change.

A data acquisition program, name `palert_svr`, to receive data in real-time from the sensors is already available in the Earthworm version 7.7. For the processing of data, a high-pass filter with a cut-off frequency of .075 Hz has been implemented to filter the data in real-time. The module for picking of the earthquake, named `pick_ew`, has been modified by (Chen et al. 2015a), which is the one used for this EEW system. The modified module has two additional parameters for acceleration and velocity threshold. These new parameters are very helpful in removing spikes created by noise. Threshold values for these parameters can be fixed for each of the sensors in the configuration files. Apart from picking the earthquake, this module also calculates peak displacement (Pd), peak velocity (Pv) and peak acceleration (Pa) of P-waves for a 3-second time window. Another module which is also developed in Earthworm, then estimates the epicentral distance, focal depth, and size of an earthquake. If all the parameters are satisfied, it creates an earthquake report file. To take decision for issuing a warning for this EEW installation, if the weighted average of estimated magnitude, from at least four stations, is found to be greater than 6, the report files are created, and simultaneously a script is also triggered, which in turn activate all the siren connected to the EEW server. While other reports for which estimated magnitude is lesser than 6, files are created, but no script is triggered to activate the siren. The magnitude estimation is a continuous process that is continued even after the creation of the first report. As soon as the new station is picked, both epicentre and weighted magnitude are estimated, and a file with a new estimated magnitude is created and sirens can be triggered. With the addition of

more stations, both epicentre and magnitude estimation is found to improve. For the purpose of future testing and archiving of data, the Winston server is used.

A Graphical User Interface (GUI) was developed using PyQt4, a Qt application framework in Python. This GUI contains two main components: a map display of the region monitored and a countdown timer to display the estimated time remaining before the arrival of a detected earthquake. The map is displayed using Leaflet JS, a JavaScript library for interactive maps.

The GUI continuously monitors the system drive for the report files that are created in the event of a detected earthquake. Each such report contains information about the sensors triggered due to the earthquake and the estimated epicentre location with respect to the triggered stations. So the epicentre location will be updated with the creation of every report. The triggered stations are then plotted on the map display after every new report. The map displays the current estimated position of the P-wave and S-wave as concentric circles based on the velocity models proposed by (Kanaujia et al. 2015). The estimated position of the seismic waves is updated every 1/10th of a second. The countdown timer displays the time remaining till the estimated earthquake reaches the user's location. The time remaining is calculated using the distance between the user's location and the epicentre location of the earthquake. After an earthquake reaches the user's location, the timer is reset to zero, and the GUI goes back to monitoring the system drive for any new event. The figure 5.1, show one example of the GUI.

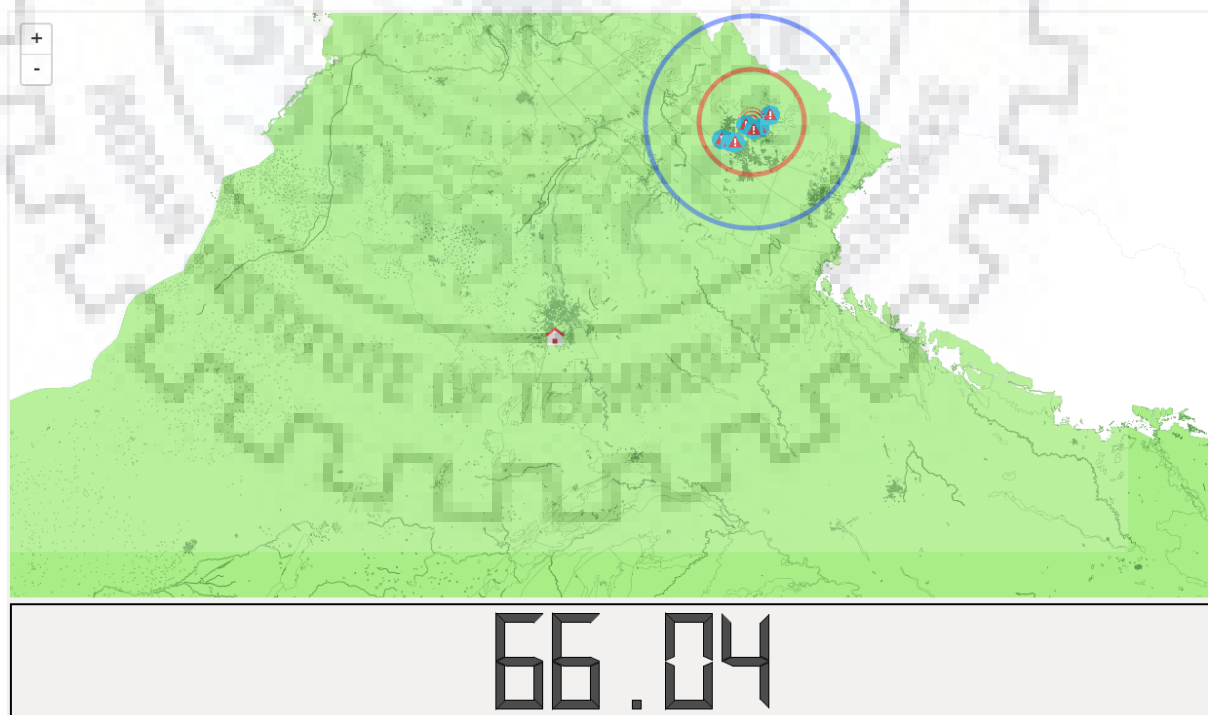


Figure 5.1: Figure shows the outcome of the warning display of Early Warning Display Program during simulation of 29th November 2015 Chamoli earthquake of magnitude 4. In the picture, blue dots are the sensors picked, innermost red circle is the estimated epicentre, red circle is S-

wave envelop, blue circle is P-wave envelop, the hut in the centre of map is target location, in this case New Delhi. 66.04 is the expected time of S-wave arrival at the target location in seconds.

5.2. Decision Making, Warning dissemination, Simulation and Performance

The module for estimation of epicentre uses the Geiger's method (Chen et al. 2015a) with grid search, using a half-space velocity model in which velocity increases linearly with depth. A 1-D velocity model has been proposed for the region around Tehri in the Garhwal Himalayas (Kannaujia et al. 2015). This study is based on the travel time inversion of 145 local earthquakes with an azimuth gap less than equal to 180 degrees and travel-time curves of crustal phases. Based on this study, P & S wave velocity model has been used for this module to estimate epicentral distance and focal depth. This velocity model is shown in Table 2 and Figure 5.2.

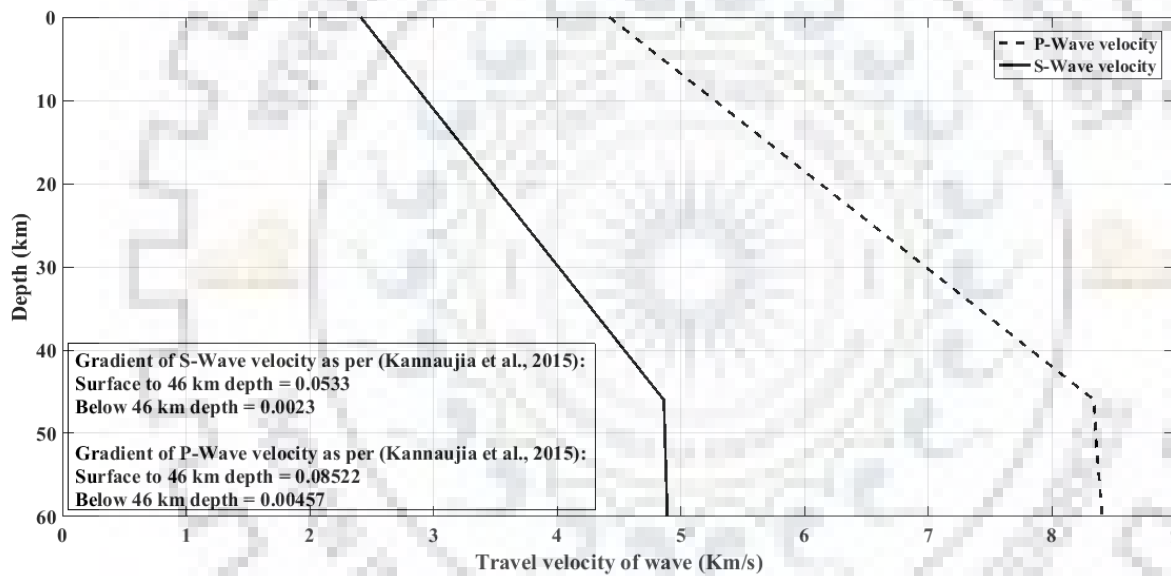


Figure 5.2: P and S wave velocity model derived from Kannaujia et al. (2015)

Table 2: Velocity model used for the estimation of epicenter and depth. (Kannaujia et al. 2015)

	P-wave velocity model	S-wave velocity model
Boundary of shallow and deep layers	46 km	46.0 km
Initial velocity in shallow layer	4.42 km/s	2.4100 km/s
Gradient velocity in shallow layer	0.08522	0.0533
Initial velocity in deep layer	8.34000 km/s	4.8600 km/s
Gradient velocity in deep layer	0.00457	0.0023

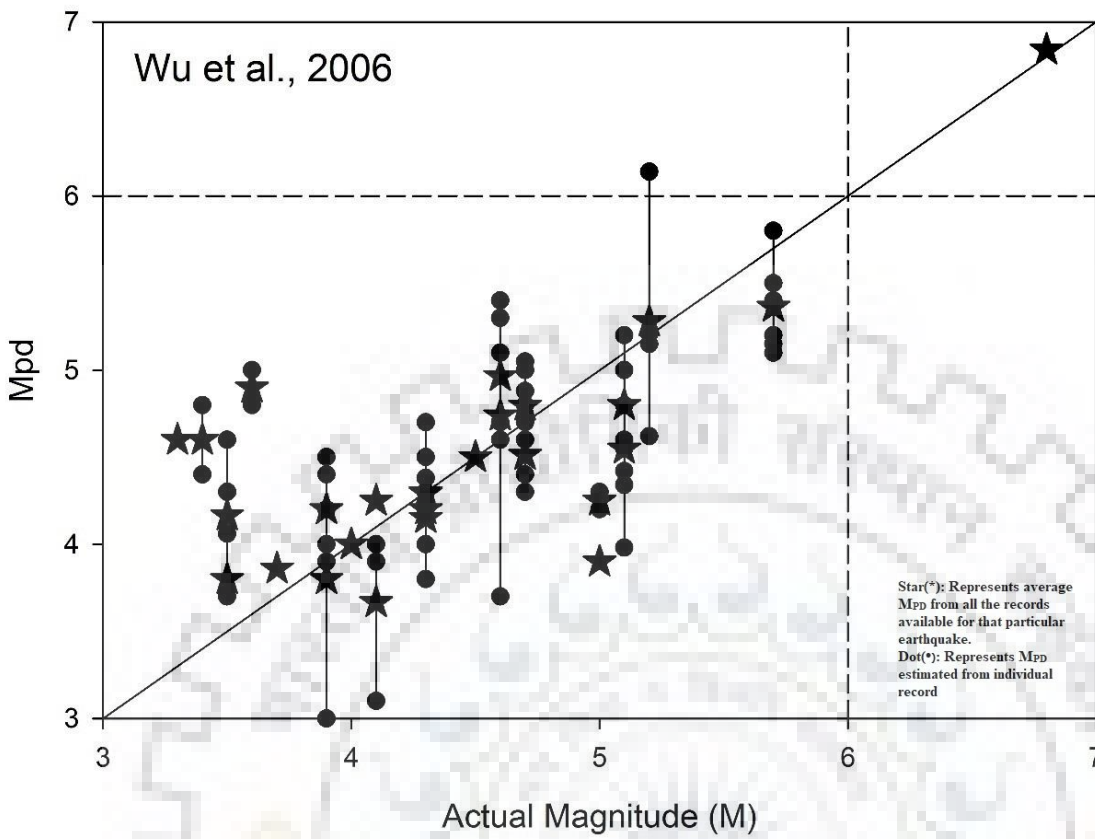


Figure 5.4: Estimated M_{PD} and error in estimation with respect to actual magnitude using Wu et al., 2006.

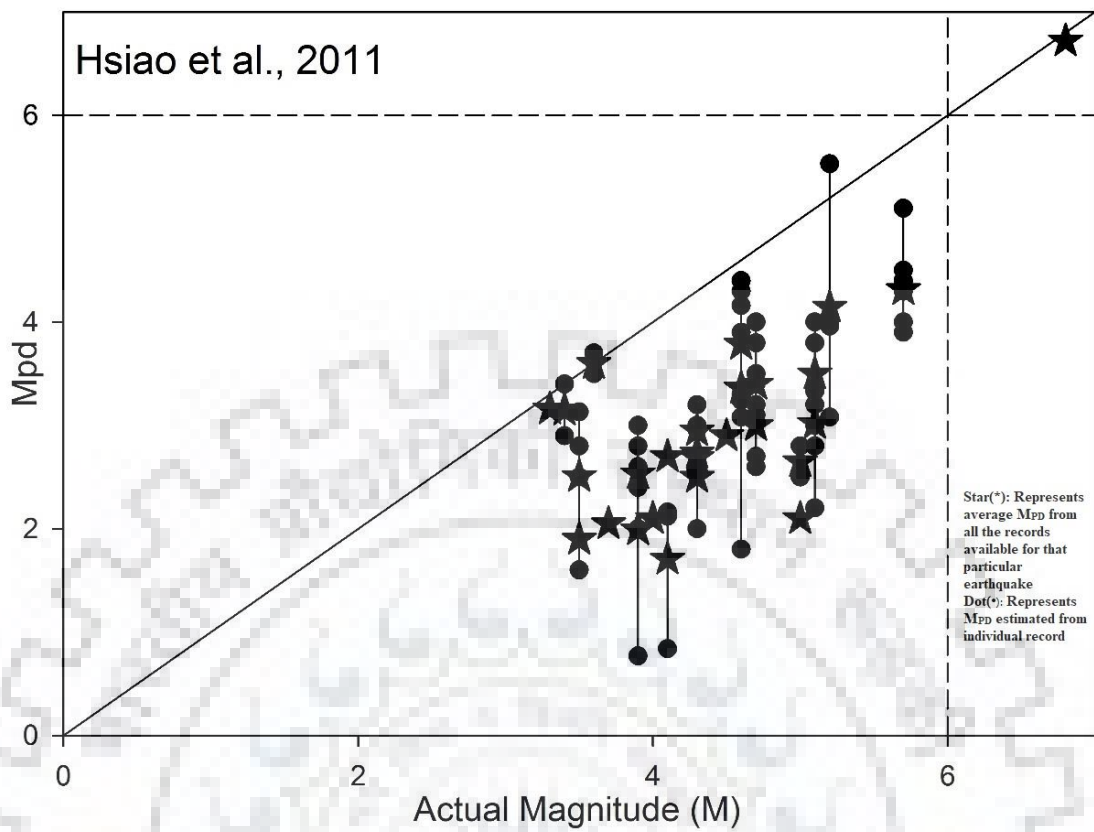


Figure 5.5: Estimated M_{PD} and error in estimation with respect to actual magnitude using Hsiao et al., 2011.

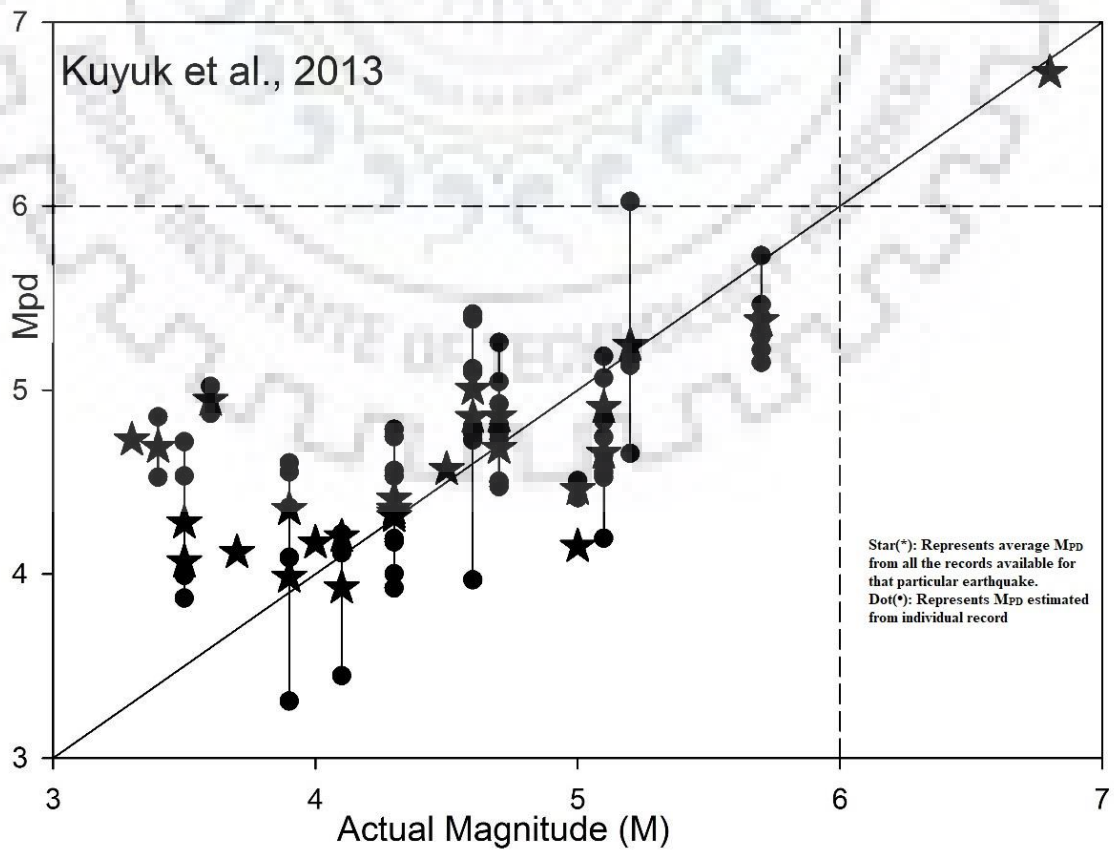


Figure 5.6: Estimated M_{PD} and error in estimation with respect to actual magnitude using Kuyuk et al., 2013.

In figure 5.4, 5.5 and 5.6 the dots represent M_{PD} estimated from individual records, and the star represents average M_{PD} from all the records available for that particular earthquake below 100 km epicentral distance.

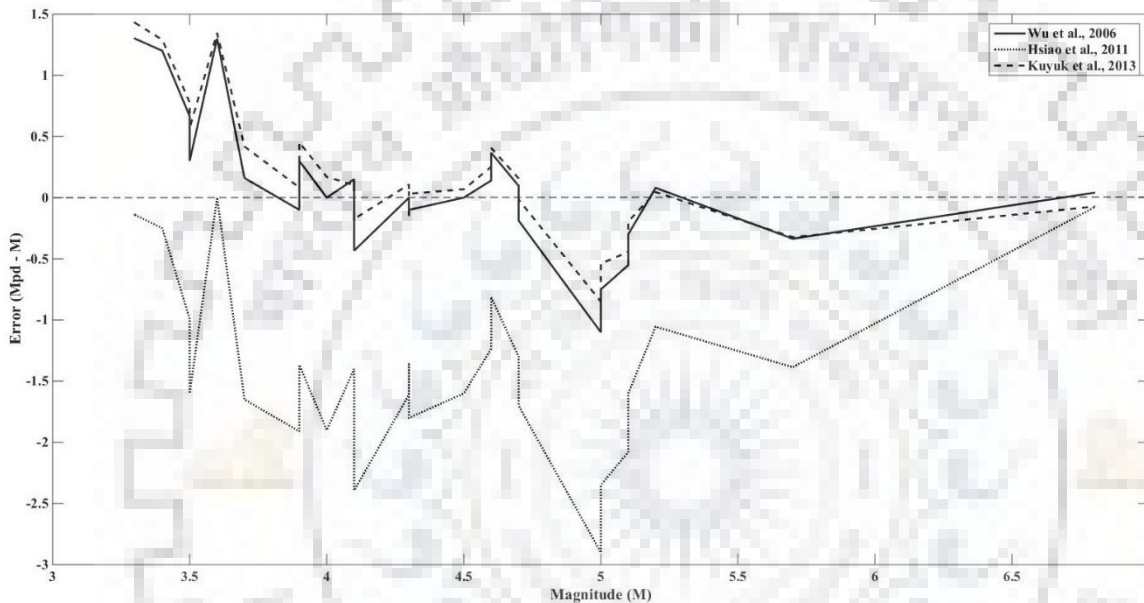


Figure 5.7: Average error in estimated M_{pd} with magnitude using Wu et al., 2006 (Solid line), Hsiao et al., 2011 (Dotted line)

Figure 5.7 shows an error in the estimation of M_{PD} with respect to the actual magnitude of the earthquake. From these figures, it can be concluded that the regression model suggested by Wu et al., 2006 and Kuyuk et al., 2013 (Equation 1 and 3) has much less error with an increase in magnitude for this dataset. Figure 5.7 has been derived from figure 5.4 to figure 5.6. Hence it was decided to use Wu et al., 2006 regression model for the current installation of the EEW system for Northern India. One example of this regression model is also shown in Figure 5.8 for the data recorded by the EEW network. The regression model will be revised in the future with the availability of more data from the networked region in order to make it more suitable for Northern India.

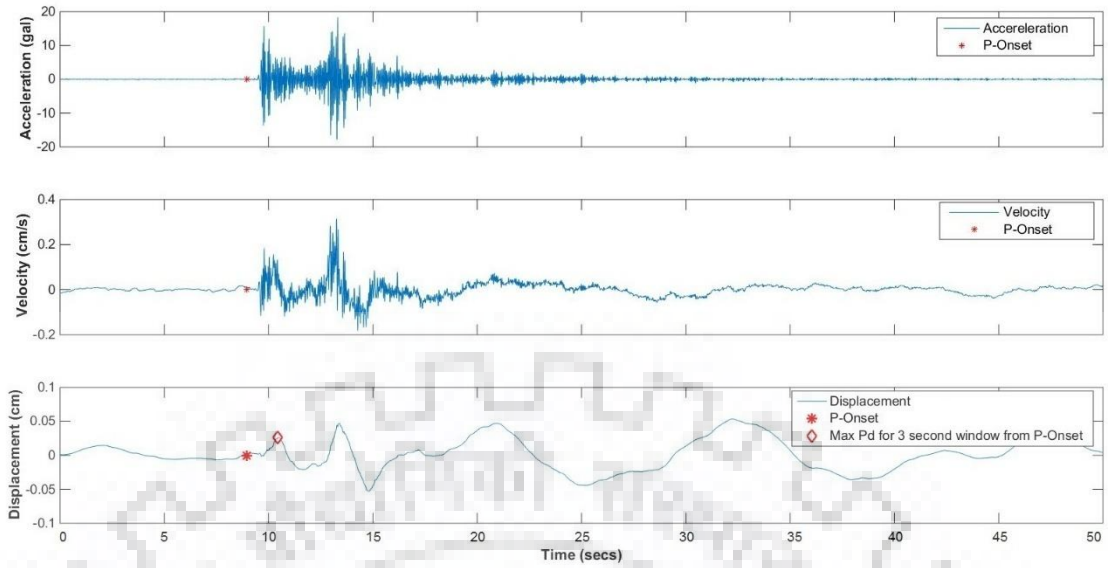


Figure 5.8: Acceleration, velocity and displacement time history of 29, November 2015 earthquake having magnitude 4 from station Chinka which was located at 13 km from estimated epicenter. Asterisk denotes the point of P-Onset and diamond shows the maximum displacement of 3 sec window from P-Onset (P_d). Magnitude estimated by EEW system, for P_d equal to 0.0264 cm, calculated at this station was 3.45.

5.2.1. Simulation and Testing

With the help of the *TANKPLAYER* module available in the standard Earthworm package, old recorded data can be re-run in the Earthworm installation. The data is streamed with a timestamp and precisely in the same manner as it would have been received from the installed sensor in real-time. The *TANKPLAYER* reads the waveform data from the recorded tank files and then passes it to shared memory. The rest of the processing from this stage onwards is exactly the same as it is on the real server. Thus by re-running recorded data from multiple earthquakes, the pick parameter, as well as the regression model used, can be tested and modified. Whenever some stations were not picked during a real event, the records from the event were rerun through *TANKPLAYER* to adjust the pick parameters for those stations. For example, in the event of 29th November 2015, Chamoli earthquake of magnitude 4.0, two stations UKMB (Ukhimath) and KKHR (Kherakhal), were not picked and thus were not shown in the initial report created by the system. Later while re-running the recorded data, the pick parameters were readjusted. After changing the pick parameters for these two stations, records were again rerun, and in the subsequent report, both the stations were picked correctly.

The selection of data for the testing purpose has been one of the major tasks for us due to the unavailability of sufficient strong motion data from India as a whole and for the networked region

in particular. Moreover, since we are using relatively low-cost sensors, it was decided to use data with similar quality. As Taiwan is also using the same sensor for the EEW network and they have a good repository of recorded data, data from Taiwan was used to test the configuration of the system and algorithms.

In order to test the configuration of the EEW server, records having an epicentral distance less than 50 km from 10 earthquakes of magnitude greater than four were used. Records consist of 3 larger earthquakes having magnitude 5, 5.5 and 6. The waveforms were passed to the earthworm installation using *TANKPLAYER*. In the first and second report which is generated when at least 5 and 10 valid triggers are available respectively, the system is able to estimate the magnitude and epicenter with an error which is well within limits for all practical purpose for EEW. The magnitude five earthquake was estimated as 4.8, the magnitude 5.5 earthquake was estimated as 5.4, and a magnitude six earthquake was estimated as 6.2 in the first report. Though the error in estimation reduces when data from more sensors are available, but considering the importance of every second, we assume that the first or second report can be used for issuing a warning with little deviation in the estimation.

Shake table tests were also performed to test the working of the system. A set of 10 sensors were mounted on the top of the shake table, and each sensor was configured with latitude/longitude such that all sensors would fall in the circumference of a circle of radius 40 km, 45 km, and 50 km. Since all the sensors would be triggered almost at the same time, it can be assumed that the epicenter should be estimated right at the center of the circle. The shake table was then excited with the data for 1999 Chamoli earthquake. In each test, it was found that in the first file itself, the epicenter was estimated precisely at the center of the circle. There was an error in the estimation of magnitude, but that was because the algorithm for estimation has been designed to work for the first few seconds of the P-wave, whereas the shake table is designed for replicating strong-motion part of the time history and hence could not reproduce the initial phase (P-phase) of earthquake motion correctly.

A schematic diagram of the whole EEW process is shown in figure

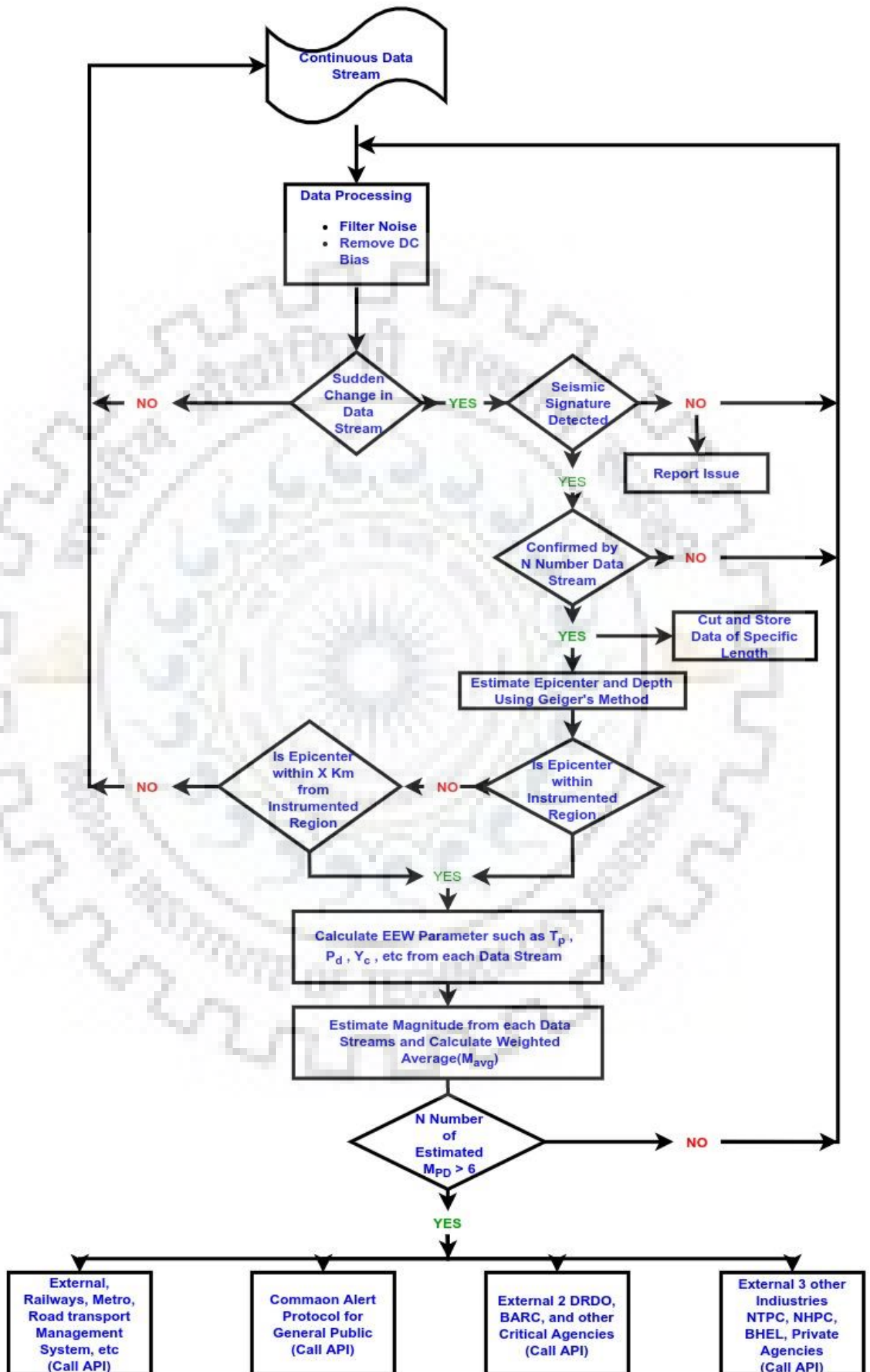


Figure 5.9 : A schematic diagram to show the EEW process being developed for EEW for Northern India.

5.2.2. Performance of the EEW system during recent earthquakes

Since the installation of the network, we have been able to record almost all the earthquakes in the region. The major events that we have been able to record are following

- 12-May-2015 Nepal earthquake of magnitude 7.3 was recorded at five stations. As it was the initial phase of installation and we had very few sensors connected to the central server, thus data was recorded at five stations only.
- 26-Oct-2015 Hindukush, M 7.5, earthquake is recorded at 31 stations
- 25-Dec-2015 Hindukush, M 6.5, earthquake is recorded at 30 stations.

The first earthquake recorded by this network, having an epicenter in the instrumented region, was recorded on 18-July-2015. This was a small earthquake of magnitude 4.3, and epicenter was located in the Chamoli district of Uttarakhand. During this event, data from 4 sensors that were near the epicenter were streamed to the central server and were picked successfully by the EEW server. As it was the initial phase of the installation of sensors, very few sensors were streaming data to the central server. Thus the report file was not generated for this event, but the following observations were made:

- India Meteorological Department (IMD) reported the origin time of the earthquake as 23:48:07 UTC
- The first sensor of the EEW network was triggered at 23:48:14 UTC. This station was at 25 km from the epicenter reported by IMD.
- Three more sensors were triggered between 23:48:16 and 23:48:18. Further, adding 10 seconds for processing, analysis, and dissemination of warning, a warning could be issued at 23:48:28.
- A seismometer (not from this network) installed at IIT Roorkee also recorded the earthquake and reported the P-wave arrival time as 23:48:35 UTC and S-wave arrival time as 23:48:50 UTC at IIT Roorkee.

It is evident from this observation that a warning time of 22 seconds could be achieved for IIT Roorkee for this case.

Later, two more small earthquakes which had their epicenters within the instrumented region were also recorded. The first earthquake on 29th November 2015 was of magnitude 4, having an epicenter at Chamoli, and another earthquake on 25th September 2016 was of magnitude 3.7, and epicenter was at Uttarkashi. The epicenter and Peak Ground Acceleration (PGA) recorded for these two events at various stations is plotted in Figure 5.10 and Figure 5.11.

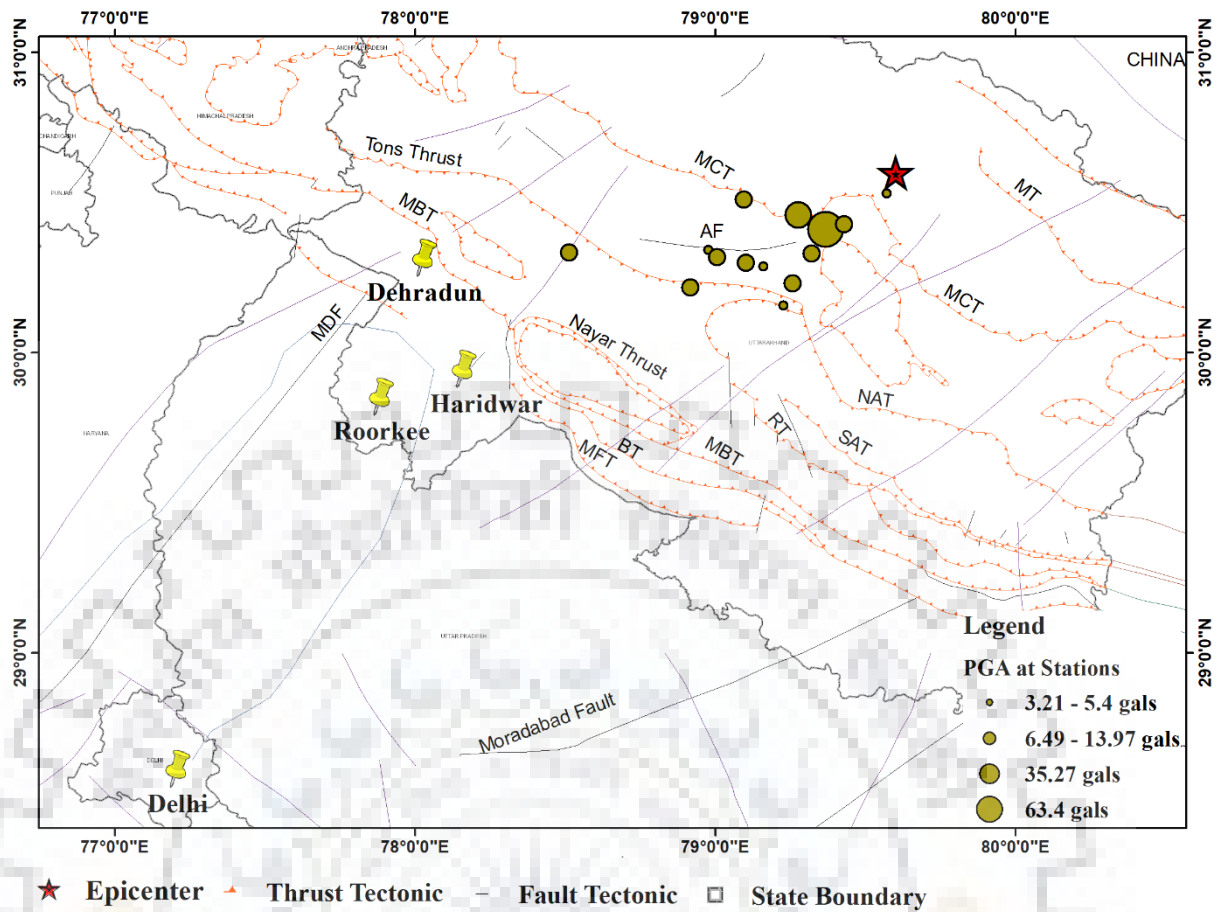


Figure 5.10: Estimated epicenters and recorded peak ground accelerations (PGA) in gals for 29/11/2015 Chamoli Earthquake of magnitude 4

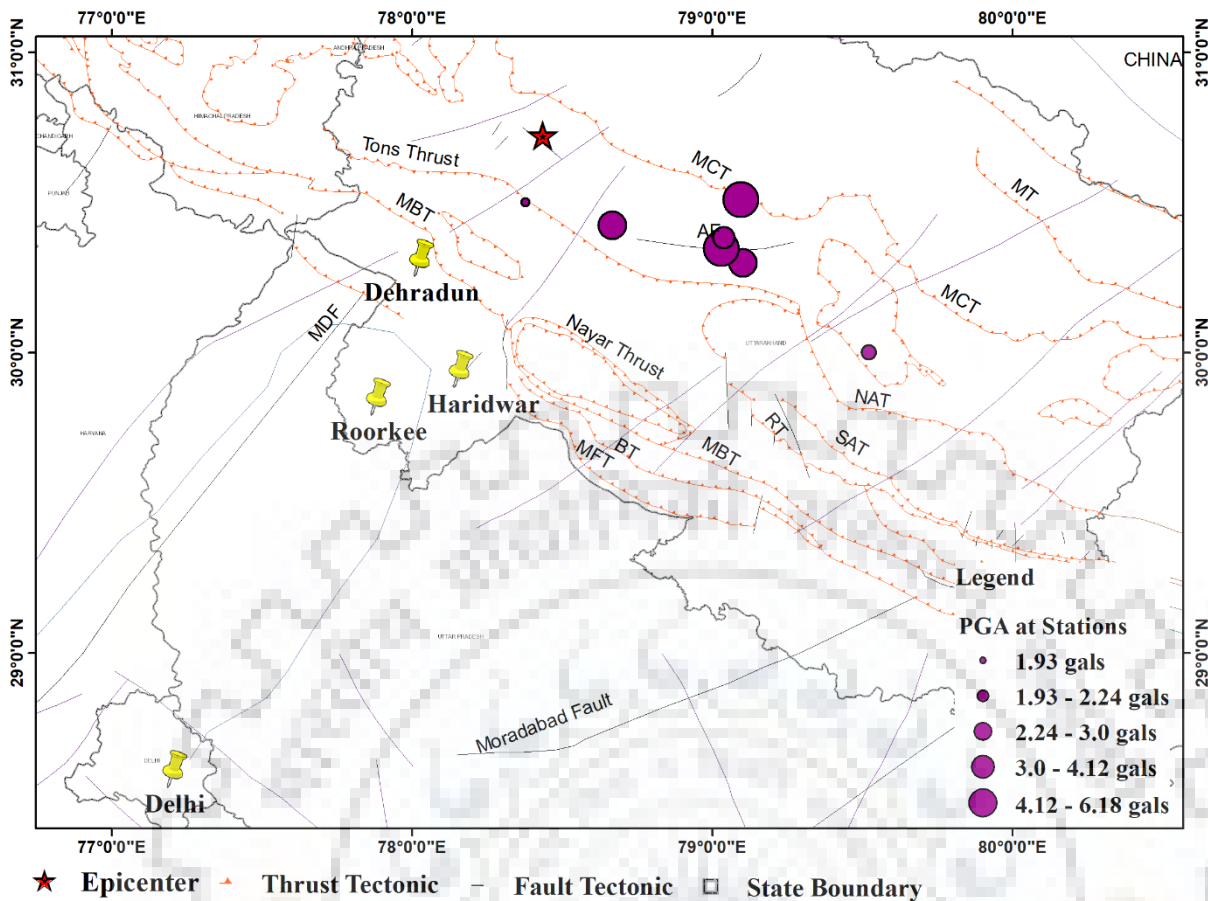


Figure 5.11 : Estimated epicentres and recorded peak ground accelerations (PGA) in gals for 25/09/2016 Uttarkashi Earthquake of magnitude 3.5

The report was created only for the first earthquake. No report was created for the second earthquake as very few sensors were triggered due to the low intensity of shaking. The observations made from the report of the first earthquake are as follows.

- The report estimated epicenter at 30.4863N, 79.3448E, whereas IMD has reported epicenter at 30.6N, 79.6E.
- Depth is estimated correctly in the report generated. The depth is estimated as 10 km in the report, and the same was reported by IMD.
- The report is created after 13.49 seconds of the estimated origin time of the earthquake, 11 seconds after the first station was picked, and ~2 seconds after the seventh and last station, in the report, was picked.
- Magnitude estimation is not correct; the report estimated 2.7, whereas IMD reported it to be 4. This is largely because of the fact that the regression model to estimate magnitude (M_{Pd}) using P_d used by us agrees well for the large magnitude earthquakes. The M_{Pd} estimated for the smaller events shows deviation from actual magnitude however, for large events, this estimate is much more accurate (Hsiao et al., 2011). However, for the Indian dataset, this was not found to be the situation for the model suggested by Hsiao et al., 2011 (Figure 2b and 3). Figures 2a, 2c and 3 suggest that model suggested by Wu et

al., 2006 and Kuyuk et al., 2013 are much more accurate at higher magnitudes compared to Hsiao et al., 2011 for the Indian dataset.

- An acceleration, velocity, and displacement time history for station CNKB (Chinka), which was nearest to the epicenter is shown in Figure 5. This figure explains the basic concept on which the EEW system for India has been developed. In this figure, the P_d for the first 3-second window after P onset was calculated to be .0264 cm and the magnitude was estimated to be 3.45. Seven more stations were triggered by the earthquake.

The network recorded a magnitude 5.5 earthquake on 6th December 2017. The EEW system worked perfectly as expected. The following observations were made:-

- The event was recorded by 30 stations.
- The magnitude was estimated 4; however, IMD reported it to be 5.5. USGS reported it to be 5.1
- The epicenter estimated by the EEW system was 30.634°N 79.09°E which is almost similar to the epicenter estimated by the USGS, which was 30.634°N 79.160°E. IMD reported epicenter at 30.4°N 79.1°E.
- The seismometer located at Roorkee recorded S-wave arrival time at 15:20:32 UTC; however, a warning from the EEW server was issued at 15:20:04 UTC. This earthquake reaffirms the possible lead time that could be achieved for Roorkee, which is approximately 25 seconds.
- Figure 5.12 shows the PGA recorded for the various station and the estimated epicenter for this earthquake.

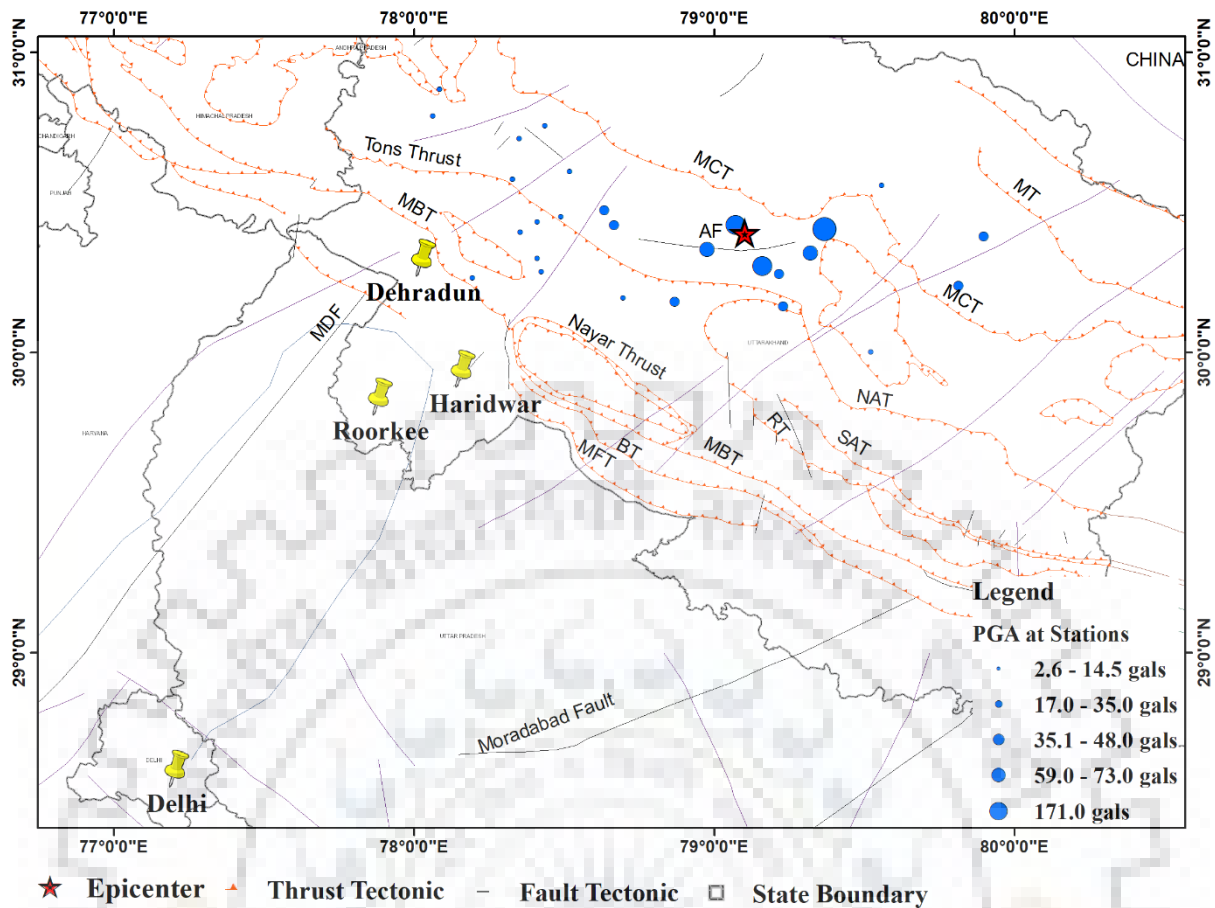


Figure 5.12: 6/12/2017 Rudraprayag earthquake of magnitude 5.5

Two large earthquakes of magnitude 6.5 and 7.5 having an epicenter in the Hindukush region were also recorded by the network. However, these earthquakes were at a distance of more than 800 kilometers from the networked region; thus level of ground shaking was too small. As a result, no station was triggered. Hence the details of those earthquakes are not discussed in this work.

5.3 New approach for P phase picking using Damage Intensity.

One of the primary tasks for any successful earthquake early warning system is to correctly pick the onset of the P-phase of the earthquake, in real-time from otherwise streaming noise. There are plenty of algorithms available for picking of onset of P-phase of earthquake record (Saragiotis et al. 2002; Gentili and Michelini 2006; Ross and Ben-Zion 2014; Ait Laasri et al. 2014; Chi-Durán et al. 2017; Wang and Zhao 2017; Zhang et al. 2018; Zhu et al. 2018, 2019). The most popular and used algorithm out of these many algorithms works on the concept of change in the ratio of short-time average (STA) and long-time average (LTA) of the data stream (Allen 1978, 1982). This algorithm was found to be quite robust and readily used in most of the EEW networks

as the STA shows a sharp rise as soon as P-phase arrives in the time history while the change in LTA is much slower (Satriano et al. 2011; Chen et al. 2015). Due to this reason, the ratio also shows a sharp change with the arrival of the P-phase, which helps in the detection of the start of seismic record by the computer program. Although this is one of the most trusted algorithms around the world for the detection of P-phase arrival, this also cannot have a 100% success rate. This is due to the inherent uncertainties, errors, ambient noise, etc., in the time history at the site of installation of sensor and equipment itself.

As discussed in earlier chapters, while developing the EEW system for northern India, the installation of strong motion sensors was carried out at the office of district/sub-divisional administration or BTS of BSNL. Most of the BTS is located in crowded places, and similarly, the administrative offices are severely crowded during office hours. Due to this, there was always a possibility of noisy zero line in the time stream sent by these sensors to the central processing unit. This in return, poses the possibility of missing the correct position of onset of P-phase in the data stream and hence miscalculation of peak displacement (P_d) in the first 3-5 seconds (as setup in EEW system) from the onset of the P-phase. As discussed earlier, the most reliable algorithms for regional warning rely on the estimation of earthquake magnitude using P_d . Due to this fact, while working on the EEW system for northern India, it was thought to adopt some other methodology for detection of the onset of P-phase, as discussed in Chapter 2. Hence, in this study, a new algorithm is developed for detection of the P-phase arrival using change in damage intensity (DI) rather than the change in the ratio of STA and LTA of the acceleration time history. DI has been widely and effectively used in Japan to estimate the intensity of earthquake (Nakamura 2004; Nakamura and Saita 2007) (Nakamura 2011).

5.3.1. Methodology

As discussed in the previous section, the focus of this chapter is to explain the requirement, methodology, and results of the developed algorithm that can be used in real-time at the server end for the detection of P-phase arrival using DI. DI is defined as the logarithmic of the dot product of acceleration and velocity and can be expressed mathematically as in Equation 5.4.

$$DI = \log(a \cdot v) \quad \text{----- Equation 5.4}$$

$$DI = \log(a_{EW} \cdot v_{EW} + a_{NS} \cdot v_{NS} + a_{UD} \cdot v_{UD}) \quad \text{----- Equation 5.5}$$

Where, a is acceleration in cm/s^2 and v is the velocity in cm/s which can be extended as shown in Equation 5.5 where subscript EW denotes East-West component, NS denotes North-South component, and UD denotes vertical component. Performing the dimensional analysis of DI gives dimensions as L^2T^{-3} , which are similar to the dimension of work done per unit time by unit

mass; in other words, power transferred per unit mass. As soon as seismic waves arrive at a location, DI shows a steep increase in its values, as shown in Figure 5.13. Figure 5.13 shows a typical trend shown by smoothed DI curve for with the onset and progress of the seismic event. It can be clearly seen that as soon as the P-wave arrives, DI started increasing steeply and then drops. DI show another steep rise with the onset of S-wave. It has been seen that the rise of DI with the onset of P-wave can be easily marked, although S-wave arrival may not be so much distinguishable in some of the cases. Due to this, it was found to be a useful parameter that can be used as a tool for the detection of P-wave arrival for EEW systems. The development of the algorithm was carried out in two phases. In the first phase, recorded data has been used to develop a suitable algorithm that can be used for P-wave detection in an EEW system effectively. In the second phase of development, recorded data has been simulated as real-time data for the purpose of testing and optimizing the algorithm.

In further sections, the development of various logic that can be used for P-wave detection, the details of the processing of data, simulation of recorded data as real-time data for testing, and further results and comparison are discussed in detail.

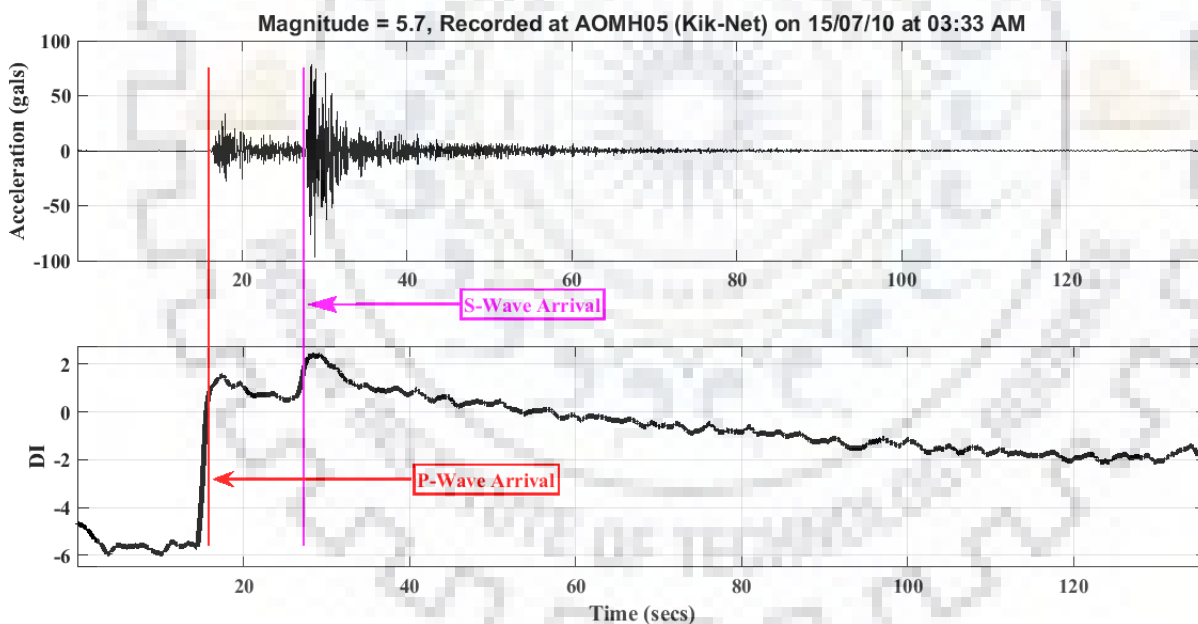


Figure 5.13 : Plot of DI corresponding to a time history of a seismic event of Magnitude 5.7 recorded at AOMH 05 (Kik-Net) on 15/07/10 at 03:33 AM.

5.3.2. Development of Pick algorithm using recorded data

For the initial development of the algorithm, around 1000 records were used, which were obtained from the Kik-Net dataset. These earthquake records are chosen such that they may contain records from magnitude 3 to magnitude 9, epicentral distance more than 10 km, and peak ground acceleration less than 30 gals. Low-intensity records are considered as they will have a

low signal-to-noise ratio, and hence if the algorithm works well for such cases, it will work fine for higher intensity records where the signal-to-noise ratio is much higher. Like the earthquake, the records used in this study are from the Kik-Net dataset, which provides the raw records for the sites. These raw records need to be converted from “counts” format to “gals” as per the conversion factor provided by the agency in the metadata of the record. Further, the acceleration time history obtained need to be processed by performing the baseline correction, which was performed using Equation 3.3.

For picking P arrival, three algorithms have been tested for DI, which are as follows:

1. Zero crossing or the first time when $\log(a. v)$ crosses zero line
2. Continuous Rise: When there is a constant rise in the value of $\log(a. v)$ for a predefined number of instances.
3. Lastly, calculating standard short time average and longtime average on $\log(a. v)$.

ZERO CROSSING

It has been noticed that vales of DI increase as soon as P-onset arrives or P-phase strikes that instrument or station, before p-onset values of DI is a function of noise and is most of the time found to be less than zero. It may reach larger values or may have values greater than zero if there is too much noise in the instrument. Also, being a logarithmic function by virtue of its property, it is non-continuous and cannot be defined. But as soon as it crosses the zero line or becomes positive from negative, it is found to be the point or time of P-Onset. It can mathematically be expressed as follows:

$$\begin{array}{ll}
 f(x) < 0 \text{ or negative} & x: \{\text{noise}\} \\
 f(x) \text{ is not defined} & x: \{0\} \\
 f(x) > 0 \text{ or +} & x: \{P - \text{onset}\}
 \end{array}$$

Thus we if we keep on calculating values of DI in a moving window of three or four seconds, as soon as this values increases and becomes positive, that point may be defined as a point of P-Onset.

Continuous Rise:

Another method, which is tested for estimation of P-onset, is the constant rise algorithm. During evaluation and testing of *zero-crossing* method, it was noticed that there were some events, especially stations where there is substantial noise, station crosses zero lines even for nonevent data. Thus a new algorithm of the *continuous rise* was evolved. In this algorithm, DI is continuously monitored, and whenever a rise in the value of DI is found, it is checked if the rise in the values is for a pre-defined number of samples or not(in our case, we tested for 15 number and 20 numbers).

Pseudo code :

```

Loop::
{
  If  $X_{n+1} > X_n$ 
     $c = c + 1$ ;
    if  $c > P$ ; “in our case
      pick_channel()
    else
      Continue;
}

```

Using above mentioned pseudo code, if a number or continuous rise were found to be more than 15-20, the start of a rising point is assumed to be a P-onset point. With this algorithm, the successful picking was found to be improved as compared to Zero crossing.

STA/LTA using DI:

In this approach standard Allen algorithm is used with a difference that instead of acceleration amplitude from sensor values of DI is used for calculation of STA/LTA. The window for STA is taken as 0.2 seconds, whereas the window of LTA is taken for 1 second.

In this approach, the dot product of acceleration and velocity is taken for a moving window, and 3 seconds and $\log(a \cdot v)$ is calculated once the ratio of the average of 15 samples in case of data at 100 SPS and the average of 45 samples has been found to be mostly at the P-phase onset.

Figure 1, shown below, explains the working of the algorithm for picking the P phase using DI as parameters. The earthquake was recorded by the Chinka station from the EEW network that has been installed for the EEW system for Northern India. The record is from a small earthquake of magnitude 4.3, and the record was re-run to replicate the scenario and analyze the algorithm. In Figure 1.a, we can see the total time history recorded, and asterisk (*) shows where the algorithm has estimated the p-phase onset.

Figure 1.b shows the

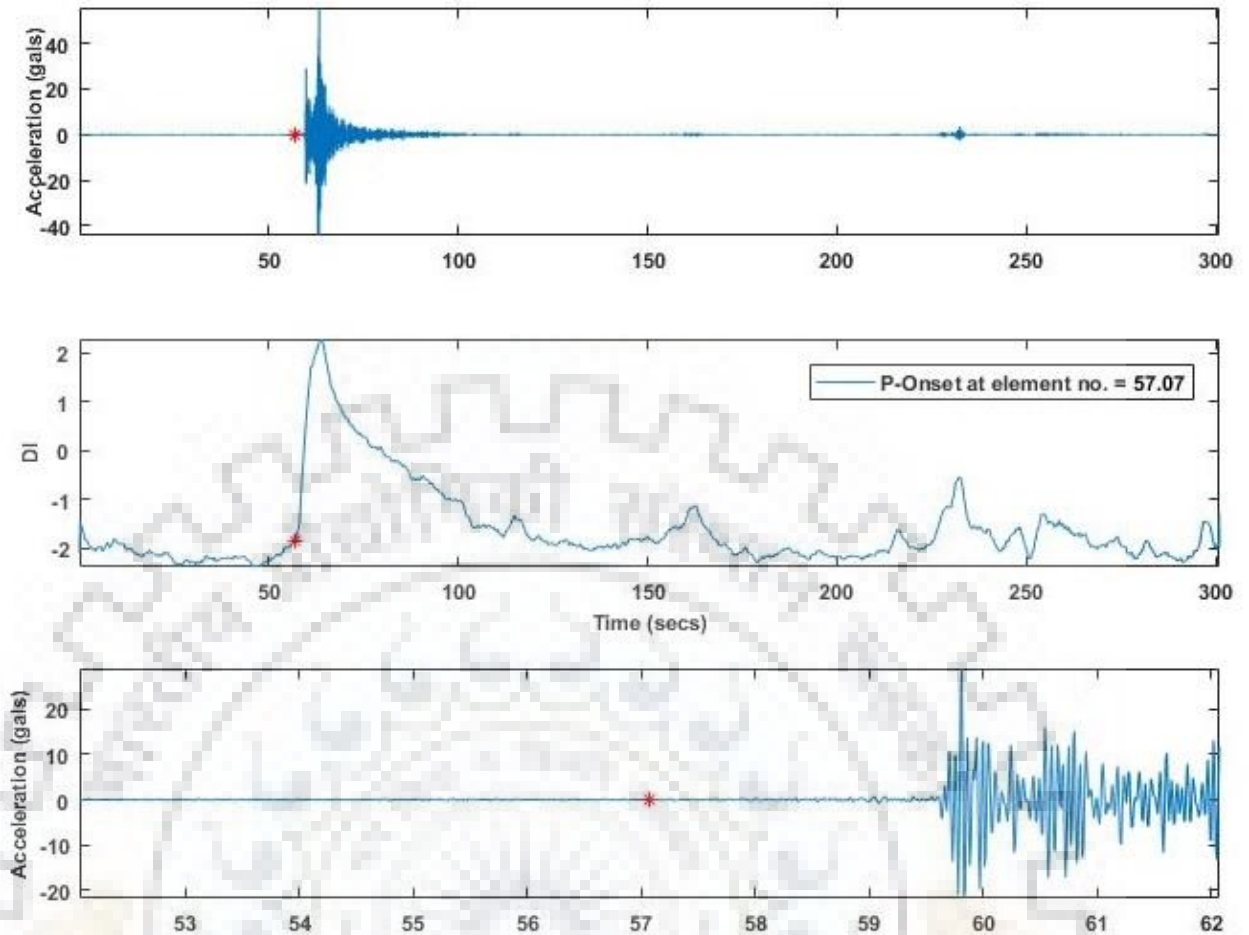


Figure 5.14: The figure representing the application of DI for picking P phase data

5.3.3. Testing of the algorithm:

The algorithm was implemented after rigorous testing using 3164 earthquake records from the Kik-Net database. To download the records, filters for epicentral distance and PGA were applied so that the data can be obtained in a wide range of PGA and epicentral distance. The selected is grouped and analyzed as per the following conditions:

- PGA less than 30 gals from any epicentral distance (1096 records)
- PGA greater than 50 gals and epicentral distance between 50 to 100 km (834 records)
- PGA greater than 50 gals and epicentral distance between 100 to 200 km (792 records)
- PGA greater than 50 gals and epicentral distance more than 200 km (442 records)

The purpose of grouping the data is to check the effectiveness of the algorithm for records with different intensity and epicentral distances.

The data thus selected has been parsed in the packets of 1 second for the analysis. The steps involved in the analysis are explained below:

1. Data in the packets of the 1-second moving window has been parsed. Baseline correction and high pass filter at the cutoff frequency of 0.075 Hz have been applied for each packet. This has been done to ensure the processing to be as similar as in the case of real-time data.
2. Velocity is calculated by numerical integration for each packet.
3. The maximum value of DI of 1-sec window data is considered as DI.
4. The window is shifted with 1 sample, and the above steps are repeated.
5. Smoothing is performed using box-car function (window length may be chosen as per requirement). For records having PGA smaller than 30 gals, a smoothing window equal to the sampling frequency has been selected for the testing of the algorithm. For example, if the sampling frequency is 100 samples per second, then the smoothing window is considered for 100 samples. For other cases, having PGA greater than 50 gals, the algorithm was tested for three different windows viz. F_s , $F_s/2$, and $F_s/4$ (where F_s is sampling frequency in samples per second).
6. Further, two filters are applied to check the change in DI. These filters are;
 - The number of continuous increasing steps should be more than 25
 - The difference between the initial point, from where continuous increasing steps are counted, and the final point (up to where DI is found to be increasing continuously) should be more than 2.
7. P-phase is picked as soon as a threshold value in step 6 is achieved.

The P-phase picked by the program is checked manually for each record, and a pick is considered to be correct if it occurred at $\pm F_s/4$ samples from the manual pick. The results of the testing of the algorithm are summarized below.

- For the dataset having $PGA < 30$ gals, analysis was performed using the smoothing window of F_s , and an accuracy of 93% was found with respect to manual pick.
- For a dataset having $PGA > 50$ gals and epicentral distance between 50 km to 100 km (834 records), the results of the analysis for different smoothing windows is as follows;
 - For F_s , accuracy = 97%
 - For $F_s/2$, accuracy = 96.3%
 - For $F_s/4$, accuracy = 93.3%

- For a dataset having $PGA > 50$ gals and epicentral distance between 100 km to 200 km (792 records), the results of the analysis for different smoothing windows is as follows
 - For F_s , accuracy = 93%
 - For $F_s/2$, accuracy = 90%
 - For $F_s/4$, accuracy = 79%
- For a dataset having $PGA > 50$ gals and epicentral distance between 100 km to 200 km (442 records), the results of the analysis for different smoothing windows is as follows
 - For F_s , correct pick = 65.4%
 - For $F_s/2$, correct pick = 58%
 - For $F_s/4$, correct pick = 40.7%

Considering the results discussed above, it can be concluded that the probability of missing the P-phase is very high for the earthquakes which are coming from a far distance. The most interesting thing to note in such cases is that the algorithm missed the whole record completely, as shown in figure 5.15. With increasing epicentral distance, it was found that the probability of picking the earthquake record decreases below 50 %. This is a favorable aspect of the algorithm while being used for EEW. This is due to the fact that the EEW system for India has been designed to issue a warning for earthquakes that are occurring inside or close to the network region. Northern India experiences long-duration shaking for the earthquakes coming from the Hindukush range in Afghanistan-Pakistan border; however they are not damaging. These earthquakes are missed by the algorithm in real-time, and no warning had been issued. Hence in this manner, the algorithm also works as a filter in identifying the near field earthquakes, which could be much more damaging.

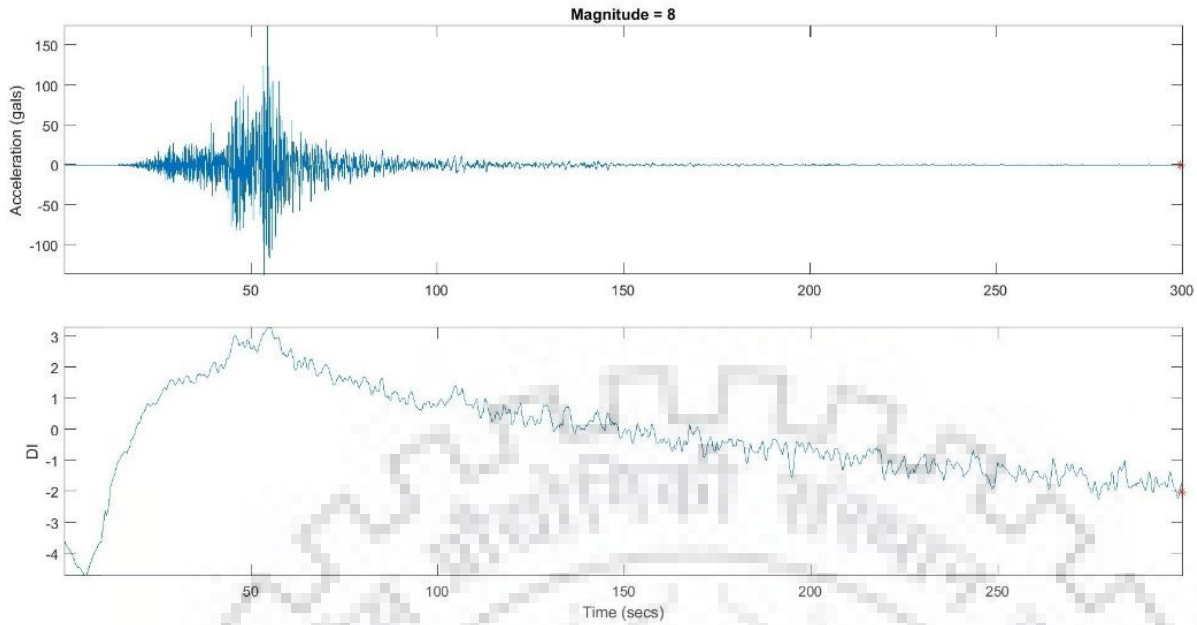


Figure 5.15: The figure gives an example of a candidate record for which event was not picked for a far-field earthquake.

The reason for the missing of far-field earthquakes by the algorithm is the slope of DI as soon as P-wave arrives. Comparing the slope between near-field earthquake DI (figure 5.16) and far-field DI (figure 5.15), it can be concluded that the slope of near-field DI is much steeper. This can also be interpreted as the change in DI is much quicker in near-field earthquakes in comparison to far-field earthquakes.

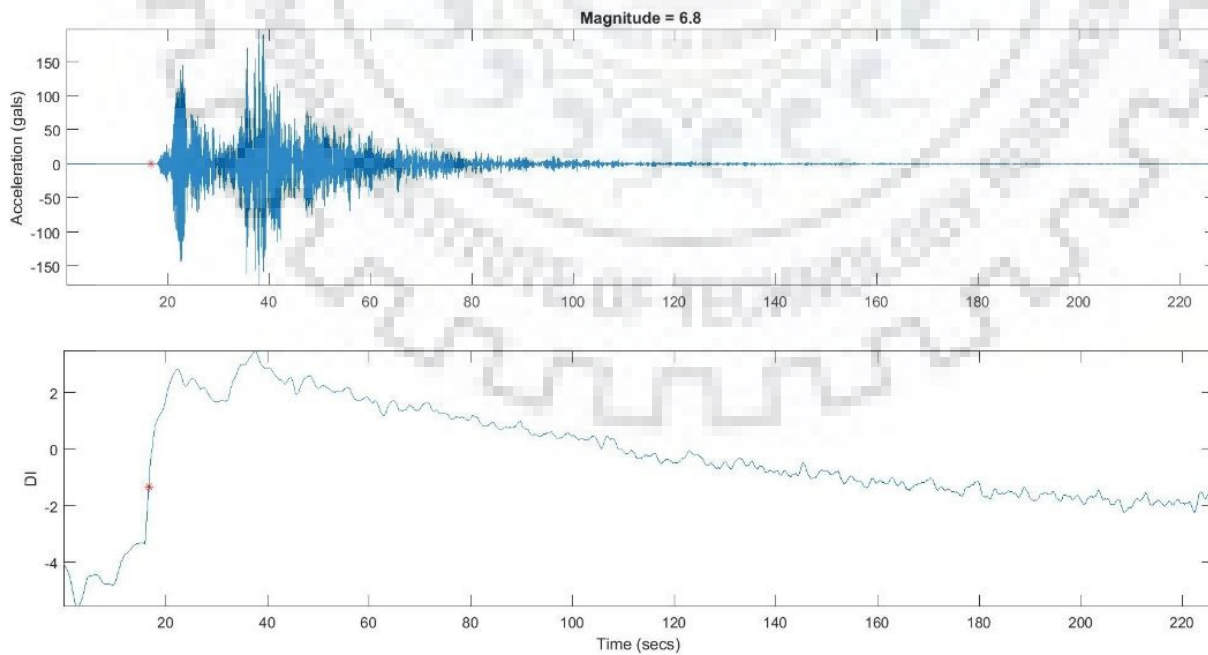


Figure 5.16: Successful pick using DI for near field event

One of the events, having a magnitude of 7.5 and epicentre in Hindukush, which occurred on 26-Oct-2015, was recorded at 31 stations by the current EEW network for Northern India. For this event, a report file was generated, though the epicentre was almost ~700 kilometres away from the network. 10 of the 31 stations were triggered and thus a report file was generated to issue a warning. However, since the peak ground displacement was too small and thus the magnitude estimated was too small to cross the warning threshold of 6, and thus, no warning was issued. However, this event led to the development of a new algorithm using which far filed events could be filtered.

The recorded data from the same earthquake was again run in the server using TANK files, and it was found that using DI not even a single station was triggered, and all of the 31 stations were filtered.



Chapter 6 Conclusion and Results

One of the prime objectives of this study was to test and confirm the feasibility of a successful EEW system for Northern India. Before the beginning of this study, a target region was already identified for instrumentation, as is discussed in chapter 3. The sensors were installed in the identified region, and the Earthworm platform was chosen for data processing and decision-making modules. The primary reason for choosing Earthworm was its readiness for the development of required modules without much getting into the details of data communication and other software and hardware-related programming. With the virtue of its design, the Earthworm has functionality that required modules can be developed or changed as per the requirement of the system, without much affecting the performance and functioning of the other modules.

As discussed after much deliberation and testing, a dedicated leased-line-based VPN is selected for communication of data from sensors to the central server, located at IIR Roorkee. In order to have all the clocks in sync with each other, an NTP server is also installed. The NTP server was also required as it was a mandate from the government to keep the network isolated from the Internet backbone.

6.1. EEW System for Northern India

The instrumentation has been created targeting the earthquakes expected between Chamoli and Uttarkashi District of Uttarakhand and between MBT and MCT. For any earthquake with an epicenter in this region and magnitude greater than 6, a warning can be issued to all the adjoining cities and towns of Uttarakhand, Western Uttar Pradesh and Delhi. The current study lacks an example of major or large earthquakes, as the current network has not recorded or observed any major event since its installation, however with the help of figure 5.4, 5.5, and 5.6, it can be inferred that the model used for estimation of magnitude works better as magnitude reaches 6. This property of the regression model is also mentioned by Hsiao et al., 2011. Thus the testing of the system with recorded data has shown that the developed system has the potential to provide early warning in case of a large or major earthquake. The EEW system has been tested, and performance is being monitored continuously. Though to have a comprehensive EEW system for Northern India, a large part of the central Himalayas needs to be networked by sensors.

In the current phase, the sirens to issue warnings have been installed only in the hostels of IIT Roorkee and some of the test users in district administration of Uttarakhand that includes government colleges, District magistrate offices, police stations, and government hospitals, along with few governments identified test users.

6.2. Sensor Selection

As discussed in chapter 3 and Chapter 4, a dense network is required for the functioning of a successful EEW system, and thus a study was performed to test and validate the suitability of low-cost MEMS-based sensors. It is a well-known fact that the cost of the sensor becomes high with an increase in the dynamic range. Thus to theoretically test the impact of lowered dynamic range in the estimation of various EEW parameters and strong motion parameters have been studied in this study. The methodology and detailed findings are discussed in chapter 4.

6.2.1 Effect on Magnitude using P_D or M_{PD} .

The results indicated that as the resolution decreases, there is a definite drop in accuracy with which M_{PD} is estimated. However, the drop in accuracy is of the order of 0.01 unit up to 16-Bit data, and thus, it can be safely assumed that sensors with up to 96dB are suitable for all practical purposes of EEW.

- For 22 Bit data or for P_D Calculated with 22-Bit data, the maximum difference in M_{PD} estimated is found to be 0.064 and minimum difference 2.4×10^{-7} , with a median at 0.000445. It is also observed that most of the estimations are well within the difference of -0.01 to 0.01.
- Similarly, for 20 Bit data or for P_D calculated for 20-Bit time history, the maximum difference in M_{PD} estimation is around 0.269, and the minimum difference is 6.9×10^{-7} , with a median at 0.00203. There is a very small or negligible difference between the estimated magnitude from 24-Bit and 20-Bit data time histories.
- The results show that for 16-Bit data also the maximum difference in M_{PD} estimation is around 0.649, with a median at 0.0083. Thus this time history is also suitable for the estimation of magnitude using P_D .

However, below 16-bit and lower resolution of ADC the error in the estimation of magnitude is high with a median value of 1.3, and more thus is not suitable for the purpose of magnitude estimation and EEW system.

P_D is extensively used for the estimation of magnitude for the EEW system, and the developed EEW system for Northern India also used the same P_D algorithm is being used. This study has justified that for the estimation of M_{pd} , the low-cost MEMS are quite suitable and can be used for the establishment of low-cost sensor networks for EEW systems.

6.2.2 Effect on magnitudes using τ_c or M_{τ_c}

In this study, the estimation of the magnitude using τ_c has been found very sensitive as the ADC resolution is decreased from 14-Bit to 10-Bit. It has been observed that the maximum error in magnitude estimation is as large as three units for 16-Bit data.

- For 22-Bit converted data, it can be seen that the error in magnitude estimated is almost in the range of -0.02 to +0.02.
- For 22-Bit records, the error in estimation is well within -0.05 to +0.05 units.
- 18-Bit converted data is almost in the order of 0.2 units only. The median error is also of the order 0.0097 units. However, the maximum error is 1 unit. Thus it appears that as the bit is being lowered, the maximum error is getting increased.
- For 16-Bit records, the median error in magnitude estimation is of the order 0.036 units only. However, the maximum error is almost of the order of 3 units. This suggests that the error is now distributed to the large range. However, most of the errors are within the range of -0.5 to +0.5.

From the above-mentioned observation, it is evident that though the median values of error is not too much, however, the large maximum error suggests that the error is more distributed in the large range and thus chances of getting false or erroneous magnitude estimation is more in case of magnitude estimation using τ_c

6.2.3 Effect on Spectral Acceleration

To access the impact of low resolution data in strong motion parameters, a study has been performed to analyze the impact on spectral acceleration. Pseudo Acceleration Spectrum and Pseudo Velocity Spectrum have been calculated by solving the equation motion for different periods and damping values using the Newmark Linear method. To study the impact, 15 important periods from .03 seconds to 10 seconds have been used. The impact has been studied for three damping ratios which are 2 percent, 5 percent, and 10 percent.

Results and observation for 5 percent damping:

- For the Zero period, it is also evident from the results that as the data is converted from 24-Bit to 10-Bit, there is a definite increase in the error with respect to original data. But the error is very small, and it reaches a median value of just 2% for 10-Bit data. Thus it would be correct to infer that for measuring or estimating PGA, therewith up to 12 or 10-Bit accuracy is also suitable.
- For 0.03 second period also the median value for 10-Bit data is only 2.7 %. It can be inferred that a lot of information could be retrieved for this period also even if ADC resolution is as low as 10-Bit.

- For 0.05 and 0.1 seconds periods also the error in 12-Bit data is also found to be as low as 1%.
- For a 0.2 second period, the error becomes more than 1% for 14-Bit data, and it is also observed that as the period increases, the sensitivity towards lowered dynamic range also decreases.
- For 0.5 second, 0.74 second, and 1 second also the error is of the order 1~2% only for data up to 14 Bit resolution.
- For larger periods, the error in SA values increased as the dynamic range of the sensor data is further reduced. However, it has been observed that even for the largest period of 10 seconds also the error is of the order 5~6 %.

Thus it can be safely inferred that for SPA values also the data from low-cost MEMS could be used for all practical engineering applications without losing much information.

Results and observation for 2 percent damping:

For 2% damping, it has been observed that the sensitivity for lowering dynamic range is more as compared to 5% damping.

- For period zero or PGA. It is observed that for 10-Bit data, the median error is 2.7%. Whereas up to 16 bit the error is well below 2%. Thus for estimation of PGA values, the low-cost MEMS with a dynamic range as low as 10-Bit can be used.
- For period 0.03 and damping 2%. The error is of the order 5% for 10-Bit data. Whereas, below 10-Bit data the error is minimal and is of the order of less than 2%. For 16-Bit and more, the error is well below 0.08%.
- For 0.1 second period, the error is well within 2% for data less than 12-Bit. For 16-Bit data, the error is less than 0.1%.
- For a 0.2 second period, the error is well within 2% for 12-Bit data. Even for 10-Bit data, the error is of the order ~6%. However, for 16-Bit, the error is less than 0.1%.
- The error in SA acceleration for 1 second period, for 14-Bit and 16-Bit data, the median error is even less than 1% and 0.2%, respectively.
- For a period of 2 seconds, the median error is of the order 2% for 14-Bit data and is even less than 0.5% for 16-Bit data.

The error in SA values increased as the resolution is reduced from 24-Bit to 10-Bit data, and the error is more prominent for larger periods. However, it has been observed that for data up to 16-Bit, for all important periods can be retrieved without much error or for all practical civil engineering applications.

Results and observation for 10% percent damping:

The observation similar to 2% damping and 5% damping have been found for 10% damping as well.

- For PGA or period, the error in SA values is of the order 2% for 10-Bit time history.
- It is observed that for 0.03 second period, up to 10-Bit, the median error is only 2%. The median error for 16-Bit data is as low as 0.048%.
- For 0.05 seconds, it is observed that error up to 12-Bit data is nearly equal to ~1%. Whereas for 16-Bit data, the median error is as low as 0.063%.
- The median and maximum error for 0.2 second period for data up to 14-Bit the median error is ~0.3%. For 16-Bit data, they are 0.08% and 1.46%, respectively.
- The median and maximum error in SA values for 1 second period, for up to 16-Bit data, are of the order 0.2% and 15%

It has been observed that for larger periods, the error with lower values of dynamic range does increase for 10% damping; however, for all practical engineering applications, the dynamic range up to 16-Bit is found to be suitable.

6.2.4 Effect on Fourier spectrum or Fourier amplitude.

For estimating error in Fourier amplitudes, 14 frequencies each corresponding to the important periods used for Spectral acceleration have been used to perform the analysis. Change in Fourier amplitude corresponding to all the fourteen frequencies has been shown for all seven groups of converted time histories viz. 22-Bit, 20-Bit, 18-Bit, 16-Bit, 14-Bit, 12-Bit, and 10-Bit.

- For the 25 Hertz frequency, the median error for 22-Bit is 0.002%, and the maximum error is 0.139%. Also, the 75th percentile value is 0.004, and the 25th percentile value is at 0.001 %. Also, up to 16-Bit, the median error is of the order 0.179 %, and the maximum error is also 11.62%
- For 20 Hz data median error for 22-Bit data is 0.002%, whereas the maximum error is 0.139% only. The 75th and 35th percentile values are 0.0038 and 0.001 % only. For 16-Bit data, the median error is 0.16% and has a maximum value of 11.49 %. The 75th and 25th percentile values are at 0.3 and 0.07%.
- For 10 hertz frequency, the median and maximum error for 22-Bit data are 0.002 and 0.07%, respectively. The 75th percentile error value is at 0.003, and the 25th percentile error value is at 0.001%. For 16-Bit data, the median error is 0.16% and has maximum values of 4.8 %. The 75th and 25th percentile values are at 0.29 and 0.09%.

- For Fourier amplitude with respect to 5 Hz, the median error for 22-Bit data is 0.0022%, and the maximum error is 0.11%. For 16-Bit data, the median error is 0.185% and has maximum values of 4.05% %. The 75th and 25th percentile values are at 0.32 and 0.092%.
- Corresponding to Fourier amplitude for 3.33 Hz the median and maximum error corresponding to 22-Bit data are as 0.002 and 0.15% only. For 16-Bit data, the median error is 0.2% and has maximum values of 7.3 %. The 75th and 25th percentile values are at 0.39 and 0.09%.
- For 0.14 Hz Frequency, the following observations are made. Median and maximum error corresponding to 22-Bit data are 0.14 and 37.6%, respectively. For 16 Bit data, the median error is of the order ~12%, whereas 75th and 25th percentile values are ~ 61 and 2.44%, respectively.
- For Fourier amplitudes for 0.1 Hertz frequency corresponding to 16-Bit data, the median error is of the order 20%. The 75th percentile and 25th percentile are at 93.12 and 4.69 %, respectively.

6.3. New Pick Algorithm using DI

A new pick algorithm has been developed and discussed in this study in chapter 5. The new algorithm uses damage index (DI), which is defined as the vector product of velocity and acceleration. Though DI has been used by Japan for estimation of intensity for the Onsite EEW system, in this study, the same approach has been used for event detection or P phase picking. It is observed that using this approach and different combinations of smoothing filters, far-field events which were not supposed to be considered for EEW purposes can be avoided. Following observations have been made regarding the same:

- The DI can be used with accuracy for real-time detection of P phase
- For soothing window equal to the sampling frequency, the accuracy of pick increase substantially.
- If a smoothing window equal to sampling frequency is used, the far-field events having epicentral distances more than 300 kilometers could be filtered.
- Recording of the 25th October 2015 Hindukush earthquake has confirmed that far fields events can be filtered if the above-mentioned approach is used.

6.4. Future scope of work

In this study, the feasibility of having an EEW system for Northern India has been performed and successfully demonstrated. However, because of the non-availability of earthquake records, soil profiles etc., there is an unlimited scope for future research.

First and foremost, a similar feasibility analysis or extension of this research needs to be done for other parts of the country, special Himachal Pradesh, Jammu and Kashmir, Laddakh, and the North-Eastern region of India. All these regions have a peculiar terrain as well as geotectonic features and thus require a thorough study for a successful EEW system.

Apart from the estimation of magnitude for issuing earthquake early warning, in order to have a comprehensive EEW system, prediction of ground motion must also be incorporated. When more data would be recorded by this network and once more accurate ground motion prediction equation, after further soil testing, would be available for the target locations, real-time intensity prediction at target places will also be included for this EEW system. This task would remain as one of the most important parts of the future scope of this project.

The current regression model has been created with three-second data of the initial P-phase; the advantage of using a small time window is that it helps in saving few seconds of time, which is very crucial for an EEW system. However, to achieve better accuracy larger time window should be tested, and a new regression model with larger window length data should also be developed in the future.

One of the most important research which is yet to be completed is in the field of local site condition because as local site effects are not known or are not available, a lot of site-specific hazards cannot be estimated and thus cannot be mitigated. Knowledge of site-specific hazards is important in order to predict actual ground motion(Kumar et al. 2015, 2016).

List of References

- Agrawal SK, Chawla J (2006) Seismic hazard assessment for Delhi region. *Curr Sci* 91:1717–1724
- Ait Laasri EH, Akhouayri ES, Agliz D, et al (2014) Automatic detection and picking of P-wave arrival in locally stationary noise using cross-correlation. *Digit Signal Process* 26:87–100. <https://doi.org/10.1016/j.dsp.2013.12.009>
- Alcik H, Ozel O, Apaydin N, Erdik M (2009) A study on warning algorithms for Istanbul earthquake early warning system. *Geophys Res Lett* 36:3–5. <https://doi.org/10.1029/2008GL036659>
- Alessandro A D', Luzio D, D'ANNA G (2014) Urban MEMS based seismic network for post-earthquakes rapid disaster assessment. *Adv Geosci* 40:1–9. <https://doi.org/10.5194/adgeo-40-1-2014>
- Allen R (1982) Automatic Phase Pickers: Their Present Use and Future Prospects. *Bull Seism Soc Am* 72:S225–S242
- Allen RM, Brown H, Hellweg M, et al (2009) Real-time earthquake detection and hazard assessment by ElarmS across California. *Geophys Res Lett* 36:1–6. <https://doi.org/10.1029/2008GL036766>
- Allen RM, Kanamori H (2003) The potential for earthquake early warning in Southern California. *Science* (80-) 300:786–789. <https://doi.org/10.1126/science.1080912>
- Allen RM, Melgar D (2019) Earthquake Early Warning: Advances, Scientific Challenges, and Societal Needs. *Annu Rev Earth Planet Sci* 47:361–388. <https://doi.org/10.1146/annurev-earth-053018-060457>
- Allen R V (1978) Automatic Earthquake Recognition and Timing From Single Traces. *Bull Seismol Soc Am* 68:1521–1532
- Anthony RE, Ringler AT, Wilson DC, Wolin E (2019) Do low-cost seismographs perform well enough for your network? An overview of laboratory tests and field observations of the OSOP raspberry shake 4D. *Seismol Res Lett* 90:219–228. <https://doi.org/10.1785/0220180251>
- Azzaro R, D'Amico S, Peruzza L, Tuvè T (2013) Probabilistic seismic hazard at Mt. Etna (Italy): The contribution of local fault activity in mid-term assessment. *J Volcanol Geotherm Res* 251:158–169. <https://doi.org/10.1016/j.jvolgeores.2012.06.005>
- Banerjee P, Burgmann R (2002) Convergence across the northwest Himalaya from GPS measurements, *Geophys. Res Lett* 29:301–304

- Bansal BK, Singh SK, Dharmaraju R, et al (2009) Source study of two small earthquakes of Delhi, India, and estimation of ground motion from future moderate, local events. *J Seismol* 13:89–105. <https://doi.org/10.1007/s10950-008-9118-y>
- Benson K, Schlachter S, Estrada T, et al (2013) On the powerful use of simulations in the Quake-Catcher Network to efficiently position low-cost earthquake sensors. *Futur Gener Comput Syst* 29:2128–2142. <https://doi.org/10.1016/j.future.2013.04.012>
- Bhardwaj R (2014) Algorithm for Earthquake Early Warning Algorithm for Earthquake Early Warning System. Indian Institute of Technology Roorkee
- Bhardwaj R, Sharma ML, Kumar A (2016) Multi-parameter algorithm for Earthquake Early Warning. *Geomatics, Nat Hazards Risk* 7:1242–1264. <https://doi.org/10.1080/19475705.2015.1069409>
- Bhatia SC, Kumar MR, Gupta HK (1999) A probabilistic seismic hazard map of India and adjoining regions. *Ann Di Geofis* 42:1153–1164. <https://doi.org/10.4401/ag-3777>
- Bilham R, Ambraseys N (2005) Apparent Himalayan slip deficit from the summation of seismic moments for Himalayan earthquakes, 1500–2000. *Curr Sci* 88:1658–1663
- Bilham R, Wallace K (2007) Future Mw > 8 Earthquakes in the Himalaya: Implications From the 26 Dec 2004 Mw = 9.0 Earthquake on India's Eastern Plate Margin. *Geol Surv India Spec Publ* 85:1–14
- Böse M, Hauksson E, Solanki K, et al (2009) Real-time testing of the on-site warning algorithm in southern California and its performance during the July 29 2008 M w 5.4 Chino Hills earthquake. *Geophys Res Lett* 36:L00B03. <https://doi.org/10.1029/2008GL036366>
- Böse M, Heaton T, Hauksson E (2012) Rapid estimation of earthquake source and ground-motion parameters for earthquake early warning using data from a single three-component broadband or strong-motion sensor. *Bull Seismol Soc Am* 102:738–750. <https://doi.org/10.1785/0120110152>
- Brown H, Allen RM, Grasso VF (2009) ElarmS in Japan, *Seismol. Res Lett* 80:727–739. <https://doi.org/10.1785/gssrl.80.5.727>.
- Caprio M, Lancieri M, Cua GB, et al (2011) An evolutionary approach to real-time moment magnitude estimation via inversion of displacement spectra. *Geophys Res Lett* 38:n/a-n/a. <https://doi.org/10.1029/2010GL045403>
- Cauzzi C, Behr Y, Clinton J, et al (2016) An Open-Source Earthquake Early Warning Display. *Seismol Res Lett* 87:737–742. <https://doi.org/10.1785/0220150284>
- Chamoli BP, Kumar A, Chen D-Y, et al (2019) A Prototype Earthquake Early Warning System for Northern India. *J Earthq Eng* 0:1–19. <https://doi.org/10.1080/13632469.2019.1625828>
- Chamoli BP, Pandey B, Kumar A, Gairola A (2020) ON-DEMAND-ON-SITE EARTHQUAKE

EARLY WARNING SYSTEM. 15

- Chen DY, Hsiao NC, Wu YM (2015a) The earthworm based earthquake alarm reporting system in Taiwan. *Bull Seismol Soc Am* 105:568–579. <https://doi.org/10.1785/0120140147>
- Chen DY, Wu YM, Chin TL (2015b) Incorporating low-cost seismometers into the Central Weather Bureau seismic network for Earthquake Early Warning in Taiwan. *Terr Atmos Ocean Sci* 26:503–513. [https://doi.org/10.3319/TAO.2015.04.17.01\(T\)](https://doi.org/10.3319/TAO.2015.04.17.01(T))
- Chen WP, Kao H Seismotectonics of Asia: Some recent progress. In: Yin A, Harrison M (eds) *The Rubey Volume IX: Tectonic Evolution of Asia*. Cambridge University Press, Palo Alto, California, pp 37–62
- Chi-Durán R, Comte D, Díaz M, Silva JF (2017) Automatic detection of P- and S-wave arrival times: new strategies based on the modified fractal method and basic matching pursuit. *J Seismol* 21:1171–1184. <https://doi.org/10.1007/s10950-017-9658-0>
- Chung AI, Henson I, Allen RM (2019) Optimizing earthquake early warning performance: ElarmS-3. *Seismol Res Lett* 90:727–743. <https://doi.org/10.1785/0220180192>
- Cochran ES, Lawrence JF, Christensen C, Jakka RS (2009) The Quake-Catcher Network: Citizen Science Expanding Seismic Horizons. *Seismol Res Lett* 80:26–30. <https://doi.org/10.1785/gssrl.80.1.26>
- Cua G, Heaton T (2007) The Virtual Seismologist (VS) method: A Bayesian approach to earthquake early warning, in *Earthquake Early Warning Systems*. Springer, Heidelberg, Germany
- D'Alessandro A, D'Anna G (2013) Suitability of Low-Cost Three-Axis MEMS Accelerometers in Strong-Motion Seismology: Tests on the LIS331DLH (iPhone) Accelerometer. *Bull Seismol Soc Am* 103:2906–2913. <https://doi.org/10.1785/0120120287>
- D'Alessandro A, Scudero S, Vitale G (2019) A review of the capacitive MEMS for seismology. *Sensors (Switzerland)* 19:1–22. <https://doi.org/10.3390/s19143093>
- Dimri VP, Pandey AK (2014) Centre for Himalayan study in Uttarakhand. *Curr Sci* 107:1647–1648. <https://doi.org/10.1029/2004JB003309.8>
- Erdik M, Fahjan Y, Ozel O, et al (2003) Istanbul earthquake rapid response and the early warning system. *Bull Earthq Eng* 1:157–163. <https://doi.org/10.1023/A:1024813612271>
- Espinosa-Aranda JM, Cuellar A, Garcia A, et al (2009) Evolution of the Mexican Seismic Alert System (SASMEX). *Seismol Res Lett* 80:694–706. <https://doi.org/10.1785/gssrl.80.5.694>
- Evans JR, Allen RM, Chung AI, et al (2014) Performance of several low-cost accelerometers. *Seismol Res Lett* 85:147–158. <https://doi.org/10.1785/0220130091>
- Feldl N, Bilham R (2006) Great Himalayan earthquakes and the Tibetan Plateau. *Nature*

- Festa G, Zollo A, Lancieri M (2008) Earthquake magnitude estimation from early radiated energy. *Geophys Res Lett* 35:4–9. <https://doi.org/10.1029/2008GL035576>
- Freeman SA (2007) Response spectra as a useful design and analysis tool for practicing structural engineers. *ISSET J Earthq Technol* 44:25–37
- Gansser A (1964) *Geology of the Himalayas*. Intersci Publ 289
- Gentili S, Michelini A (2006) Automatic picking of P and S phases using a neural tree. *J Seismol* 10:39–63. <https://doi.org/10.1007/s10950-006-2296-6>
- Ghosh C, Pal I (2017) Geotechnical measures for Uttarakhand Flash flood-2013. *Geotech Meas Uttarakhand Flash flood-2013, Geotech Eng J SEAGS AGSSEA* 48:
- Gutenberg B, Richter CF *Seismicity of the Earth*. Princeton University Press, Princeton, New Jersey
- H. LD, Singh Y, Prasad JSR (2012) Comparing Empirical and Analytical Estimates of Earthquake Loss Assessment Studies for the City of Dehradun, India. *Earthq Spectra* 28:595–619
- Horiuchi NJ, Negishi SH, Abe K, et al (2005) An automatic processing system for broadcasting earthquake alarms. *Bull Seism Soc Am* 95:708–718
- Hoshiaba M, Kamigaichi O, Saito M, et al (2008) Earthquake early warning starts nationwide in Japan. *Eos Trans AGU* 89:73–74
- Hsiao N-CC, Wu Y-MM, Shin T-CC, et al (2009a) Development of earthquake early warning system in Taiwan. *Geophys Res Lett* 36:3–7. <https://doi.org/10.1029/2008GL036596>
- Hsiao NC, Wu YM, Shin TC, et al (2009b) Development of earthquake early warning system in Taiwan. *Geophys Res Lett* 36:3–7. <https://doi.org/10.1029/2008GL036596>
- Hsiao NC, Wu YM, Zhao L, et al (2011) A new prototype system for earthquake early warning in Taiwan. *Soil Dyn Earthq Eng* 31:201–208. <https://doi.org/10.1016/j.soildyn.2010.01.008>
- Hsieh CY, Wu YM, Chin TL, et al (2014) Low cost seismic network practical applications for producing quick shaking maps in Taiwan. *Terr Atmos Ocean Sci* 25:617–624. [https://doi.org/10.3319/TAO.2014.03.27.01\(T\)](https://doi.org/10.3319/TAO.2014.03.27.01(T))
- <https://isti.com/products/eq-monitoring-seismic-software/earthworm/> No Title.
<https://isti.com/products/eq-monitoring-seismic-software/earthworm/>
- Ionescu C, Böse M, Wenzel F, et al (2007a) warning system for deep Vrancea (Romania) earthquakes. In: Gasparini P, Manfredi G, Zschau J (eds) *Earthquake Early Warning Systems*. Springer, Heidelberg, Germany, pp 343–349
- Ionescu C, Böse M, Wenzel F, et al (2007b) An early warning system for deep Vrancea (Romania) earthquakes. *Earthq Early Warn Syst* 343–349. <https://doi.org/10.1007/978-3->

- Iyengar RN, Ghosh S (2004) Microzonation of earthquake hazard in Greater Delhi area, *Curr. Sci* 87:1193–1202
- Jade S, Mukul M, Bhattacharya A, et al (2007) Estimates of interseismic deformation in northeast India from GPS measurements. *Earth Planet Sci Lett* 263:221–234., <https://doi.org/10.1016/j.epsl.2007.08.031>
- Jain SK (2016) Earthquake safety in India: achievements, challenges and opportunities. *Bull Earthq Eng* 14:1337–1436. <https://doi.org/10.1007/s10518-016-9870-2>
- Johnson CE, Bittenbinder A, Bogaert B, et al (1995) Earthworm: A flexible approach to seismic network processing. *IRIS Newsl* 14:4
- Jon P (1993) Observations and modelling of background seismic noise. *US Geol Surv Open-File Rept* 92–322
- Joshi GC, Sharma ML (2011) Strong ground-motion prediction and uncertainties estimation for Delhi, India. *Nat Hazards* 59:617–637. <https://doi.org/10.1007/s11069-011-9783-y>
- Kamigaichi O, Saito M, Doi K, et al (2009) Earthquake early warning in Japan: Warning the general public and future prospects, *Seismol. Res Lett* 80:717–726. <https://doi.org/10.1785/gssrl.80.5.717>
- Kanaujia J, Kumar A, S.C G (2015) velocity structure and characteristics of contemporary local seismicity around the Tehri region, Garhwal Himalaya, *Bull.Seismol. Soc Am*105 1852–1869
- Kayal JR (2001) Microearthquake activity in some parts of the Himalaya and the tectonic model. *Tectonophysics* 339:331–351
- Kayal JR (2008) *Microearthquake Seismology and Seismotectonics of South Asia*, First Ed. Springer and Capital Publishing Company, Heidelberg, Germany and New Delhi, India, ISBN
- Khatti KN, Tyagi AK (1983) Seismic patterns in the Himalayan plate boundary and identification of areas of high seismic potential. *Tectonophysics* 96:281–297
- Kumar A, Baro O, Harinarayan NH (2016) Obtaining the surface PGA from site response analyses based on globally recorded ground motions and matching with the codal values. *Nat Hazards* 81:543–572. <https://doi.org/10.1007/s11069-015-2095-x>
- Kumar A, Harinarayan NH, Baro O (2015) High Amplification factor for Low Amplitude Ground Motion : Assessment for Delhi. *Disaster Adv* 8:1–11
- Kuyuk HS, Allen RM (2013) A global approach to provide magnitude estimates for earthquake early warning alerts. *Geophys Res Lett* 40:6329–6333.

<https://doi.org/10.1002/2013GL058580>

- Lawrence JF, Cochran ES, Chung A, et al (2014) Rapid Earthquake Characterization Using MEMS Accelerometers and Volunteer Hosts Following the M 7.2 Darfield, New Zealand, Earthquake. *Bull Seismol Soc Am* 104:184–192. <https://doi.org/10.1785/0120120196>
- Melgar D, Hayes GP (2019) Characterizing large earthquakes before rupture is complete. *Sci Adv* 5:eaav2032. <https://doi.org/10.1126/sciadv.aav2032>
- Milne J (1911) Catalogue of destructive earthquakes—A.D. 7 to A.D. 1809, British Assoc. Adv Sci Rep, Portsmouth Meet Append 1:649–740
- Minson SE, Meier MA, Baltay AS, et al (2018) The limits of earthquake early warning: Timeliness of ground motion estimates. *Sci Adv* 4:1–11. <https://doi.org/10.1126/sciadv.aaq0504>
- Mittal H, Kamal, Kumar A, Singh SK (2013a) Estimation of site effects in Delhi using standard spectral ratio. *Soil Dyn Earthq Eng* 50:53–61. <https://doi.org/10.1016/j.soildyn.2013.03.004>
- Mittal H, Kumar A, Kumar A (2013b) Site effects estimation in Delhi from the Indian strong motion instrumentation network, *Seismol. Res Lett* 84:33–41. <https://doi.org/10.1785/0220120058>
- Mittal H, Kumar A, Ramhmachhuani R (2012) Indian National Strong Motion Instrumentation Network and Site Characterization of Its Stations. *Int J Geosci* 03:1151–1167. <https://doi.org/10.4236/ijg.2012.326117>
- Mittal H, Kumar A, Rebecca (2013c) No Title. Strong Motion Instrum Netw its site Charact *J Geosci* 3:1151–1167
- Molnar P, Lyon-Caen H (1988) Some simple physical aspects of the support, structure, and evolution of mountain belts, in *Processes in Continental Lithospheric Deformation*, *Geol. Soc Am Spec Pap* 218:179–207
- Nakamura Y (1984) Development of earthquake early-warning system for the Shinkansen, some recent earthquake engineering research and practical in Japan. In: *Proc. of The Japanese National Committee of the International Association for Earthquake Engineering*. Tokyo, Japan, pp 224–238
- Nakamura Y (1988) On the urgent earthquake detection and alarm system (UrEDAS). In: *Proc. of the 9th World Conference on Earthquake Engineering*. Tokyo-Kyoto, Japan, pp 673–678
- Nakamura Y (2004) UrEDAS, urgent earthquake detection and alarm system, now and future. *13th World Conf Earthq Eng*. <https://doi.org/ISBN 4-89580-010-5>
- Nakamura Y (2011) ON THE EFFECTIVE EARTHQUAKE EARLY WARNING SYSTEMS FOR BOTH DISTANT AND NEAR EVENTS. In: *8th International Conference on Urban Earthquake Engineering* (ed). Tokyo, Japan

- Nakamura Y, Saita J (2007a) the earthquake warning system: Today and tomorrow, in Earthquake Early Warning Systems. In: Gasparini P, Manfredi G, Zschau J (eds) Chapter 13. Springer, New York, New York, pp 249–282
- Nakamura Y, Saita J (2007b) UrEDAS, the earthquake warning system: Today and tomorrow. Earthq Early Warn Syst 249–281. https://doi.org/10.1007/978-3-540-72241-0_13
- Nakamura Y, Saita J (2007c) FREQL and AcCo for a quick response to earthquakes. In: Gasparini P, Manfredi G, Zschau J (eds) Earthquake Early Warning Systems. Springer Berlin Heidelberg, pp 307–324
- Nof RN, Allen RM (2016) Implementing the elarms earthquake early warning algorithm on the Israeli seismic network. Bull Seismol Soc Am 106:2332–2344. <https://doi.org/10.1785/0120160010>
- Odaka T, Ashiya K, Tsukada S, et al (2003) A new method of quickly estimating epicentral distance and magnitude from a single seismic record, Bull. Seism Soc Am 93:526–532
- Olson EL, Allen RM (2005) The deterministic nature of earthquake rupture. Nature 438:212–215. <https://doi.org/10.1038/nature04214>
- P. R, Joshi GC, Bhaisora B, et al (2010) Seismic vulnerability of the health infrastructure in the Himalayan township of Mussoorie, Uttarakhand, India. Int J Disaster Resil Built Environ 2:200–209. <https://doi.org/10.1108/17595901111167088>
- Parvez IA, Vaccari F, Panza GF (2003a) A deterministic seismic hazard map of India and adjacent areas. Geophys J Int 155:489–508. <https://doi.org/10.1046/j.1365-246X.2003.02052.x>
- Parvez IA, Vaccari F, Panza GF (2003b) A deterministic seismic hazard map of India and adjacent areas. Geophys J Int 155:489–508. <https://doi.org/10.1046/j.1365-246X.2003.02052.x>
- Peng C, Chen Y, Chen Q, et al (2017) A new type of tri-axial accelerometers with high dynamic range MEMS for earthquake early warning. Comput Geosci 100:179–187. <https://doi.org/10.1016/j.cageo.2017.01.001>
- Peng C, Jiang P, Chen Q, et al (2019) Performance Evaluation of a Dense MEMS-Based Seismic Sensor Array Deployed in the Sichuan-Yunnan Border Region for Earthquake Early Warning. Micromachines. <https://doi.org/10.3390/mi10110735>
- Peng HS, Wu ZL, Wu YM, et al (2011) Developing a prototype earthquake early warning system in the Beijing capital region, Seismol. Res Lett 82:394–403
- Picozzi M, Parolai S, Mucciarelli M, et al (2011) Interferometric analysis of strong ground motion for structural health monitoring: The example of the L’Aquila, Italy, seismic

- sequence of 2009. *Bull Seismol Soc Am* 101:635–651. <https://doi.org/10.1785/0120100070>
- Portnoi M, Schlachter S, Taufer M (2014) Study of the Network Impact on Earthquake Early Warning in the Quake-catcher Network Project. *Procedia Comput Sci* 29:453–464. <https://doi.org/10.1016/j.procs.2014.05.041>
- Rautela P (2015) Traditional practices of the people of Uttarakhand Himalaya in India and relevance of these in disaster risk reduction in present times. *Int J Disaster Risk Reduct* 13:281–290. <https://doi.org/10.1016/j.ijdr.2015.07.004>
- Rautela P, Joshi GC (2010) Earthquake-safe Koti Banal architecture of Uttarakhand, India, *Curr. Sci* 95:475–481
- Rautela P, Joshi GC, Bhaisora B Seismic vulnerability and risk in the Himalayan township of Mussoorie, Uttarakhand, India. *Curr Sci* 99:521–526
- Rautela P, Joshi GC, Bhaisora B, et al (2015) Seismic vulnerability of Nainital and Mussoorie, two major Lesser Himalayan tourist destinations of India. *Int J Disaster Risk Reduct* 13:400–408. <https://doi.org/10.1016/j.ijdr.2015.08.008>
- Rautela P, Sati D (1996) Recent crustal adjustments in Dehradun valley, western Uttar Pradesh, India, *Curr. Sci* 71:776–780
- Ross ZE, Ben-Zion Y (2014) Automatic picking of direct P, S seismic phases and fault zone head waves. *Geophys J Int* 199:368–381. <https://doi.org/10.1093/gji/ggu267>
- Rydelek P, Wu C, Horiuchi S (2007) Comment on “Earthquake magnitude estimation from peak amplitudes of very early seismic signals on strong motion records” by Aldo Zollo, Maria Lancieri, and Stefan Nielsen. *Geophys. Res. Lett.* 34
- Santos-Reyes J (2019) How useful are earthquake early warnings? The case of the 2017 earthquakes in Mexico city. *Int J Disaster Risk Reduct* 40:101148. <https://doi.org/10.1016/j.ijdr.2019.101148>
- Saragiotis CD, Hadjileontiadis LJ, Panas SM (2002) PAI-S/K: A robust automatic seismic P phase arrival identification scheme. *IEEE Trans Geosci Remote Sens* 40:1395–1404. <https://doi.org/10.1109/TGRS.2002.800438>
- Satriano C, Elia L, Martino C, et al (2011) PRESTo, the earthquake early warning system for Southern Italy: Concepts, capabilities and future perspectives. *Soil Dyn Earthq Eng* 31:137–153. <https://doi.org/10.1016/j.soildyn.2010.06.008>
- Seeber L, Armbruster JG, Quittmeyer R (1981) Seismicity and continental subduction in the Himalayan Arc. *Geodyn Ser* 3 D:215–242
- Singh RP, Aman A, Prasad YJJ (1996) Attenuation relations for strong seismic ground motion in the Himalayan region. *Pure Appl Geophys* 147:161–180. <https://doi.org/10.1007/bf00876442>

- Singh SK (2002) Ground Motion in Delhi from Future Large/Great Earthquakes in the Central Seismic Gap of the Himalayan Arc. *Bull Seismol Soc Am* 92:555–569. <https://doi.org/10.1785/0120010139>
- Srivastava HN, Verma M, Bansal BK, Sutar AK Discriminatory characteristics of seismic gaps in Himalaya, *Geomatics. Nat Hazards Risk* 6:224–242,. <https://doi.org/10.1080/19475705.2013.839483>
- Suárez G, Espinosa-Aranda JM, Cuéllar A, et al (2018) A dedicated seismic early warning network: The mexican seismic alert system (SASMEX). *Seismol Res Lett.* <https://doi.org/10.1785/0220170184>
- Tandon AN, Srivastava HN (1954) Focal mechanism of some recent Himalayan earthquakes and regional plate tectonics. *Bull Seism Soc Am* 65:963–969
- Tandon AN, Srivastava HN (1974) Earthquake occurrence in India. In: Tandon AN, Srivastava HN (eds) *Earthquake Engineering*. Meerut, India
- Tu R, Wang R, Ge M, et al (2013) Cost-effective monitoring of ground motion related to earthquakes, landslides, or volcanic activity by joint use of a single-frequency GPS and a MEMS accelerometer. *Geophys Res Lett* 40:3825–3829. <https://doi.org/10.1002/grl.50653>
- Valdiya KS (1980) *Geology of the Kumaun Lesser Himalaya: Dehradun*. 289
- Wang Z, Zhao B (2017) Automatic event detection and picking of P, S seismic phases for earthquake early warning and application for the 2008 Wenchuan earthquake. *Soil Dyn Earthq Eng* 97:172–181. <https://doi.org/10.1016/j.soildyn.2017.03.017>
- Wenzel F, Onescu M, Baur M, F. (1999) Fiedrich (1999). An early warning system for Bucharest, *Seismol. Res Lett* 70:161–169
- Wu Y-M, T.-LTeng (2002) A virtual subnetwork approach to earthquake early warning, *Bull. Seism Soc Am* 92:2008–2018. <https://doi.org/10.1785/0120010217>
- Wu Y-M, Zhao L (2006a) estimation using the first three seconds P-wave amplitude in earthquake early warning, *Geophys. Res Lett* 33, L16312:. <https://doi.org/10.1029/2006GL026871>.
- Wu YM (2015) Progress on Development of an Earthquake Early Warning System Using Low-Cost Sensors. *Pure Appl Geophys* 172:2343–2351. <https://doi.org/10.1007/s00024-014-0933-5>
- Wu YM, Chen DY, Lin TL, et al (2013) A high-density seismic network for earthquake early warning in Taiwan based on low cost sensors. *Seismol Res Lett* 84:1048–1054. <https://doi.org/10.1785/0220130085>
- Wu YM, Kanamori H (2008a) Development of an earthquake early warning system using real-

- time strong motion signals. *Sensors* 8:1–9. <https://doi.org/10.3390/s8010001>
- Wu YM, Kanamori H (2008b) Exploring the feasibility of on-site earthquake early warning using close-in records of the 2007 Noto Hanto earthquake. *Earth, Planets Sp* 60:155–160. <https://doi.org/10.1186/BF03352778>
- Wu YM, Mittal H, Huang TC, et al (2019) Performance of a low-cost earthquake early warning system (P-ALert) and shake map production during the 2018 M w 6.4 Hualien, Taiwan, earthquake. *Seismol Res Lett* 90:19–29. <https://doi.org/10.1785/0220180170>
- Wu YM, Zhao L (2006b) Magnitude estimation using the first three seconds P-wave amplitude in earthquake early warning. *Geophys Res Lett* 33:4–7. <https://doi.org/10.1029/2006GL026871>
- Yeats RS, Thakur VC (1998) Reassessment of earthquake hazard based on a fault-bend fold model of the Himalayan plate-boundary fault, *Curr. Sci* 74:230–233
- Zhang H, Jin X, Wei Y, et al (2016) An Earthquake Early Warning System in Fujian, China. *Bull Seismol Soc Am* 106:755–765. <https://doi.org/10.1785/0120150143>
- Zhang Y, Chen Q, Liu X, et al (2018) Adaptive and automatic P- and S-phase pickers based on frequency spectrum variation of sliding time windows. *Geophys J Int* 215:2172–2182. <https://doi.org/10.1093/gji/ggy400>
- Zhao W (1993) Deep seismic reflection evidence for continental underthrusting beneath Southern Tibet. *Nature* 366:557–559. <https://doi.org/10.1038/366557a>.
- Zhu L, Peng Z, McClellan J, et al (2019) Deep learning for seismic phase detection and picking in the aftershock zone of 2008 Mw7.9 Wenchuan Earthquake. *Phys Earth Planet Inter* 293:106261. <https://doi.org/10.1016/j.pepi.2019.05.004>
- Zhu M, Wang L, Liu X, et al (2018) Accurate identification of microseismic P- and S-phase arrivals using the multi-step AIC algorithm. *J Appl Geophys* 150:284–293. <https://doi.org/10.1016/j.jappgeo.2018.01.007>
- Ziv A (2014) New frequency-based real-time magnitude proxy for earthquake early warning. *Geophys Res Lett* 41:7035–7040. <https://doi.org/10.1002/2014GL061564>
- Zollo A, Iannaccone G, Convertito V, et al (2009a) *Encyclopedia of Complexity and Systems Science*. Springer New York, New York, NY
- Zollo A, Iannaccone G, Lancieri M, et al (2009b) Earthquake early warning system in southern Italy: Methodologies and performance evaluation. *Geophys Res Lett* 36:L00B07. <https://doi.org/10.1029/2008GL036689>
- Zollo A, Lancieri M, Nielsen S (2006) Earthquake magnitude estimation from peak amplitudes of very early seismic signals on strong motion records. *Geophys Res Lett* 33:2–7. <https://doi.org/10.1029/2006GL027795>

PUBLICATION AND CONFERENCES

Publications

1. **Chamoli, B.P.**, Kumar, A., Chen, D.-Y., Gairola, A., Jakka, R.S., Pandey, B., Kumar, P., Rathore, G. (2019). A Prototype Earthquake Early Warning System for Northern India. *Journal of Earthquake Engineering*. 0, 1–19.
2. **Chamoli B.P.**, Pandey B, Kumar, A., Kumar, P., “A new approach to pick P Phase using DI”, (*To be submitted*)
3. **Chamoli B.P.**, Pandey, B., Kumar, A., “Theoretical analysis of sensor dynamic range and its impact on Earthquake Early Warning Parameters, (*To be submitted*)
4. Kumar, P., **Chamoli, B.P.**, Kumar, A., Gairola, A. (2019). Attenuation Relationship for Peak Horizontal Acceleration of Strong Ground Motion of Uttarakhand Region of Central Himalayas. *Journal of Earthquake Engineering*. 0, 1–18.

Patent

1. **Chamoli, B.P.**, Pandey, B., Kumar, A., Gairola, A., (2020) “*On-Demand-On-Site Earthquake Early Warning System.*” 26/2020 (Chamoli et al. 2020) (Chamoli et al. 2020) (Chamoli et al. 2020)

Conferences

1. **Chamoli B.P.**, Pandey, B., Kumar P, Rathore, G., Jakka, RS., Gairola, A., and Kumar, A. (2015) “Development of Earthquake Early Warning System for Northern India.” ISPRS WG VIII/1 Workshop on Geospatial Technology for Disaster Risk Reduction, Jaipur, India.
2. **Chamoli, B.P.**, Kumar, A., Gairola, A., Jakka, RS., Mittal, H., and Srivastava, A. (2015) “Development of Earthquake Early Warning System” Proceedings VI Annual Conference of the International Societies for Integrated Disaster Risk Management., New Delhi, Oct 2015.
3. Rathore, G., Kumar, A., Jakka, R. S., and **Chamoli, B. P.** (2018). *Development of Earthquake Early Warning Siren for Regional Earthquake Early Warning System in India*. (154), 2018. Roorkee, India: 16th Symposium on Earthquake Engineering, 20-22.
4. Ashok Kumar, Mittal, H., **Chamoli B.P.**, Gairola, A., Jakka, RS., and Srivastava, Amit. (2014) “Earthquake Early Warning System for Northern India” Proceedings 15th Symposium on Earthquake Engineering, IIT Roorkee, Dec 2014, pp231-238.
5. Kumar, P., **Chamoli, B.P.**, Kumar, A., Gairola, A. (2018). “Mock drill of Earthquake Early Warning and its benefits”, Japan Geoscience Union Meeting 2018, Makuhari Messe, Chiba, Japan, 20th – 24th May.
6. Kumar, P., **Chamoli, B.P.**, Kumar, A., Gairola, A. (2018). “Real-Time Generation of ShakeMap through Earthquake Early Warning System for Northern India”, EGU General Assembly 2018, Vienna, Austria, 08th – 13th April.

7. Kumar, P., **Chamoli, B.P.**, Kumar, A., Gairola, A.(2017).“Parameters and Methodologies for Earthquake Early Warning System”, 3rd World Congress on Disaster Management, Visakhapatnam, Andhra-Pradesh, India, 6th – 10th Nov.

